PERSISTENT CIRCULATION ANOMALIES IN OBSERVATIONS AND IN A GENERAL CIRCULATION MODEL

by

© Bernard Dugas

This thesis is submitted to the Faculty of Graduate Studies and Research, in partial fulfillment of the requirements for the degree of Ph.D. in Meteorology.

Department of Meteorology
McGill University
Montréal, Québec

July 1989

PERSISTENT CIRCULATION ANOMALIES IN OBSERVATIONS AND IN A GCM by Bernard Dugas

Résumé

Une étude diagnostique, comparant des évènements persistants de la haute atmosphère, tels que simulés par un modèle de circulation générale (MCG) et tels qu'observés, est présentée Nous commençons d'abord par un survol des différentes théories tentant d'expliquer l'existence de ce genre de phénomenes Nous nous attardons tout particulièrement au modèle propose par Shutts (1983) Ensuite, nous montrons que les distributions dans l'espace d'évenements simulés et observés sont qualitativement tres similaires Les situations ayant cours au-dessus de l'Atlantique-Nord sont retenues dans le troisième chapitre, ou une analyse de ces donnees en termes de fonctions empiriques orthogonales ayant subies une rotation (REOF) est effectuee Les deux ensembles de modes qui resortent de cette analyse, l'un pour les donnees du MCG et l'autre pour les observations, se ressemblent étonnament. Tous deux expliquent approximativement 50% de la variance contenue dans leur donnees respectives Les relations entres les modes d'un même ensemble sont également présentees, illustrant ainsi l'*évolution* probable des situations ou ces derniers sont importants Le quatrième chapitre contient une évaluation de la théorie de Shutts Les résultats de l'analyses du troisième chapitre sont alors utilises afin de n'extraire que les evènements correspondants à un type bien particulier, *i e* les dipoles prononces +ATL2 Les champs de tendance temporelle associes aux ondes synoptiques de courtes durees sont évalués à l'aide des *vecteurs E*, tout en prenant bien soin de distinguer entre le début, la phase mature et la fin des évènements Il en ressort que ces ondes synoptiques semblent avoir un effet déterminant sur le cycle de vie moyen des evenements du genre +ATL2, et ce dans le MCG et dans les analyses du NMC americain

Abstract

A comparative diagnostic study of upper-air persistent atmospheric events, as simulated by a general circulation model (GCM) and as observed, is presented We start with an overview of the several theories that attempt to explain such phenomena. Particular emphasis is put on the model approach of Shutts (1983) We next show that the spatial distributions of persistent events is qualitatively similar in the GCM and observational data The North-Atlantic events are extracted and a rotated empirical orthogonal function (REOF) analysis is done on the resulting data sets The two REOF sets that are thus obtained are shown to greatly resemble one another Both explain roughly 50% of their original data's variance The relationships between the modes within a set are presented, so as to understand their probable combined *evolution* The fourth chapter contains an evaluation of Shutts' theory There, the third chapter's results are used to isolate a particular class of events, namely the strong +ATL2 dipoles. The time-tendencies associated to short time-scale synoptic waves are evaluated, using an *E-vectors* approach, taking care to distinguish between the onset, mature and demise phases of the events. It seems that these synoptic waves have a significant impact of the average life-cycle of this +ATL2 type of events, whether they be simulated by a GCM or obtained from a NMC set of analyses.

Remerciements

Je voudrais tout d'abord remercier ma compagne, France-Line Carbonneau, pour sa comprehension et son support constant tout au long de la duree de cette these En second lieu, je tiens egalement a remercier mon directeur, le professeur Jacques Derome, pour la façon qu'il a su diriger ce travail et pour la confiance qu'il a manifeste a mon égard en acceptant de diriger un projet purement diagnostique tel que celui-ci De plus, je remercie le Dr Roger Daley pour sa suggestion de considerer les rotations de fonctions empiriques orthogonales (REOF)

Le service de l'environnement atmospherique (SEA) du gouvernement du Canada a lui-même grandement contribue a ce travail Je lui suis reconnaissant pour son important support financier au cours des trois premieres annees de ce doctorat De plus, mes calculs furent tous effectues a l'aide des ordinateurs du SEA a Dorval Finalememt, je remercie le departement de meteorologie de l'univerité McGill pour son support financier de mars a août 1989

En dernier lieu, je remercie egalement Mme Hélene Potvin qui a expertement relu une version finale du texte, afin de suggerer certaines améliorations de caractère purement stylistique.

Table of Contents

List of Figures.

List of Tables.

Statement of originality

The contributions to original knowledge to be found in this thesis are the following:

1) A time-wise breakdown of the upper-air streamfunction variances and kinetic energies of observations and of simulated data is first presented. This shows that a further, more exhaustive, comparative study of modelled and observed mid-latitude persistent events is indeed possible.

2) An objective criterion is proposed by which most instances of these persistent atmospheric anomalies can be identified in either the northern or the southern hemispheres

3) This permits a complete rotated empirical function analysis of these events, thereby producing a classification of the principal modes accompanying strong mid-Atlantic 50 kPa persistent anomalies The model and observation classifications are shown to closely parallel each other

4) We finally use this classification to determine the influence of high-frequency (synoptic-scale) transients on the life-cycle of one of these types of modes, the so-called ATL2 mode. The synoptic events are found to either enhance or hinder the ATL2 mode, depending on whether we consider the mode's onset or demise stages, respectively.

Chapter 1
Blocking theory survey

1.1 Introduction

A great deal of work has been done in the last ten years or so with regards to the persistent circulation anomalies known to the meteorological community as blocks, their initiation, maintenance and eventual demise. While some of this work has been concerned with a better observational description of the phenomenon, quite a few theories have been proposed that attempt to explain one or another aspect of these important atmospheric events We propose in the following to evaluate these theories using, when appropriate, diagnostic tools applied both to observations and to a long-term atmospheric simulation by a general circulation model (GCM).

This first chapter starts by giving a quick review of the main points modelers have tried to reproduce from atmospheric observations of blocks. Secondly, a more extensive overview is given of the more prominent modeling approaches taken in blocking studies, and the important results obtained in each are discussed. No attempts are made to mention ***all*** of the different variations pertaining to a given approach A third section will concentrate on one of the theories that seems most promising and is also more amenable to numerical evaluation using a GCM The entire chapter should be viewed as the prerequisite step in an evaluation process of recent blocking theories in a primitive equations context. The goal is to identify the better documented or more promising theories pertaining to blocking so as to verify or invalidate them (if possible) using a higher level model.

Certain main references turn out to be extensively used in this chapter. They are the March 1983 issue of the *Australian Meteorological Magazine* and Hoskins and Pierce's 1983 *Large Scale Dynamical Processes in the Atmosphere*. More classical reviews such as Bengston's contribution to the 1979 ECMWF summer seminar have also been found useful.

The second chapter describes certain aspects of the basic (seasonal and annual) climatology of the simulated and observed data sets, with special emphasis on blocking. An objective criterion will be given with which the events can be defined. Both Northern and Southern Hemispheres statistics are considered. The work of Dole and Gordon (1983) is particularly relevant to this part of our thesis.

The third chapter presents a rotated empirical functions (REOF) analysis of certain of the anomalies that are identified in the second chapter. The mathematical and statistical methods that are used throughout are discussed in more detail in Appendix A. This Appendix should be consulted by readers not already acquainted with the principles and properties of REOFs. The main result of the analysis is a breakdown of the simulated and observed persistent anomalous events in terms of a small number of physically meaningful modes of atmospheric variations. Each of these can be immediately identified to a specific atmospheric situation. The GCM and observed versions of these modes are shown to be very similar. The mutual and self interactions of these modes (in terms of lag-correlation statistics) is discussed in an attempt to understand their probable time-wise evolution.

The fourth chapter contains a short diagnostic study where a particular physical mechanism, the theory of which is reviewed later in this first chapter, is evaluated whereby blocks could be either created, maintained or destroyed. This should be compared to the work of Mullen (1987), where the same mechanism is indeed considered but with different diagnostic tools and without our particular emphasis on the different stages of the events.

1.2 Observational model

All of the *blocking* theories try to fit some accepted observational model of atmospheric blocks. A very extensive such model is the one presented by Dole (1982). Except when specifically stated otherwise, we will refer to this study when comparing theoretical results to observations in this chapter.

A quick qualitative description of the main points modelers have tried to reproduce would be that :

1) Full blown blocks exhibit equivalent barotropic vertical structures. Their vertical temperature structure is that of warm anomalies throughout the troposphere and cold anomalies in the lower stratosphere with very little anomaly line tilt in the vertical, except at the surface and tropopause

2) The three preferred northern hemispheric (NH) geographical positions for the blocks are the North-Atlantic, North-Pacific and northern USSR, the first two being the most important. Although blocks do occur in the Southern Hemisphere (SH) (Van Loon, 1956, Taljard, 1972, and Trenberth and Mo, 1985), very few modelers have tried to model them The preferred position seems to be south of New Zealand with a secondary preferred position south-east of South America.

3) Blocks occur all through the year but are most frequent in late winter, early spring and late summer, early autumn (Knox and Hay, 1984, for the NH and Hirst and Linacre, 1981, for the SH).

4) The accepted duration and amplitude criteria are of the order of five to ten days with an amplitude in the NH of 100 gpm at 50 kPa (lower in the SH). It has to be remembered though, that Dole's study shows no preferred time duration for circulation anomalies.

5) Blocks can occur in groups of one, two or three. Solitary blocks are not at all uncommon. In fact single blocks are more the rule than the exception in the SH (Wright, 1974).

6) The spatial extent of blocks is smaller in the SH than in the NH where Austin (1980) associates them to a wavenumber 4 amplification occurrence in the Pacific sector, consistent with the Rex (1950a) criterion of at least 45 degrees of longitudinal extent (or compare Dole's NH blocks with Wright's SH blocks).

Other aspects will be mentioned as required by specific theories.

1.3 Theoretical overview

We now consider, in order, the ***modon*** blocking theory of McWilliams, followed by considerations of some of the ***asymptotic approaches*** that have been attempted. Charney and DeVore's ***multiple equilibria*** theory is discussed after that, followed by a section on ***linear stability analysis*** and their possible application to blocking. The section ends with a few of the ***resonance*** theories.

1.3.1 Solitary eddy solutions (SES) or Modon solutions

Many authors have used numerical approaches but very few analytic theories have been produced In the latter, simplifications are generally introduced to obtain a more tractable problem, such as to impose weak nonlinear interactions, in Malguzzi and Malanotte-Rizzoli (1984), leading to weak (i.e. small amplitude) perturbations, or to simply specify constant zonal winds, which then results in a linear problem, in Tung and Lindzen (1979a)

As of now, however, the only fully nonlinear and finite amplitude theory of blocking of realistic flows has been the modon, solitary eddy solution or SES (Flierl *et al.*, 1980, McWilliams, 1980, and Baines, 1983). Modons specifically address the equivalent barotropic, stationary and local features relevant to blocks. The solutions are required to be steadily translating, local structures of the equivalent barotropic stream function. McWilliams has named them *equivalent modons*. One finds, in Flierl *et al.* (1980), the analytic derivation of the solutions for the more general two-layer model While there is a family of such solutions, McWilliams is concerned with only one of them (see Berestov (1981), for a discussion of the other solutions). The shape of the retained solution is that of a vortex pair similar to certain occurrences of blocking such as the January 1963 North-Atlantic occurrence (see O'Conner, 1963) and, in the case where the zonal wind far enough upstream of the blocking region is zero, the range of acceptable translating speeds turns out to be disjointed from the one pertaining to the linear Rossby wave problem. The current problem's solutions are thus fundamentally different from the more usual Rossby solutions of the linear problem.

It is interesting to note that once the translating condition has been used, the resulting boundary value problem is very similar to the *noninteraction* condition used by Mitchell and Derome (1983), that is, the potential vorticity is a function of the streamfunction (or rather *streakfunction* in Flierl *et al* , 1980). This condition will be discussed again later in more detail when reviewing Mitchell and Derome's paper.

The modon solutions have an inner (blocking) and an outer (normal) region The local wind (defined in this normal outer region) is supposed to be uniform As of now, this is an essential ingredient in Flierl *et al* 's problem, but clearly, it would be interesting to know if modon solutions exist in a variable upstream wind field McWilliams seems to imply that they do, but does not use them. This generalization would strengthen the theory and could possibly ease its verification. It could also help explain the preferred positions that blocks exhibit

The range of modon translation speeds depends linearly on the value of the local wind. This proves to be one of the points causing problems in the theory's verification since it is difficult to know how one defines in practice. A simple time-averaging procedure to determine this local wind is unsatisfactory since the combination of nonlinear solutions will not automatically yield another nonlinear solution. McWilliams tried to fit the 1963 case to the theory and his results were at best inconclusive The problem seems to be that the transient nature of the real atmospheric flow is not taken into account in the modon theory. The solution itself is purely steady-state. There is little need to point out that climatological winds such as those found in Oort and Rasmusson (1971) failed the verification test even more seriously than did the 1963 North-Atlantic winds

The theory as presented by McWilliams does not include any forcing and, given the dissipative nature of the real atmosphere, this proves to be unsatisfactory Baines (1983) included such forcing relevant to the New Zealand sector, without changing the structure of the equation. The solutions were thus of the same type as in the original problem and the diabatic forcing required by Baines' modification could very well be produced by certain local SST patterns Baines remarks that there would not need be so strange as to completely rule them out.

We can ask ourselves to what extent such modon solutions can really be identified within a transient fluid such as the atmosphere. It seems that the necessary simplifications (here, stationarity) permitting analytic solutions render the results difficult to verify A point that can help to explain the difficulty in identifying atmospheric modons is the fact that their north-south asymmetries can be masked by additional stationary solutions to the basic equations, solutions termed as *riders* in Flierl *et al.* (1980). The stationary nature of this theory should be compared with the essentially transient nature of the blocking theory presented in Shutts (1983), to be discussed later

The local aspect of the SES theory should be stressed as it is an essential part of it Baines (1983) considers that this makes it the theory that explains most satisfactorily the maintenance of blocks in the SH. Whether this local characteristic of modon solutions can be invoked to explain NH blocks, which appear to be more of a planetary scale than in the SH, remains to be seen. On the other hand, consider Held (1983). In his review paper on stationary eddies, Held presents the combined and separate responses of a barotropic channel model with zonal basic winds and realistic Ekman damping time (as defined by Charney and Eliassen, 1949, to be of the order of five days) to the two main 45^{0}N topographic forcings. The Tibetan Plateau and Rockies forcings display very little interference between each other and he concludes that one could "think in terms of wavetrains emanating from localized features" This local view of NH eddies is encouraging for the modon theory proponents. To our knowledge, verification of the SES theory has not yet been attempted in the SH

Another encouraging aspect of the theory is that presented in

McWilliams *et al.* (1981). Numerical experiments presented by these authors, done with a grid point barotropic model, show that the modon solutions are robust with respect to the inclusion of various scales of perturbations and are stable with respect to change in spatial resolution.

1.3.2 Asymptotic theories

There is a family of asymptotic theories, and a wide range of approximations have been used to build them, that rely on expansions of the governing atmospheric variables about one or more small parameter. The latter can, for example, represent the weakly nonlinear nature of the flow, the long longitudinal scale, the slow time scale on which dispersion takes place or the weak forcing which is applied to the equations.

This approach gives exact solutions to the (at some finite order) expansion of the (appropriately simplified) governing equations in terms of its small parameter It thus allows us to isolate and understand different processes that, in a more general framework, can be masked and/or occur in conjunction with other processes The main limitations of this approach are, firstly, that the small parameters that are used do not necessarily remain so and the approach then breaks down, and secondly, that the relevance of these small parameters to observations is not always obvious from the start.

One justification of the weakly nonlinear approach can be found in Illari and Marshall (1983) and Illari (1984). These authors show that there exist a nearly linear relationship between the geopotential height Φ and the potential vorticity q on a given pressure surface in the vicinity of an observed block (July 1976, Northern Europe) In other words, q was found to be nearly constant along quasi-geostrophic streamlines so that the Jacobian of the geostrophic streamfunction ψ_g and potential vorticity was then minimal (*i e.* $J(q,\psi_g)\approx 0$), leading to small nonlinear interactions over the blocking region. The only event studied, though, is the July 1976 Northern Europe block. Derome (1984) finds that this assumption holds (although to a lesser degree than in Illari's study) at the top of the troposphere when considering zonally- and time-averaged data (here, January 1979) north of the tropospheric jet stream. We now examine theories using this weakly non-linear hypothesis.

This asymptotic theory discussion will be restricted to the work of Malguzzi and Malanotte-Rizzoli (1984), Patoine and Warn (1982) and Warn and Brasnett (1983).

Malguzzi and Malanotte-Rizzoli (1984)[1] consider quasi-geostrophic inviscid motion on a β-plane They find analytic weakly nonlinear solutions to the stationary potential vorticity equation They thus model the mature steady phase of blocks. Their (artificial) background zonal wind U has meridional as well as vertical shear and the solutions are horizontally as well as vertically trapped by this profile, this being done to ensure energy confinement (and initial buildup) in the zonal wave guide defined by U Note that this is also an appropriate condition if the mechanism responsible for the block's initiation is supposed to be some kind of Rossby wave resonance, as in Tung and Lindzen (1979a, b), where it is indeed required.

Of the two fashions in which nonlinearities can be considered a higher order phenomenon, the more desirable one in the problem of blocks is to have a weak perturbation streamfunction. The other fashion, weak meridional shear, can be shown to produce solutions that have zero vertical means (see Flierl, 1979, and Malanotte-Rizzoli, 1984) and the desired solutions would not be equivalent barotropic.

It is possible to separate the longitude dependence in the problem so that the latitude-height problem is described by a linear Schroedinger eigenvalue problem at finite order while the longitude structure obeys a *KdV* equation at first order. This is obtained by balancing the weak nonlinearities by the weak dispersion. The linear prob-

[1]Hereafter referred to as MMR4. Their 1985 article will be called MMR5.

lem then has a complete set of orthonormal eigen solutions (in MMR5).

The perturbation streamfunction solution is of the well-known soliton type. that is, hyperbolic secant squared in longitude, times one of the eigenfunctions of the linear problem in latitude and height The latter have to be found numerically, given the $U(y,z)$ profile The eigenfunction is then chosen to ensure an equivalent barotropic solution The combination of the gravest acceptable eigensolution, which turns out to be the second one, and the *KdV* solution yields idealized but recognizable vortex pair blocks and perturbation geopotential amplitudes of up to 100 m at 50 kPa, consistent with expected values

The main difficulty these authors identify is that the same wave confinement condition they require may also ensure baroclinically unstable background winds On the other hand, they also qualitatively show that the interior region of their block has enhanced stability with respect to its surroundings. The other (conceptual) problem of the small amplitudes of the perturbations is addressed by the authors in their 1985 paper where they use a finite amplitude nonlinear truncated spectral model that essentially manages to reproduce the analytic results.

In an earlier study, Patoine and Warn (1982) had used an approach similar to that of MMR4 with a weakly nonlinear asymptotic theory In fact, they arrived at the same unforced stationary small order KdV equation as MMR4 but did not solve for the finite order problem Their main result involves the (asymptotic) time evolution of their soliton solutions in response to weak local topographic forcing The case of weak periodic forcing had been addressed in Trevisan and Buzzi (1980) In Patoine and Warn, the solitons end up being attached to (or captured by) different parts of the topography, depending on aspects of the latter

Warn and Brasnett (1983) extended the previous work by including Ekman damping and comparing the effect of the relative amplitudes of the (initially traveling) soliton and topographic forcing on the amplitude response of the (finally captured) soliton. When the capture mechanism is operative, significant (resonant) amplification is shown to occur and the final soliton position is upstream of the topography.

The relevance of weak topography is not entirely clear in the case of observed blocks when significant topography may not even be present, as in the North-Atlantic, or may simply not be weak at all, as in the North-Pacific. On the oher hand, land surfaces are indeed found east of these two preferred blocking positions

1.3.3 Multiple Equilibria

Since the works of Charney and DeVore (1979) and Wiin-Nielsen (1979), where the possibility of multiple atmospheric equilibrias first mentioned, quite a few studies on the subject have been produced The former authors put this result in the context of atmospheric blocking while a more cautious Wiin-Nielsen only hints that it "(·) corresponds to the general synoptic experience that certain wave configurations in the atmosphere may persist for a relatively long time while others, presumably corresponding to the unstable cases, will break cown ataa fast rate". One of the aspects shared by most authors is their use of severely truncated models Leith (1983) in a review article dealing with predictability of atmospheric flows considers that "The main concern with these studies has been their severe truncation As more and smaller modes are included, will they serve as random stochastic elements increasing the transition probability between states ( )"

In a recent review article, Tung and Rosenthal (1985) (TR) have shown that although multiple equilibria do in fact occur in barotropic models, the necessary conditions for that may be quite unrealistic. An essential distinction here is the one between steady and periodic or regime equilibria. In their article, TR are concerned with steady equilibria of barotropic flows as in Charney and DeVore (1979), Charney, Shukla and Mo (1981) or Legras and Ghil (1985) Regime equilibria is a concept introduced in Reinhold and Pierrehumbert (1982) and is discussed later[2] Gravel (1989) discusses periodic equilibria of barotropic

[2]The first three are respectively referred to as CD, CSM and LG while

flows.

In the steady equilibria theory, the unrealistic parameters or conditions can be very weak Ekman damping and very low spectral resolution of the forcing (as in Leith's comment) as in CD and CSM, or very high zonal winds and sources of vorticity that prove to be unphysical as in LG.

To be more specific, it was found by CSM that under certain parameter values, the zonal flow of their system exhibits several equilibria values between mountain torques produced by a one meridional mode topography and the transient momentum flux in a β-plane channel One of the stable equilibria corresponds to a (normal) high zonal index and the other a low (blocking-like) zonal index The mechanism maintaining the low-index solution is seen to be a form of damped resonance to (form drag) topographic forcing. In fact, resonance of this or another type is an essential part of all multiple equilibria theory

TR first point out that instead of a five-day Ekman damping time CD and CSM actually use a 14-day one. Secondly, if the topography is allowed to have more than one meridional mode (which TR term the nonlinear case) the multiple equilibria disappear Finally, they point out that the momentum driving term used by CSM is unrealistically large

Note that Mitchell and Derome (1985) also run into this last type of problem in their topographic resonance theory They show that it is related to the choice of background wind profiles It would seem that, if instead of choosing a basic sine wave in latitude (as in CSM and Mitchell and Derome, 1985), one were to add a constant value to this, the zonal wind for which the external (barotropic) large scale Rossby wave becomes resonant (stationary) is greatly reduced, as in Dionne *et al* (1988) In this latter case, the zonal momentum driving term need not be as large

---

the last is referred to as RP.

TR also discuss the energy source used in the different equivalent barotropic models to balance the presence of dissipation. They stress that one should not use a momentum driving term that appears in the potential vorticity equation as a vorticity source since that equation has no such term, even though many authors have used it, as CD, LG and Kalnay-Rivas and Merkine (1981) The forcing should instead appear in the zonal index equation as a (climatological) momentum flux across the lateral boundaries Taking this forcing into account, as in LG, eliminates steady multiple equilibria in these barotropic models, unless one considers unreasonably high zonal momentum driving.

TR's ideas are here in agreement with zonal budgets of the different terms in the vorticity (or potential vorticity) equation On the other hand, transient vorticity sources can locally be of the same order as the dominant advection terms, as presented in Lau (1979) This is certainly true over the main oceanic storm tracks Baroclinic processes convert potential to kinetic energy in these regions This latter could then conceivably be made available to purely barotropic processes. The question of advisability of including or not such mid-channel energy sources in equivalent barotropic models does not seem obvious to this author.

Others have tackled the multiple equilibria problem from a more numerical point of view and RP are among those. They present results from a very long (257 years, 1.5 million timesteps) numerical integration of a two-layer (severely) truncated spectral channel model. They include modes with barotropic and baroclinic components and are thus able to examine the minimum interaction of one type of wave on the other, particularly in regards to the transition between the different preferred circulation regimes they find.

One of their first conclusions is that "knowing the large-scale equilibria and their respective stabilities ( ) is insufficient information in determining the qualitative aspects of the quasi-stationary time-independent flow". For one thing, synoptic scale disturbances mask the large scale equilibria patterns so that they seem to appear and disappear.

In fact, the presence of these disturbances as well as the interactions between them and the large scale flow turn out to be essential aspects of RP's simulation This is shown by removing the wave-wave interactions In that case, transition from one type of regime to another does not occur. This is quite interesting in view of the proposition made by Green (1977), developed by Austin (1980) and Shutts (1983) and partially substantiated by Mullen (1987) from observations and GCM simulations In Austin's theory, these interactions provide the mechanism that maintains blocking episodes as a resonant response of a planetary scale wave to transient synoptic forcing We will come back to this theory

RP present a theory of feedbacks between synoptic and planetary scale waves, the former set up the transition from one circulation regime to another while the latter modulate the transient synoptic-scale transports They arrive at the first result through a budget analysis of their simulated data and at the second one by a linear stability analysis of their regimes and their implied transports. The results are more of a qualitative nature and exact criteria for transition are not presented However, the theory would not only explain the start of blocking episodes but also their demise The transition time scale in the model is of the order of the synoptic time scale, in concordance with the observation that blocks appear and disappear fairly rapidly, independently of their duration.

Dole's finding that blocks do not have preferred duration is one of the characteristics well reproduced in RP's simulation. They also find evidence that more than one dynamical process may be active and dominant throughout the regime lifetime, again in agreement with Dole Mullen (1987) also suggests this in concluding his diagnostic study of blocks The initial and mature phase of blocks could very well be controlled by processes having different persistence statistics. Baroclinic and barotropic processes could very well be both relevant.

The value of the parameters used in RP's model are not those found in nature, but they are rather chosen so that the simulated flow be itself similar to the observed one in terms of scale behaviors The topographic and latent heat forcings are of the single meridional mode variety. In view of all this, one can wonder to what extent the criticism of TR on stable multiple equilibria for equivalent barotropic models applies to RP's model, if they do at all In fact, Ceheleski and Tung (1987) have investigated RP's model dependence on severe truncations, but without changing any of its other parameter values. They establish, with the aid of bifurcation theory, that under these circumstances, only one weather regime eventually survives the increase in the number of modes The resulting regime is already *qualitatively stable*, when only four longitudinal and four latitudinal degrees of freedom are considered. Ceheleski and Tung explain that, by relaxing the severe truncation constraint, a vorticity cascade (arising from triad interactions) to smaller scales is now permitted so that the larger scale flow is less chaotic (but still unpredictable in detail) Reinhold (1989) has, in turn, criticized Ceheleski and Tung for using parameter values that are inappropriate for these higher resolution models

Gravel (1989) seems to answer most of TR's objections[3] and, accordingly, her model does not contain multiple *stationary* equilibria. Rather, she finds, again with the methods of bifurcation theory, two branches of solutions for the same parameter values, one of which corresponds to the stationary zonal flow found by TR and the other is a very slowly oscillating blocking mode. As her model is hemispheric, TR's objection to either the channel width or to the boundary conditions used by previous authors are also answered Note that a β-plane version of her model was also found to display these two types of *multiple equilibria*, but then, only for an unacceptably large 20-day diffusion

All that can be said in the end is that while the multiple equilibria approach seems in the first instance to be a reasonable one, both Tung and Rosenthal (1985) and Ceheleski and Tung (1987) have cast

[3]For example, she has high model resolutions (to triangular-hemispheric T9), realistic jet speeds and realistic 8-day diffusion

very serious doubts as to its simple application. It still remains one of the attractive theories (or concepts) attempting to explain why different weather patterns, including blocks, occur and why the atmosphere shifts from one to another.

1.3.4 Linear Normal Modes

Once the equations describing atmospheric motions have been linearized around a certain basic state and the choice of spatial basis functions on which to project the different fields has been made, one is left with an ordinary first order set of equations in time. If we further choose the time projection as a complex exponential, we obtain a complex eigenvalue problem in frequency Eigenfunctions corresponding to eigenvalues having non zero imaginary parts will be amplifying or decaying exponentially in time, while the others will be oscillating.

The resulting eigenfunctions are termed linear normal modes. The most unstable modes to linear perturbations are the ones having largest imaginary frequency components and the idea is that these should come to dominate the perturbation flow in the absence of dissipation and nonlinearities One of the basic hypotheses in this approach is that the anomaly spatial structures can be deduced from the normal modes even if the eventual amplitudes cannot be.

None of this is particularly new but it has found renewed interest in atmospheric dynamics. The reason for this interest is that to accurately represent atmospheric motions, quite a few spectral modes have to be retained in the first projection and the eigen problem that follows has degree equal to the number of independent spatial components The problem quickly became impossible to handle on any of the older generations of computers Shortcuts exist that can simplify this problem. The most obvious is the use of zonal basic states and barotropic channel evolution equation and this was done as far back as 1949 by Kuo. But now, modern super-computers allow the solution of the problem with ever more complex basic states and ever more realistic equations.

In the last few years, contributors on the subject of linear modes have used full spherical geometry to represent their basic states and either baroclinic (see for example Frederiksen, 1983) or barotropic models (as in Simmons *et al*., 1983, hereafter referred to as SWB). SWB couple linear normal modes with extensive linear and nonlinear time integrations of their model where the resolution, damping and forcing change, thus verifying the normal mode calculations under more general assumptions.

The barotropic calculation, when done using NH winter latitude-longitude-dependent flows as basic states, have shown a strong resemblance between the observed low-frequency winter variance over northern oceans and northern USRR (Wallace and Blackmon, 1983), and the most unstable barotropic normal modes. Blocking episodes do in fact contribute to this range of frequencies and the preferred blocking positions will correspond to centres of high variance in these frequencies. Nonlinear damped integrations of the model produce flows that oscillate about new mean flows not too different from the integration's initial basic state. We are shown synoptic maps of relevant parts of one such oscillation. The flow actually takes on the aspect of an East-Atlantic split flow for some time during this period. Normal mode calculations show that the new mean state remained linearly unstable to barotropic disturbances. But, it is still not clear to what extent the (mature and equivalent barotropic) blocking patterns (in the NH at least) are barotropically unstable or even the result of barotropic instability. Similar calculations for SH winter cases would be interesting.

Frederiksen's approach seems to yield modes that operate on smaller spatial and temporal scales, as would seem appropriate since he considers baroclinic (synoptic) processes. In fact, his older results seem to have more relevance to the high-pass frequency region identified by Blackmon (1976) than on the band-pass or low-pass regions. In any event, he shows that in one case, where the vertical profile of the wind was allowed to be moderately unstable, the NH winter preferred baroclinic normal mode somewhat resembled the composite blocking precursor for unfiltered data found in Dole (1982) for his Pacific composite positive anomaly case. Dole's precursor anomaly centre also exhibits strong westerly tilt with height, consistent with a strong baroclinic traveling wave component. The conclusion would then be that baroclinic instability can trigger blocking episodes and nonlinear (or barotropic) effects would afterward change the preferred scale and positions at which the process occurs

One aspect one has to consider with this type of approach is the dependence of its results on the basic state itself. This apparent problem is discussed in SWB. The regions of maximum instability changes with the basic state and this agrees with the fact that blocks do not always occur in the same location. Some of the preferred instabilities in SWB show a striking resemblance to certain teleconnection patterns presented in Wallace and Gutzler (1981). Depending on the basic wind, the PNA or EA patterns seem to emerge from SWB's results Tropical SST anomalies could, for example, be considered as an excitation source for mid-latitude stationary disturbances occurring in certain preferred locations. This, in turn, could lead to enhanced mid-latitude blocking. The latter mechanism does not, by any means, explain all types of blocks, but it seems reasonable to expect that it may account for some blocking occurrences. Karoly (1983) discusses this possibility. An example of a situation where such external forcing of middle latitude waves seems important is the enhanced ridging over the North-Western North America region found during the 1982/83 ENSO event and the PNA pattern of which it was part (see Rasmusson and Wallace, 1983, on this). Boer (1989) cautions that this kind of simple explanation may be just that, too simple, as the nonlinear terms cannot be disregarded in this context.

One problem in both of these linear instability studies is that the actual spectral resolution and the equations used are still very restrictive. Finally, the approach is still linear and cannot really be expected to give the full answer. Rather, it still has to be considered in conjunction with other (nonlinear) theories.

But even if the linear instability mechanisms were important in blocking situations, as seems probable, this just pushes the problem one step back. One would now have to find which processes set up the unstable basic flow

1 3.5 Resonance

Most blocking theories we have reviewed until now rely on a certain form of resonance, that is, forcing of a (quasi-) stationary Rossby wave by a stationary (or periodic) mechanism such as topographic lifting, oceanic latent heating or transient forcing by a baroclinic zone The time and space scales on which blocking occurs and the mere existence of such stable phenomena in a dissipative, advective and damped system seems to require this general type of mechanism

Observational evidence for the resonance theories can again be found in Dole (1982) and also in Austin (1980) The former mentions the striking phase reversals and amplification for low-pass filtered zonal wavenumbers 1 to 5 corresponding to blocking when comparing climatology and his composite Pacific positive anomaly He also remarks that these "phase relationships ( ) are somewhat reminiscent of the responses seen in simple models when crossing through a resonance"

After several individual case analyses, Austin concludes that blocking can be associated with a sudden amplification of a few zonal wavenumbers displaying constructive interference She concludes that "In the Atlantic sector this reinforcement is either between wavenumbers one and two or between wavenumbers two and three In the Pacific sector this initial reinforcement is between wavenumbers two and three, but this manifests itself as blocking only if wavenumber one is small"

This last conclusion is not supported by Dole's study On the other hand, Austin does not find phase changes in the stationary planetary waves, in her turn contradicting Dole However, both agree on the sudden amplification of planetary scale waves It is probably relevant to note that, in the NH middle latitudes, the main forcing mechanisms have very large amplitude zonal Fourier components at these wavenumbers.

We end this part of our *recent historical* overview of blocking with four studies relating persistent anomalies to different types of resonance, namely those of Egger (1978), Kalnay-Rivas and Merkine (1981), Mitchell and Derome (1983) and Tung and Lindzen (1979a, b).

The mechanism Egger (1978) considers for the production of blocking situations is a resonant triad interaction between two topographically forced waves (having zonal wave numbers 1 and 3) and a stationary Rossby wave (having zonal wave number 2). The models he uses are very low resolution spectral channel models Barotropic and baroclinic versions are studied All of these versions are inviscid and since the forcing is independent of the actual wind field, energy is actually being brought into the system as can indeed be seen from Egger's Fig. 2 This fact and the implied spatial periodicity of the model are the most bothersome aspects of the work. This type of *topographic* forcing means that the same two standing forcings will always be present, with the same constant amplitudes Egger's approach is necessarily global and all but the very largest scale waves are ignored The initial (or background) zonal wind is chosen so as to ensure the desired (triad) interactions.

Egger's study shows that, with the special conditions it allows, blocking-like patterns lasting for something like five to ten days can be produced by all versions of the model that have orography. Allowing for wave-mean flow interactions does not significantly change this. The change one then gets is jet stream splitting, associated with the blocks, produced by momentum transport from the centre toward the channels lateral boundaries. When using a baroclinic two-layer model, the author finds a decreased thermal wind associated with blocking episodes, as one would hope to see in realistic blocks.

The main point made here is that removing the orographic forcing, or forcing only one standing mode, removes the blocks The orographic wave interaction being the only mechanism present here able to force the free wave at the right scale to produce resonance, the result somehow does not surprise us Triad interaction could still be important in distributing energy between modes if more than one such can be made stationary simultaneously (as in Mitchell and Derome, 1983, where the three-dimensional wavenumber controls this) The triad interaction idea has not been picked up by other works Note that the spatial periodicity and inviscid nature of Egger's model are modified in the work of Kalnay-Rivas and Merkine (1981), discussed next

Kalnay-Rivas and Merkine (1981) take pains to ensure a kind of locality to their blocks in agreement with the comment taken from Held (1983) as to localized features in the atmosphere They adopt the viewpoint that the block production is dominated by resonant energy transformations "via wave-induced Reynolds stress fields while baroclinic process ( ) are necessary only as far as" a possible mechanism "triggering the traveling disturbances" (note that this point of view is very similar to that of Shutts, 1983) They have a basic setup producing a steady Rossby lee-wave upon which a positive vorticity pulse is added every three days Their model is nonlinear and barotropic in nature

The blocks arise from (large and steady) lee-waves resonantly responding to traveling disturbances The resulting patterns are somewhat like an Ω-block A certain phase relationship between the pulse source and the mountain (corresponding in fact to the perturbation pressure gradient being in the same direction as the main flow when the disturbances pass over the mountain) has to be satisfied and the pulses themselves have to be strong enough (seemingly ruling out small amplitude instability mechanism). The blocks remain as long as the eddy forcing is active

The authors point out that the pulse source could be another mountain or a baroclinically active region such a the northern oceanic storm tracks (again considered in Shutts, 1983) Nonlinearity is also essential to produce blocking-like structures an integration where the only retained interaction is that of the perturbations with orography does indeed manage to produce a resonant response but this latter did not look at all like a block Note that the production mechanism being upstream of the blocking region could possibly explain such features as very similar local budgets for blocking and non-blocking situations, found by Hartman and Ghan (1980).

The evidence presented for the verification of the theory is of an indirect and qualitative nature, rather than of a quantitative nature. As we have remarked several times already, the theory bears a strong conceptual resemblance to Shutts' theory (1983), but the emphasis, as to the means by which their standing wave come about, is quite different. In the end, it is not clear if this resonant mechanism could produce dipole-like structures similar to the ones found in numerous blocking episodes (as in diffluent jet stream patterns) or even, what observed blocking patterns are explained. For instance, the Pacific blocks are certainly not accounted for, as their geographical setup is not the one the theory requires[4] The same seems true of Atlantic blocks Dole's northern USSR positive anomalies geographical setup may correspond to what Kalnay-Rivas and Merkine's theory describes.

The next work presented in this overview considers a special type of flows, namely, *noninteracting* flows in which the Jacobian of the streamfunction and potential vorticity is zero. This is the same type of condition solved analytically by Flierl *et al.* (1980) in their SES theory. Under these conditions, stationarity is ensured and resonant responses to a potential vorticity source, such as a diabatic heating having the right horizontal and vertical structure, are then made possible. This *noninteraction* condition is not a bad one, as it is what Illari (1984) essentially verifies in a particular blocking situation. Moreover, Illari finds that the implied relationship between the potential vorticity q and streamfunction ψ turns out to be linear, which is exactly what Mitchell and Derome (1983) assumed.

One of the main advantages of such flows is that the growth mechanism for the resonant waves does not imply energy extraction from the mean flow, so that the system can thus stay at resonance, which is not

[4]The *resonant* orography has to be between the eddy-producing region and the block which is obviously not the case here.

necessarily the case in other situations We must consider though the result of Tung and Lindzen (1979b), where significant off-resonant responses are also achieved in a similar type of study The question is then, will the system have enough time to grow before going too far out of resonance? The answer seems to depend on the type of wave that is excited, as we will later see.

Mitchell and Derome (1983) use a three-level inviscid spectral quasi-geostrophic potential vorticity channel model with no flow across the lateral boundaries and $\omega=0$ at the top and bottom of their domain A Newtonian thermal forcing is included, as well as thermal dissipation Choosing a certain zonal initial wind for which the (4,1) and (2,2) waves satisfy the *noninteraction* condition, the flow is shown to be numerically stable when unforced and the desired waves to be the resonant ones when forcing is applied at either only their scale or at a whole range of scales. The equilibrium (steady-state, unforced) flow is also shown to be nearly equivalent barotropic in good agreement with observations and the zonal mean of the zonal wind associated with it has realistic tropospheric amplitudes.

The blocking configurations could not be forced from zero wave amplitudes though, because then an excited free mode dominated the resulting flow It was found that "the configuration under discussion can be forced and maintained by Newtonian heating if the model atmosphere is in some neighborhood of the equilibrium flow configuration at initial time". This theory would tend to explain the maintenance of certain blocking situations in the β-plane geometry rather than their creation This may not be too surprising as the condition on which it lies (*noninteraction*) certainly applies more to mature blocking events than to developing ones.

Would a developing (by some kind of resonance) blocking situation automatically *fall* into some such *noninteraction* flow situation? The answer is that it is not clear why it should As well, the authors only consider thermal forcing, which is in general by no mean sufficient (see Section 5 of Austin (1980) on this subject) A few blocking situations may be explained here, but what is proposed seems more like a particular case than a general solution.

One of these objections is addressed in Derome (1984). There, it is shown that, when the zonal mean of the zonal flow is such that its index of refraction depends only on the vertical coordinate (a condition that once integrated gives us the same *noninteraction* condition as above), topographically excited waves can coexist with some diabatically forced waves without interacting with them

We now discus the work of Tung and Lindzen (1979a, b)[5] These authors relate blocking to the resonant responses of Rossby waves to stationary topographic and/or diabatic forcing and as such their theory is obviously more global than local The first paper presents one of the very few analytical solutions to the atmospheric blocking problem. The simplification making this possible is their choice of uniform zonal basic wind U. The second paper extends TLa's results to more general (vertically sheared basic wind) conditions, so that the treatment cannot be entirely analytical, but must turn to numerical methods The solutions found in TLa are barotropic, but such is not the case in TLb, where the response is rather equivalent barotropic with an $e^{(Z/2)}$ increase in height, with $Z=ln(P_0/P)$.

In both cases (TLa and TLb), the resonant response is linear in time (previous to the imposition of damping, of course). Also, TL investigate the off-resonance responses. It turns out that for the considered damping, if an horizontal wave's frequency is less than 1/(14 days), its actual response to stationary forcing can be 90% of its resonant maximum. Exact stationarity is then not essential, it seems, to get a significant response, but the free wave still has to be nearly stationary. We find in Mitchell and Derome's (1985) Appendix that exact resonance is less and less important, as the zonal wavenumber decreases. So, the larger the scale of the wave, the less important is exact stationarity

[5] Hereafter TLa and TLb.

In fact, TL's strongest responses can be found for a Rossby wave that has zonal wavenumber 1 or 2, no meridional nodes and the fewest possible nodes in the vertical (so that the first external mode seems to be the best candidate). An accompanying lowering of the stratospheric jet maximum, acting so as to reduce the number of vertical nodes in the case of a wavenumber 1 or 2, will then produce a resonant response of that wave for reasonable jet speeds.

While zonal wavenumbers 3, 4 and 5 can be resonantly excited by topographic/diabatic forcing, the responses are much smaller than in the case of zonal wavenumbers 1 and 2 and they are also generally more subject to damping. Furthermore, their resonant responses are confined below the tropospheric mid-latitude jet.

The strong points of this theory are, first, a fairly precise set of criteria determining the possibility of resonant waves and, second, blocking-like amplitudes associated with realistic damping and wind profiles. Its first limitation is the fact that the background zonal wind does not have meridional shear. Another limitation, and this one is shared by numerous blocking studies, is the fact that self-interactions and/or nonlinear interactions are not included. Thus, the effect of the growing wave on the basic flow, on itself or on any other waves is disregarded from the very start and the maintenance of blocks cannot be accounted for.

Mitchell and Derome (1985) and Dionne *et al.* (1988) extend TL's work by taking into account horizontal shear of the zonal wind, wave-mean flow and wave-wave nonlinear interactions. Both these studies use the same model and nearly identical setups. They restrict themselves to topographic forcing. As the maximum topographic component in zonal wavenumber domain is in zonal wavenumber 2 and since TL show that the stratospheric jet speeds are the important ones to consider for these wavenumbers, the background (or initial) zonal mean of the zonal wind will consist of a stratospheric jet only. There is no tropospheric jet in these experiments. From TLa and TLb, it is clear that the authors are now interested in major blocking episodes only, at least in terms of strength.

The theory they present manages to account for the initial growth of a free Rossby wave by resonant response to topographic forcing. The effect of the β-plane geometry still has to be evaluated by going to spherical geometry and, as of now, the theory's practical verification has come mainly from the fact that the predicted total growth rate agrees with observations and the attainable blocking sizes are of the same order as what we expect from blocks On the other hand, Dole's onset compositing does not display amplification of unique zonal wavenumbers as is the case here, but rather a whole range of waves seem to amplify simultaneously As well, the topography does not produce forcing at a single zonal wavenumber as is also done here

1.4 Baroclinic wave/Planetary wave interactions

A last theory attempts to explain either the onset or the maintenance of blocking events of the split stream variety, against advection by the mean flow and dissipation. The actual mechanism by which it proposes to do this, as in Shutts (1983), is a resonant one inasmuch as the (planetary-scale) perturbations and their (baroclinic wave induced) forcings are stationary and of the same scales. Several authors have since considered the same type of interactions, generally building upon Shutts' work.

Green (1977) first proposed that momentum forcing by baroclinic eddies could have maintained the 1976 summer block over Northern Europe against dissipation. In support of this idea it should be recognized that although the transient eddy vorticity flux terms are not the globally dominant ones in the time-mean vorticity budget, they cannot be neglected in certain regions where they can indeed be very important. This is especially true over and around the baroclinically active storm track regions, where they are of the same order, although slightly smaller, than the dominant linear advection terms (see Mullen, 1985, for vorticity budgets of GCM blocking events or Dugas and Derome, 1986, for a January 1979 FGGE vorticity budget). In fact, it now seems that during blocking events these transient eddy terms could locally balance the advections of relative vorticity by the mean flow (that tends to push the block downstream) and of planetary vorticity by the meridional perturbation wind (from Mullen, 1987). Green's calculations of the transient momentum flux around the block showed that it was strong enough to produce the observed mean blocking vorticity in about four days. Finally, it has long been recognized that the major oceanic winter blocks have climatological positions just downstream of the major storm tracks.

One essential [illegible] tween the maximum eddy forcing [illegible] relationship [illegible] stationary disturbance [illegible] (1980) shows [illegible] having its maximum a quarter of a wavelength upstream of the standing wave (so that the forcing and block are in quadrature) would, if applied at the level of the tropopause, produce vertical structures similar to those found in blocks. The diagnostic study of Illari (1984) on the July 1976 block would tend to support this phase relationship The disturbances themselves would consist of warm highs below cold highs or cold lows below warm lows. The tropopause level is chosen because it is one where the transient momentum flux is known to be maximum in certain blocking events, as can be seen in Oort (1983), for the January 1963 case.

The blocks (or stationary patterns) are here regions outside of which one finds a split jet stream The two north-south oriented regions of eddies traveling on the two branches of the jet would then enhance the positive and negative vorticity patterns found inside the stationary blocks by momentum transports towards them, the anti-cyclonic vorticity pattern being poleward of the cyclonic one, in accordance with observations of split-stream blocking events. A necessary resonance condition is that the north-south oriented dipole disturbance be in fact stationary with respect to the mean flow

Shutts (1983) extends Austin's work with a series of time-dependent linear and nonlinear integrations of a channel equivalent barotropic model. Furthermore, he relates the baroclinic eddy forcing mechanism to energy transfers that can be found in the case of smaller eddies embedded in a larger (two-dimensional and quasi-geostrophic) flow, when the latter acts as a deformation field on the former The eddies "are, on average, strained into filaments so that the constraints of energy and enstrophy conservation demand that energy should appear at progressively lower wavenumbers (Fjortoft, 1953)" The energy necessary to hold the block steady against advection and dissipation could then come from such a straining process Diagnostic studies such as Berggren *et al.* (1949) and Rex (1950a), with his shock front found just upstream of blocks, support the idea that such deformation processes play an important dynamical role in blocking situations.

A fundamental aspect of this work, as proposed by Green (1977), is that the "time-averaged blocking flow field does not satisfy the equations of motion in itself - in other words, blocking is essentially an unsteady phenomenon" It is achieved by a periodic eddy forcing on a scale close to that of a certain stationary Rossby wave and the total flow is quite variable in time. The model results of Shutts (1983) verify this quite well This tenet has to be compared with the fundamentally stationary solutions of McWilliams and the apparent difficulties this latter had in verifying his theories with observed flows, at least in the NH Note also that, as in Kalnay-Rivas and Merkine (1981), perturbations that are too weak do not produce blocking patterns

As was previously mentioned, the numerical experiments with a two-layer truncated model, presented in Reinhold and Pierrehumbert (1982), also support the synoptic-planetary wave interaction theory There, removing this kind of interaction essentially prevented the regime transitions that otherwise occur, transitions that can be associated with the flow going in and out of blocking regimes.

It is very interesting to note that a recent paper by Haines and Marshall (1987) ties both the modon and transient eddy forcing theories together. They show that the same type of forcing as is considered by Shutts can as well maintain a modon-like structure for extended periods of time Their equivalent-barotropic model is very similar to that of Shutts (1983) and they also consider linear and nonlinear integrations At the same time, Malanotte-Rizzoli and Malguzzi (1987) extend the results of MMR[6] by considering, again, the eddy transient forcing of their blocking-like solutions in a low-order baroclinic model They report that "(···) the interaction of our highly nonlinear dipole solution with traveling synoptic scale systems is very similar to what was found by Shutts (1983) ( )" Finally, both of these studies give some indications as to how their respective theories could be investigated in actual observations

[6] See section 1 3.2 for details

A feature of observed blocks that Shutts' equivalent barotropic theory cannot explain is their relative warmth. Also, in view of Tung and Rosenthal's (1985) comments on the derivation of the equivalent barotropic equation and the forcings that can be included in it, the reliance of this theory on a wavemaker is a bothersome feature, as it is in Kalnay-Rivas and Merkine (1981) However, the strongest point about Shutts's theory is the degree to which it has recently been supported by observational studies.

Mullen (1985, 1987) in a diagnostic study of long series of GCM (specifically, NCAR's CCM) and NMC data shows that the quadrature relationship Shutts requires between eddy vorticity forcing and blocking anomaly maximum can be verified, at least for NH flows, in both types of data. The eddy forcing is specifically found for high pass filtered data, *i.e* , the eddy forcing is essentially produced by synoptic features, as in Shutts' model. The quadrature relationship does not necessarily hold for unfiltered or low pass data, so that Dole (1982) was unable to identify it. Mullen states that "During blocking episodes (···) eddy vorticity forcing tends to cause the block to retrograde" adding to the retrograde action of advection of planetary vorticity to balance advection of relative perturbation vorticity by the mean flow. He also shows that eddy heat forcing acts to dissipate the blocking pattern temperature anomaly The mechanism mostly responsible for the maintenance of this temperature anomaly seems to be advection of time-mean temperature by the time-mean flow.

A last set of conclusions one can find in Mullen (1987) is that it appears that "barotropic processes associated with deformation of the transient eddies are predominantly responsible for the eddy forcing of the upper level circulation". Indeed, the 30 kPa and 100 kPa eddy vorticity forcing seem to be highly correlated, displaying an equivalent barotropic nature, with a maximum in the higher troposphere. This barotropic feature dominates the total eddy forcing in the block's vicinity.

1.5 Concluding remarks

To summarize what has just been discussed in this chapter, the most promising theory seems to be a resonant response theory of planetary scale free Rossby waves with respect to a specific forcing mechanism, namely that of the synoptic scale eddies. It should be noted though, that from Dole's and Reinhold and Pierrehumbert's persistence analysis of either observed circulation anomalies or of simulated regimes, we can already expect more than one mechanism to be responsible for different periods in the lifetime of blocks.

Although the theory presentation and verification have so far made use of NH conditions, there does not seem to be any reason why it could not be applied to the SH. Indeed, the SH main blocking position (the area south of New Zealand) is again downstream of the major hemispheric storm track (over the southern Indian Ocean). An important aspect here is that the blocking events are intrinsically considered to be transient phenomena, more easily identified in time-mean maps than in instantaneous flows. A first verification of the theory has been attempted by Mullen (1987), with model and observational data. The theory cannot yet explain the relative warmth of blocks and this proves to be one of its few important weaknesses.

Some of the other theories also turn out to be interesting even though not quite as well documented or promising as the two previous ones. For example, linear normal mode analysis does seem to present us with the baroclinic type of precursor state alluded to in Dole's work. It also gives us indications of what happens in the mature barotropic phase of the phenomenon. The actual resolutions and models used here are still coarse (because of the very heavy resource requirements implied by its use). As well, the method is linear by definition, and one wonders if its application to more complex models would not drown out the significant information that has been found to date.

The theories presented by Kalnay-Rivas and Merkine (1981) and Mitchell and Derome (1983) do not seem general in their application, in the sense that the first considers a Rossby lee-wave resonance (that we cannot see applied anywhere except maybe the Russian blocks), while the second limits the resonant forcing to diabatic mechanisms. Topographically excited waves can coexist with the diabatically forced waves, as Derome (1984) mentions. Would this theory explain the warm structure of blocks? It also has not been verified, except to the extent that the particular kind of flow it requires do effectively occur in conjunction with blocking events.

As for the the modon theory, its main and glaring weakness is exactly what makes it possible, that is, the (forced) stationary nature of the solution. This may be what caused McWilliams problems in verifying it and the theory should be compared to the transient blocking theory of Shutts. There exist, though, a simple verification for modon-like behavior, as can be seen in Haines and Marshall (1987). That is, the (q,ψ) scatter plots should display two distinct linear relationships, one applying to the inner modon region and the other to the outer one.

The multiple equilibria theory has been under serious attack (from Tung and Rosenthal, for example). Reinhold and Pierrehumbert's work in analyzing and reproducing regime transitions in this framework, is one of the high points of the theory. But the poor results of Ceheleski and Tung (1987), when the low spectral (or modal) resolution used by RP is increased, is quite bothersome. The low resolution seems to have been what permitted the (clear) results of Reinhold and Pierrehumbert. As of now, such results as those of Gravel (1989), where periodic rather than stationary solutions are addressed, remain the most promising. But even then, this kind of analysis on observation or GCM data may prove impossible, the number of possible unambiguous regimes not being necessarily small (or limited at all).

Tung and Lindzen's resonance as well as Mitchell and Derome's (1983) diabatic maintenance mechanisms could perhaps be tested in a GCM A linear version of the latter could also be used to find the model's (linear) normal modes, possibly using an approach of the kind SWB used.

The model basic states would then be the precursors of the initiation and/or demise of blocks

Finally, Malanotte-Rizzoli and Malguzzi (1987) also propose a necessary condition for the presence of a blocking-like, finite amplitude version of their previously discussed asymptotic solution. This criterion stipulates that a particular (specified) function of the background flow must have the form of a potential well

Chapter 2
Anomaly climatology: Distributions

2.1 Introduction

This chapter deals with an evaluation of persistent circulation anomalies in a GCM, namely the Canadian Climate Centre (CCC) GCM, and in atmospheric data. A climatology of the 50 kPa events in terms of position and time of year is presented in what follows.

2.1.1 Model

A complete description of the model and its climatology, as described by a few standard fields, can be found in the two articles by Boer *et al.* (1984a, b) Briefly, the model is a 10 sigma vertical level, spectral primitive equation model. It has mainly been run at a triangular T20 horizontal resolution although T30 and T40 extended runs have been made. Most runs (including the one used here) also include daily and annual cycles in solar radiation and a daily cycle in long-wave radiation. The physical parameterization includes gravity wave drag (as described in McFarlane, 1987), surface hydrology and energy budgets as well as a Leith-type of (scale-dependent) horizontal dissipation. The model climatology has been found to be quite reasonable both in the winter and summer Hemispheres throughout the year, most of the well known climatological features of the atmosphere being rather well reproduced.

Climate models are run at relatively low resolutions when compared to that used in medium range weather predictions such as the T106 version of the ECMWF spectral forecast model. The effect of truncation on the quality of the simulation are beginning to be known[7] with respect to the very few high resolution models. Whether these effects are found to be generic to the whole class of climate models remains to be seen. However, these potential problems will have to be taken into consideration in any use of simulation data from the as of yet normal "low" reso-

[7]As an example, see Jarraud's contribution to the March 1986 ECMWF seminar.

lution[8] models. In the meantime, hardware and funding restrictions will ensure continued use of the latter type of model in climate studies.

2.1.2 Observations

Quite a few studies have been made on persistent anomalies in the atmosphere, nearly all of them proposing their own *new* set of criteria to define anomalies. Rex' (1950a, b) work, however, could be regarded as the archetype of the whole class and as such, it is still instructive to quickly review the approach he used. His work is concerned with the 50 kPa Northern Hemisphere (NH) winter geopotential height patterns called blocks (or positive circulation anomalies). The approach is entirely subjective and the criteria he used to identify blocking are the following:

1) The basic westerly flow is *split*[9] into two branches,
2) Each current branch must transport an *appreciable mass*,
3) This *double jet* system must extend over *at least 45 degrees* of longitude,
4) A *sharp transition* from zonal type flow upstream to meridional type downstream must be observed across the current split,

and finally,

5) The pattern must persist with recognizable continuity for *at least ten days*.

The words in italics refer to the subjective aspects of the criteria, the parts that to a certain extent characterize the winter oceanic patterns in which Rex was interested. This choice of criteria may not be adequate to study patterns occurring elsewhere or at other times. Furthermore, using this type of method on a very long data set quickly becomes prohibitive as it can hardly be implemented on a present day computer due to its subjective aspects.

Recent studies tend to be more objective in their specification of

---

[8] R15 NCAR CCM and GFDL GCM, T20 CCC GCM

[9] The italics are added by this author

what constitutes a persistent event, but most of them still retain some preferred time-and-space scales (as in parts three and five of the Rex set). Two examples of these are found in Dole[10] (1982) and Lejenas and Økland (1983). Recent comparisons of these two criteria by Lejenås (1987), using Southern Hemisphere FGGE and Australian data sets, seem to indicate that the former is less sensitive to the quality of the data as well as being less restrictive as to the type of events it identifies. The Rex-type of events are in fact a sub-class of the new ensembles of events.

A supplementary type of criterion of interest when considering more general methods of identifying persistent events is the locality one, an example of which is that the ***events end*** *if they move by more than 10 degrees in 12 hours* ***or*** *if their total movement is more than 30 degrees*, from Hartman and Ghan (1980). This (angular) migration criterion corresponds to the known feature that very few, if any, atmospheric patterns remain absolutely fixed geographically for any extended time period but, at the same time, they tend to remain in limited areas.

Indeed, the fixed type of patterns appear to be quite exceptional[11], whereas the moderately persistent patterns we want to study do not seem to be so rare at all . In fact, using a looser five-day duration requirement, Treidl *et al.* (1981) find that over half of the NH winter days are blocked at one place or another Using a locality criterion, defined in terms of angular instead of cartesian distances, could favor lower latitude events over the more poleward events since the former are then permitted greater spatial deviations from their centre of definition. However, as we shall see, the preferred anomaly positions occur in a fairly small latitude belt so that this bias may be safely disregarded.

To a certain extent, Dole (1982) manages to take into account the

---

[10] Some of this material has been published either in Dole and Gordon (1983) or in Dole (1986).

[11] A maximum of 10 positive events, lasting at least 10 days, at the 100 gpm level in the North-Atlantic winter, from Dole's work with 14 years of 50 kPa NMC data.

locality of the events. Indeed, Dole filters out the shortest time-scale fluctuations (periods smaller than one to two days) from the observations before applying his criterion What arises from this is that a few cases, where rapidly moving synoptic events mask and/or interrupt larger- and longer-scale events, can be identified As well, there are persistent events for which this masking or interrupting is done by locally shifting their centre This technique, however, is by no means sufficient, as will be shown later, since most "non-stationary" events are still disregarded by it.

2.1.3 Criteria used in the present study

We use Dole's (1982) objective criteria, modified to take into account the possibility that the events move about their geographical centres Thus, *an* ***anomnaly event*** *is identified at a geographical position* $\vec{X}$ *if, for a given duration time* $\boldsymbol{T}$, *the field under observation is continuously larger than a certain value* $\boldsymbol{M}$ *at any point within 8 (latitude or longitude) degrees of* $\vec{X}$. This latter value is arbitrary and is chosen because it is the approximate separation between grid points in the smallest gaussian grid onto which a T20 spectral field can be projected without linear aliasing Therefore, from a practical point of view, only the four immediately adjoining grid points are considered when applying the locality part of the criteria at a certain geographical point, in addition to the point itself Only quasi-stationary events are likely to be captured by this criterion, even though it is conceivable that a series of waves travelling at the right (relatively high) speed could also (but wrongly) be retained as an event An indication that only large-scale (and thus slowly moving) features are identified here, is that most cases found to satisfy the full set of criteria eventually do satisfy the amplitude part of it at every adjoining position around their centre, at one moment or another of their lifetime. We will discuss the main cases for which this is not verified, such as the Atlantic negative anomalies

2.1.4 Data sets and anomaly criterion values

The model data used in this section of the study are the 50 kPa rotational streamfunction ψ from a 20-year T20 simulation. The data are available at 18 simulated-hour intervals, for a total of 9732 different time values.

Various combinations of amplitude M and duration T values were tested in the preliminary stages of this work. The objective was to unambiguously eliminate synoptic scale events from the set of persistent anomalies and, at the same time, retain a sufficiently large number of events so as to get stable statistics from this set. It was found that the qualitative nature of the spatial distributions of positive and negative anomalies is maintained over a fairly wide range of possible values. The values retained are representative of this range and will also permit comparisons with certain other recent works[12] The same values are used in both the Southern and Northern Hemispheres Thus, M is set to 1.0×10^7 m^2/s. From geostrophy, this is roughly equivalent to 100 gpm at 45^0 latitude. The duration T that is used is nine days (that is, twelve model sampling intervals).

The time mean and the seasonal cycle[13] are removed from ψ before applying the criteria. The reasoning behind this step is, firstly, that the anomaly events under study are *a priori* supposed not to be directly related to the variations in solar radiation and, secondly, that we want to be able to compare events throughout the years or at least throughout seasons. Indications of the independence of the annual cycle signal from the rest of the time spectrum are presented in the next section.

The observational data used for comparisons are either a 14-year (1965-78) NMC NH or a five-year (1980-84) global ECMWF data sets. The observed variable is the 50 kPa geopotential height. However, this is

[12] Again, mainly Dole (1982) but also Trenberth and Mo (1985) are considered.

[13] Unless otherwise specified, this is defined as the annual cycle plus its first five harmonics.

generally transformed to the geostrophic streamfunction ψ_g, following the comment by Hoskins *et al.* (1977) as to the appropriateness of this variable when studying two-dimensional energy propagations and/or interactions between tropical and extra-tropical regions. When dealing with statistics derived from yearly data, the ECMWF data will be preferred to the NMC, at least in the current chapter. The reason for this is that the former are global, more recent than the latter, and we expect them to be of generally higher quality. On the other hand, when dealing with statistics derived from seasonal data, the relatively smaller ECMWF sample seems to become problematic[14] and the longer NMC sample will be preferred.

Throughout this thesis it should be noted that we will use the term "anomalies" to describe both the upper-air events satisfying our criterion, but also to distinguish between the complete data sets and those from which the time-mean and seasonal cycle components have been removed, *i.e.* anomalies. Whether the word "anomalies" refers to the events or to deviations from the climatic averages will depend upon the context.

---

[14] Problems with noisy statistics.

2.2 Anomalies in the frequency domain

2.2.1 Anomalies in the frequency domain: Northern Hemisphere overview

A known problem in GCM simulations is their low level of transient activity[15]. Note that, at least in the NH, this effect is one of those presently ascribed, to a certain extent, to resolution deficiencies. What is not as well known is how this feature is distributed in the frequency domain Is this deficiency more important in the high[16] frequencies or the low[17] frequencies? Is there a relative difference in the importance of the frequency range mainly concerned with persistent anomalies, the medium frequencies, with respect to the other ranges? One would hope that the distributions of such quantities as the anomaly kinetic energy are, if not quantitatively, at least qualitatively similar in the models and the observations.

It should be noted here that the low- and medium-frequency ranges adopted here correspond to what Blackmon (1976) calls "low-pass data". The high frequencies are made up of Blackmon's (1976) band-pass and high-pass data. Our frequency breakdown is closer to the one used in Blackmon *et al* (1984), i.e. low, intermediate and high frequencies. Please also note that no use is made here of the Blackmon-type of digital filters. Rather, the time filtering is done by directly operating on the timewise spectral components representation of the data sets, obtained via FFTs at each spatial grid points.

Pratt (1979) presents ratios of simulated to observed geopotential height variances for a range of zonal wavenumber/frequency values. The simulation data are from earlier versions of the NCAR and GFDL GCMs (his Figures 3a and 3b) We already know these ratios to be generally less than unity. For our purpose, the question of qualitatively similar behavior translates here into whether the ratios are independent of fre-

---

[15] See Jarraud (1986) as noted earlier, Lambert (1987) on inter-comparisons of model and observation energy budgets; Tribbia and Baumhefner (1987) on the CCM model predictability

[16] Mainly baroclinic waves, with periods shorter than a week

[17] Mainly planetary waves, with periods longer than a month

quency. Both models unfortunately turn out to be significantly better behaved in the synoptic range of values than at other ranges. For example, the zonal wavenumber seven results for the NCAR model range from a ratio of 20% at low frequency to better than 80% at synoptic frequencies and back again to 20% at the highest frequencies available in the simulation

TABLE 1

Comparative kinetic energy of the CCC rotational V^* and NMC, ECMWF geostrophic components in a Northern Hemisphere 50 kPa zonal channel from 25^0N to 55^0N The percentages quoted under the ECMWF and NMC columns are calculated with respect to the corresponding CCC results. The high frequencies correspond to periods shorter than a week, the medium frequencies to periods between a week and a month and finally, the low frequencies to periods longer than one month, excluding the seasonal cycle Then, Box(1) = Box(2+4+5) and Box(5) Box(6+7+8)

(m^2/s^2)		CCC (20 years)	NMC (1965-79)	ECMWF (1980-84)
Total KE	1	152.22	200.32 (131%)	191.57 (126%)
KE Time Mean	2	79.40	89.26 (112%)	87.53 (110%)
Yearly cycle	3	17.17	16.74 (98%)	17.68 (103%)
Tot Seasonal	4	19.63	19.20 (98%)	22.06 (112%)
Total Anomaly	5	53.19	91.86 (173%)	81.98 (154%)
Low Frequency	6	14.13	25.54 (181%)	21.21 (150%)
Med Frequency	7	20.70	36.88 (178%)	33.26 (161%)
High Freq.	8	18.38	29.43 (160%)	27.[illegible] (150%)

This change with frequency band is not found in the CCC model, at least in the NH as can be seen from Table 1, containing a breakdown of NH mid-latitude channel rotational kinetic energy. Comparing NMC or ECMWF analyses to a CCC simulation, we find qualitative agreement in their anomaly energy. The overall NMC and ECMWF anomalies are respectively 73% and 54% more active than the CCC model anomalies, but these proportions are roughly the same in all three frequency ranges considered. What this means is that the nature of anomalous events may be sim ilar in the model and the observations but their number and/or their strength will be smaller in the GCM. A surprising aspect of this NH kinetic energy breakdown is that the seasonal cycle signal is very well reproduced in the model data. To a lesser degree, the time-mean values are also well reproduced by the GCM.

2.2.2 Southern Hemisphere overview

Turning to the Southern Hemisphere statistics found in Table 2, the picture is not as clear. The total and total anomaly kinetic energies are both about 30% greater in the ECMWF data set than in the GCM simulation. These proportions turn out to be, respectively, the same as for the NH total and slightly better than what holds for the NH total anomalies. The annual cycle contribution is only a small part of the total SH kinetic energy in both SH data sets This is a marked contrast to what was found in the NH. It apparently has to do with the relative absence of land-sea contrast in this SH latitude band, with respect to what is found in the NH channel used for Table 1. The higher harmonics of the SH annual signal are appreciably stronger in the atmosphere but they are still negligible with respect to the other components of the spectrum.

The partitioning of the total SH anomaly energy in terms of low-, medium- and high-frequency bands does not yield the same qualitative results as for the NH The lack of anomaly energy in the GCM simulation, while generally smaller than in the NH, is not as uniform as what was found there. The lower the frequency, the greater the lack (or difference) Whereas the high and medium frequencies are about as important in the analysis, the former are 25% stronger than the latter in the simulation.

2.2.3 Overview conclusion

What is to be expected from these differences? First of all, a smaller number of anomalous events (*i.e.* those satisfying our anomaly criterion) and/or smaller events, both in the NH and SH. Secondly, an even greater importance of the locality aspect of the criterion in the

TABLE 2.

Comparative kinetic energy of the CCC rotational V and ECMWF geostrophic components in a Southern Hemisphere 50 kPa zonal channel from 25°S to 55°S. The percentages quoted under the ECMWF column are calculated with respect to the corresponding CCC results. The designation of the different boxes are the same as in Table 1.

(m^2/s^2)	CCC (20 years)	ECMWF (1980-84)
Total KE	1 218.16	284.48 (130%)
KE Time Mean	2 134.58	171.22 (127%)
Yearly cycle	3 1.33	2.28 (172%)
Tot Seasonal	4 1.75	4.88 (280%)
Total Anomaly	5 81.48	108.70 (133%)
Low Frequency	6 13.04	19.79 (152%)
Med Frequency	7 30.42	43.81 (144%)
High Freq.	8 38.02	45.10 (118%)

SH with respect to the NH, due to the relatively greater importance of the high frequencies in the GCM SH. It should finally be noted that there seems to be a better overall quantitative agreement between analysis and simulation in the SH than in the NH, even though the qualitative agreement is better in the NH. While NH analyses are generally accepted to be of high quality, the same certainly could not be said, up to very recently, of the SH analyses, mainly due to the sparseness of the observation network. To what extent the discrepancies between simulation and analysis data, noted in the preceding paragraphs, can be traced back to this feature is not at all clear.

2.2.4 Seasonal cycle

Let us come back to the seasonal cycle and the fact that, from Table 1, its amplitude is quite well reproduced in the model SH. This different statistical behavior for the two types of signal, the anomaly and the seasonal cycle components, is a first indication that they can probably be considered separately. Another more substantial indication of this can be found by considering the loading vectors of the principal components[18] (PC) of the covariance matrix constructed from the model total ψ NH transients (not shown) We notice that, poleward of 30^0N, the square of the first loading vector (first in terms of explained variance) is essentially identical to the variance of the model ψ seasonal cycle[19] (Fig 1a) The model seasonal cycle components thus seem to be uncorrelated with the rest of the spectrum. It should also be stressed that, due to the relatively greater importance of the seasonal cycle in the NH model data compared to what is obtained in the observations, filtering it out completely is even more important in the first type of data. All this does not mean that the seasonal cycle is independent of the rest the spectrum. Indeed, we will shortly find an increased anomaly activity towards mid-winter and a subsequent decrease towards mid-summer, so that an indirect seasonal cycle is still manifest.

The horizontal structure of the transients' frequency distribution in terms of the seasonal cycle, the low, medium and high frequencies is discussed next in greater detail. We compare the variances of the GCM streamfunction, ψ, and the ECMWF geostrophic streamfunction, ψ_g. The latter field is set to zero within 20 degrees of the equator, the geostrophic approximation being inappropriate at those latitudes.

2.2.5 Horizontal distributions, A: NH seasonal cycle

Figure 1b displays the seasonal cycle variance of the NH ψ_g The CCC and ECMWF functions are very similar as to amplitudes and spatial patterns. Pronounced maxima are found over the mid-latitude eastern coasts of the major land masses, but these are closer to the pole in the simulation, by 10 degrees in the Pacific and even more over North America. The minimum found over the Northeastern-Atlantic/Western-Europe region is more pronounced in the CCC simulation while the reverse holds

[18] See Appendix A for a presentation of the EOF/PC techniques used (mainly) in the next chapter.

[19] Note that half the variance explained by the EOF/PC(1) component pair when replacing ψ by the rotational wind vector $\vec{V}$ is again identical to the seasonal cycle kinetic energy.

over the North American west-coast. These seasonal cycle maxima and minima are obviously related to the differing land-sea temperature gradients found at their respective positions. The same applies to the third maximum found over (or near) the area of the Mediterranean and Caspian seas. Perhaps due to resolution problems, this feature is somewhat washed out in the simulation, although it is still quite clearly present. Consider that the land-sea mask used in the GCM simulation represents the Mediterranean by a total of only twelve grid points while the Black and Caspian seas rate two grids points each. It is thus not unduly surprising that such relatively small local differences as the ECMWF double maximum in that area do not get captured by the model.

The model's sea surface temperature (SST) is specified and is essentially made up of a crude annual cycle. This does not seem to be too bad an approximation at the planetary scale we now investigate. When the phase of the modelled annual cycle signal is considered (not shown), we find that it is such as to promote the deepest eastern continental troughs at approximatively the end of February. There is surprisingly little variations in these phases north of 30^0N. Values for the dates of the negative extremum essentially range from mid-February to mid-March. This places the seasonal cycle nearly in phase with the SST. The annual cycles found in continental areas such Siberia and the American Great Plains precedes that of oceanic areas but then only very slightly, that is by less than 20 days.

Overall, the agreement between the simulated and observed 50 kPa variances on the seasonal time scale is quite good, as was to be expected from Table 1.

2.2.6 Horizontal distributions, B: NH anomalies

We have seen from Tables 1 and 2 that the agreement between the simulation and observations is not as good for the anomalies. What are exactly these discrepancies? Parts a and b of Figures [illegible] 3 and 4 display the low-, medium- and high-frequency NH [illegible] and [illegible] variances for the CCC simulation and ECMWF analyses, respectively. Similar figures derived from other observation data can be found in Blackmon *et al.* (1984), for example[20].

The main qualitative difference between our two sets of variance is that, as we consider lower-frequency ranges, the main model patterns tend to split into latitudinal dipoles, whereas the observations display monopole patterns at all frequencies. This difference is greatest over the North-Atlantic, to the extent that, in the low-frequency range, the absolute maximum of the model variance now appears over Greenland, Fig. 2a, whereas the observed absolute maximum is in the Pacific, Fig. 2b. The North-Pacific region suffers from this dipole problem only for the lowest frequencies The observations do have local maxima northward of their main oceanic patterns, but the intensities of the former is negligible compared to that of the latter

Another difference is that the Northern Soviet Union maximum found in the analysis (and only) in the low-frequency range is not as clearly defined in the model data. This latter position is the third preferred NH winter (NHW) observed anomaly position as determined by Dole (1982). The two other NHW anomaly positions can be very clearly identified in the simulation low and medium frequencies.

In light of the transient high-frequency resonance theory discussed in the first chapter, it is of some importance to note that the relation between the two high-frequency storm tracks and the medium- and low-frequency oceanic patterns is qualitatively the same in both kinds of data. The lower frequency patterns are found downstream of the higher frequency centres Any possible causative link between these frequency ranges is likely to be the same in the simulation and the observations.

In the high-frequency range, the Pacific storm track seems to be relatively well simulated by the model, Fig. 4a, both in terms of position and amplitudes. The Atlantic storm track is well positioned but

[20]Same frequency ranges but for the winter geopotential heights standard deviations.

its amplitude is only 50% of its observed counterpart, Fig. 4b. At the same time, it is only 2/3 as active as its Pacific counterpart, whereas both storm tracks are about as strong in the observations. Also, it appears to possess an extension towards Spitsbergen, along Greenland, not found in the observations. The Atlantic type of persistent anomalies has been most often presented, both by theoreticians and data analysts, as a possible example of events either forced or maintained by interactions with high-frequency transients.[21] Thus, this mechanism would be noticeably weakened in the model and, if present, it could possibly operate at more northerly latitudes. When comparing with other similar observation or simulation[22] analyses, we should keep in mind that most authors, including those previously cited, consider the winter season data exclusively. While this is not the case here, the patterns and values we find are generally quite similar.[23]

In the medium-frequency range, the model Pacific pattern, Fig. 3a, is 30 degrees upstream of the observation pattern, Fig. 3b. The model Pacific persistent anomalies are thus expected to be closer to the date-line than the observed ones. Also, due to the dipole structure found over the model Atlantic, its preferred persistent anomaly position in that sector is also expected to be split in two. In contrast to the high-frequency anomalies, the model medium range ψ variances in the Pacific and Atlantic are of comparable magnitude.

It is in the low-frequency range that the Pacific and Atlantic model dipoles are the clearest. The southern sections of these patterns are found at slightly lower latitudes than the observation patterns, and their northern parts, 20 degrees poleward of that. The model Atlantic patterns are now stronger than their Pacific counterparts. Note that this is not the case in the observations. Thus, we should not be too surprised to find more model persistent events over the Atlantic than over the Pacific Ocean.

---

[21] See chapter 1 for more details.

[22] As, Lau (1981) on a 15 years GFDL simulation.

[23] Lau's results, after translation to ψ variances, show Pacific and Atlantic high frequency maxima of [illegible] and [illegible], respectively.

We now conclude this section. The model seems to display a greater number of NH centres of action than the atmosphere. The reason for this may have to be investigated[24]. The atmosphere's centres of action are all present in the model, including the NSU centre, although to a lesser extent, but their relative importance is not quite the same as in the observations An intriguing result is the difference between the Atlantic and Pacific model values The Pacific is more active at the synoptic time scale, while the Atlantic dominates the longer time scales. This is not verified in the ECMWF observations, where the Pacific is at least as active as the Atlantic, at all time scales.

2.2.7 Horizontal distributions, C: SH anomalies

In view of their weakness, the model and the atmosphere's SH seasonal cycle are not discussed in any great detail. It is sufficient to mention that the only location where both are relatively important is over the Antarctic, where they represent about 30% of the total model transients and over 50% of the atmospheric transients. Everywhere else, this percentage is much less. Maybe due to the shorter sample available, the ECMWF streamfunction variance is not as smooth at this time scale as the model's.

Again, parts a and b of Figures 5, 6 and 7 display the low-, medium- and high-frequency SH ψ and ψ_g variances for the CCC simulation and ECMWF analyses, respectively.

The model and observation variances display qualitatively similar distributions at all time scales. The relative importance of maxima and their positions at different frequencies are well reproduced in the model In fact, the agreement seems better than what is found in the NH, inasmuch as the simulation's centres of activity closely resemble the atmosphere's centres. The Antarctic is a region of minimum activity. The SH important centres are located equatorward of this continent

[24] For example, could the Greenland centre be in some way related to the apparent northward extension of the Atlantic storm track?

but generaly poleward of 40^0S.

The biggest difference appearing at long time scales is in the South-Pacific, downstream of New Zealand The main model pattern at low frequencies is located closer to South-America as well as poleward of the corresponding observations At medium frequencies, the observed split between the South-American and New Zealand maxima is not as clear in the simulation Still, New Zealand itself appears to be important in both types of data as it marks the beginning of the South-Pacific maxima. This may again be related to the extensive high-frequency storm track that is to be found in the longitudinally elongated region centred at 45^0S over the Indian Ocean. This storm track *ends* just upstream of New Zealand We are indeed reminded of the similar situation noted in the NH where low-frequency maxima *follow* the high-frequency

Another difference is that the observation's maxima are sharper than the model's. For example, the high-frequency maximum is 50% stronger in the atmosphere. But we already know, from Table 2, that the gross atmospheric and model anomaly statistics compare best at this time scale A closer look at Figs 7a and 7b reveals that the difference is mainly confined to the immediate vicinity of the maximum The background activity over which the Indian Ocean maximum pattern is superimposed is quite similar in the CCC and ECMWF data sets and is by no means negligible The channel average values from 30^0S to 60^0S would then again be comparable

The preceding comment on the importance of the high-frequency SH background activity holds at all time scales considered here This is the single most important difference between the SH and NH results, where no such background activity can be found This may very well be explained by an anchoring effect of the topographic forcing[22] and/or land-sea contrasts, both mechanisms being much more important in the NH than in the SH Lower frequency activity cannot be said to be confined to certain particular SH longitudes, which is the case in the NH There

---

[22]See Held (1983) for a discussion of this idea in a NH context

are admittedly certain preferred longitudinal positions, but these are by no means exclusive. This is most obvious in the medium-frequency range, Figs 6a and 6b. The model and observation background activity levels are there respectively greater than 4.0×10^{13} m^4s^{-2} and greater than 5.5×10^{13} m^4s^{-2}, at 45^0S.

SH longitudinal anchoring effects, if such can be said to exist, are clearest in the low-frequency ECMWF data, Fig 5b, and to an even lesser degree in the corresponding CCC data, Fig. 5a The three centres that can be identified happen to be downstream (and poleward) of the major SH land masses These positions are the same as the SH preferred persistent anomaly positions, as determined by Trenberth and Mo (1985). The South-Atlantic maximum does not show as a distinct extremum in Fig 5a, but is still discernible as such from the figure's contours

We expect from the preceding discussion that the model SH persistent anomalies resemble quite closely their observational counterparts. Their frequency of occurrence and/or amplitudes will be reduced, but their positions should be nearly correct. The anomaly distributions themselves, to be discussed next, should not be as geographically concentrated in the SH as in the NH, due to the greater background activity present in the SH medium and low frequencies.

2.3 Anomalies in the space domain

We now present the spatial distributions of positive and negative anomalies in the Northern and Southern Hemisphere winters and summers (NHW,NHS and SHW,SHS, respectively) These anomalies are those that satisfy the criterion discussed in Sections 2 1 3 and 2.1 4 The intermediate seasons will not be discussed in detail. In terms of the anomalies as we define them, they are transition periods, not periods of activity extrema.

It should be noted that Treidl *et al*. (1981) conclude that the maximum and minimum periods of NH blocking activity are precisely the spring and autumn intermediate seasons Their approach, however, is subjective[26] and, because of this, does not include removing the seasonal cycle prior to attempting an identification of the events While the former just means that reproducing all their results could be technically difficult, the latter presents a more fundamental problem, as we have already pointed out From our discussion on the importance of the seasonal cycle, it is not too surprising to find that Treidl *et al*.'s annual cycle of blocking high frequencies is exactly out of phase with the atmosphere's annual cycle. They observe more blocks when the annual cycle is such as to promote the deepest east-coast troughs, *i e*. when the climatological flow itself gives the impression of being partially blocked, and fewer when this flow pattern is at its lowest activity level.

The figures that will be presented in this section have not been scaled in any way, in that the model values are valid over a 20-year simulated period and the NMC values are valid over a 14-year observed period For ease of comparison, whenever we quote specific distribution values, we will as well translate these to values appropriate for a ten-year period

[26]Consisting of a visual analysis of 23000 50 kPa meteorological charts

2.3.1 Positive and negative NHW events

Using our anomaly criteria, the NHW model results are now compared to NMC analysis results. We present only the sum of the distributions of positive and negative anomalies. The individual distributions are quite similar, both for model and atmospheric data. The differences between the positive and negative will be mentioned as they arise.

As is shown in Fig. 8a, for the NHW model total distributions, the three centres of anomalies identified by Dole (1982) are clearly present in the CCC model The relative importance of the three seems, however, to be somewhat different from what holds in the corresponding NMC observations, Fig. 8b Indeed, we see in the latter figure that the Atlantic and Pacific cases are about as frequent in the NMC data (56 *vs* 62 cases, *i.e* 40 *vs* 44/10 year). This equipartition also holds true if we consider the distributions of positive and negative events separately (not shown). On the other hand, the CCC simulation would strongly favour Atlantic events (44 *vs* 33 cases, *i.e.* 22 *vs* 17/10 year). The model seems to overemphasize positive Atlantic events with respect to positive Pacific events (not shown). This is not the case for negative events. The model northern Soviet Union (NSU) events are too frequent both with respect to the Pacific and to the Atlantic events: the proportion is correct for the positive NSU events but not for the negative events

As we anticipated in the preceding section, the main oceanic patterns have more of a meridional extension in the CCC data than in the NMC data. The observations' maxima straddle the simulation's patterns, as was the case for the low-frequency variances. We now have an Alaska and a Greenland preferred sub-area, but the main areas are still close to the traditional ones. It is interesting to note that this problematic extension is also found for the NCAR/CCM Pacific anomalies as can be seen in Blackmon *et al.* (1986)[27].

The model anomaly distributions may be reflected by new circulation

---

[27]Their Figure 5b.

patterns arising in conjunction with their extensions For example, we will later see, when discussing the variances associated with individual types of events, that some of the model NSU negative events are in fact linked to the previously identified Greenland positive and mid-Atlantic negative events This connection is absent in the atmosphere, but a link seems to exist there between the Atlantic and NSU negative events This link does not include a Greenland component, but rather a Scandinavian positive component. This is quite clear either from Dole's (1982) Atlantic or NSU negative composites or from the composites obtained with our criterion (to be discussed later) The main difference, however, between the NMC and CCC results is the smaller number of events in the CCC data, as was to be expected from our discussion on anomalies in the frequency domain Please note that the NMC results should again not be considered equatorward of 20^0N or 30^0N, here as well as in Fig. 9

As we alluded to when presenting our modified Dole criterion, quite a few more events are now found than would be the case with the standard Dole criterion, of the order of fourfold if we refer to the observations, even when we use essentially the same thresholds as he does The number of positively blocked days per winter is now of the same order as that found by Treidl *et al* (1981). When the negative anomalies are considered as well, we find, for example over the North-Atlantic, that something noteworthy is occurring on two out of every three winter days The mean event duration is also quite comparable with what was earlier found, either by Dole or Treidl's team, that is, of the order of 15 days for Atlantic events The atmospheric events found by this local criterion are in fact a superset of the original Dole set In an attempt to capture certain events that may have been briefly interrupted by fast transients, Dole filters out the very highest frequencies in his data set. We have found that applying this additional procedure does not yield a greater number of events What this may point out is that there are no other persistent mid-latitude events to be identified with this type of method, *i e* our anomaly set seems *complete* The same would hold for the GCM simulation We have also verified that the observed and model anomaly distributions within the winter season are not biased towards spring Thus approximatively a third of the total winter blocked days are found in February.

Persistent events can be seen to occur at any particular geographical position in the NH. However, their distributions are by no means spatially homogeneous, the preferred positions (*i e.* the two mid-oceanic and NSU regions) being three times more frequent than any mid-continental positions. This holds both in the atmosphere and in the model With respect to a possible link with high-frequency phenomena, both of the oceanic maxima of the NHW persistent anomaly distributions can be found immediately downstream of the two main regions of high-frequency activity This is again the case for the observations and model.

2.3.2 Positive and negative NHS events

The model and atmospheric NHS total distributions of persistent positive and negative events, found in Figs 9a and 9b, respectively, differ more than their corresponding NHW distributions The two oceanic patterns are still present, but so are new model continental patterns missing in the observations The latter patterns could well be linked to a model tendency for extremely high surface temperatures[28] and heat domes over areas such as the American Great Plains and Iran. Indeed, the new extrema reflect the presence of negative circulation anomalies over their regions The NSU maximum is now appreciably weaker in the model with respect to the two other main centres. This is not the case in the atmosphere

One consistent summer feature found both in the model and the atmosphere is a shift in the Atlantic maxima towards Europe. The model Greenland extension is still present, although much weaker than in the NHW. In view of the previously mentioned North-Atlantic/Greenland/NSU link in the model, this may or may not be related to the weaker NSU centre. The NHS Pacific maxima found in both data sets are now shifted towards Asia with respect to their wintertime positions

[28] Mean summer surface temperatures of the order of 37 ^{o}C to 40 ^{o}C.

The maximum number of events is drastically reduced from their NHW value, approximately by a factor two. The longitudinal differences in the distributions are even greater than in the NHW There are practically no mid-latitude NHS persistent continental events in the atmosphere; the same holds in the model, apart from the afore-mentioned probable model deficiency Whatever the mechanism causing them in the NHW, it seems to be inoperative in the NHS. The oceanic events do not seem to be as affected, as their number is not reduced as much

2.3.3 Positive and negative SHW events

We now turn to the sum of SHW distributions of positive and negative cases presented in Fig 10a and compare it with the anomaly analysis of Trenberth and Mo[29] (1985) The model reproduces the two main action centres south and downstream of both New Zealand and South America, over the South-Pacific and South-Atlantic oceans. When the events of the two South-Pacific model extrema are totaled, the relative importance of the two regions is similar in the GCM, the South-Pacific region being more frequent by far A third centre in the southern Indian Ocean, again downstream of a major land mass, Africa, is present in both the model and the WMO observations but seems much weaker in the latter, although van Loon (1956) also identifies this third centre, using surface pressure data.

Our criterion was not applied to a sufficiently long time series of SHW observations, so a direct comparison of the frequencies of anomaly occurrences is not yet directly available As we have already seen (Fig 8a), the NHW model results differ from both the NMC frequencies presented by Dole (1982) and our own NMC anomaly frequency analysis (Fig 8b) in a more quantitative than qualitative manner If, as we can reasonably expect, those quantitative differences also apply to the SH, we can again say, while referring to the statistics of Trenberth and Mo (1985) for the observed positional information, that the model has fewer anomalies than the atmosphere, but the anomalies it has are at roughly

[29] Done with twice-daily operational analyses from the WMO Melbourne centre, valid from May 1972 to November 1980

the right positions.

One obvious difference is the split in the New Zealand/South-Pacific model centre. Trenberth and Mo identify only one observational pattern in this region, while the GCM clearly has two, resulting in four overall maxima. It is also interesting to note the nearly regular positioning of these four SHW event maxima Indeed, the three southernmost maxima are separated in longitude by approximatively 120 degrees and the two northernmost by 180 degrees

Comparing the southern and northern winter hemispheres and using the same criterion, the GCM has fewer anomalies in the SHW than in the NHW (as is the case in the atmosphere) Inasmuch as the spatial scales displayed by an anomaly distribution will to a certain extent reflect the scales of the anomalies themselves, the spatial scales associated with the SHW events are slightly smaller. This may or may not be related to a more local type of explanation being appropriate for the SHW events, as discussed in Baines (1983).

The major centres in both winter hemispheres are found immediately downstream of the most intense high-frequency activity. As such, the high to low frequencies link still seems to hold and the former frequencies could very well be part of a triggering or maintaining mechanism for certain low-frequency (persistent) events. We have also commented on the fact that the SH high-frequency activity is much more geographically widespread than in the NH. This may in turn be related to the SH's weaker pattern of (climatological) standing waves, as these latter are known in the NH to provide for locally unstable regions where high-frequency events tend to grow. That these regions are found immediately downstream of the NH land-masses is again hardly accidental All of these points are quite consistent with the SH's comparatively weaker longitudinal anchoring of persistent events, in the sense that the events seem less constrained to occur in relatively limited areas.

2.3.4 Positive and negative SHS events

We now end the discussion on anomaly distributions by quickly considering the sum of the SHS positive and negative model anomaly distributions, Fig 10b This field is quite similar to the corresponding figure of Trenberth and Mo (1985) The events now tend to occur at about 50^{0}S and no splitting of the New Zealand pattern can be observed, compared to the SHW model cases The three SH major centres can again be clearly identified

At the same time, the SHS background anomaly activity is more important with respect to the extrema than what is found in the NHS A final point we wish to make is that the reduction in anomaly activity from the SHW to the SHS is not as severe as what is observed (and modeled) in the NH

2.4 Composite events

2.4.1 General considerations

Overall, as we expected from the discussion of model and atmospheric variances, the model anomaly activity is in better agreement with that of the atmosphere in the SH than in the NH. This seems particularly true in the SHS We can still conclude that the model does reasonably well in both Hemispheres and both extreme seasons Thus, we can expect to find useful model analogs to atmospheric situations The next point we explore is the spatial structures of certain time-mean events This is done in order to ascertain to what degree these model events possess the same characteristics as the atmospheric ones A complete catalog of model events is obviously out of the question Firstly, we have already seen that some of these anomalies may not have atmospheric counterparts Studying these latter types, while interesting in itself, would probably not help us in increasing our understanding of the atmosphere's behavior with regards to its persistent patterns. Secondly, even if we restrict ourselves only to the types of events that do have atmospheric correspondence, some of them are probably linked together, as we have already alluded to when discussing a possible NSU/North-Atlantic NHW connection Also, there are probably a limited number of processes leading to the persistent structures we now investigate An equally limited number of event types would then be appropriate For these reasons, we limit the following discussion to events found in the winter North-Atlantic and North-Pacific and finally, in the summer New Zealand/South-Pacific sectors

We choose to present maps of the composite total and anomaly streamfunctions for each case, in order to display the mean horizontal structure of the events As such, the reader will find in Figures 11 to 16 the total streamfunctions displayed as unlabelled alternating stippled and clear bands, superimposed on the anomaly field, which is itself displayed using heavier contour lines The high and low values referenced on the maps are those of the anomalies The same type of maps are also constructed from observations when they present important differences from the composite maps of Dole (1982). As well, the anomaly contour intervals remain identical throughout the series, *i.e.* $2.0 \times 10^6\ m^2 s^{-1}$. The contour intervals of the total streamfunctions are $1.5 \times 10^7\ m^2 s^{-1}$ and $1.0 \times 10^7\ m^2 s^{-1}$ for the NH and SH fields, respectively.

At this point, a few comments on the compositing itself are probably appropriate While the events are identified using daily data, the composites are defined from pentadic data This modification is only introduced so that, in light of the decoupling times that can be inferred from their lag correlation statistics, the atmospheric or modelled states that make up the final composites are such that one would normally consider them to be essentially independent from one another[30] This will become important in the next chapter when we discuss the variance patterns associated with certain types of events

We retain pentads when any part of an event occurs within them The composites will thus generally contain part of the build-up and decay phases of the events One immediate consequence of this is that an event that lasted longer will have greater weight in the compositing than a shorter event, even tough every pentad is given the same weight This is particularly true of the relatively short events that barely satisfy the criterion The longer lasting events do not suffer too much from this problem Another consequence of the compositing method is that the composite events appear weaker than their individual events

The total sample used in the composite is much larger than what is found to have been used in previous studies As an example, when Dole (1982) built his composites, he gave each event the same weight by considering only the individual event means His Atlantic NHW negative composite is thus made up of the means of the six events he identifies,

[30]This is verified over the modelled wintertime continental landmasses and over most of the NH oceans, as the five-day pointwise lag correlations of 50 kPa ψ then become statistically insignificant The same cannot be said over certain other oceanic regions, particularly in the Azores high region, where strong lag correlations persist well beyond ten days Small values of lag correlations are even more prevalent in the SH

while our NMC NHW Atlantic negative composites are calculated from at least 90 to 120 five-day periods. This will also become important in the next chapter.

2.4.2 Composite Atlantic NHW events

We now discuss the type of composite anomalies presented the most often, the North-Atlantic events. Figs 11a and 11b show the positive and negative model composite NHW anomalies, respectively, when a centre position of (18^0W, 44^0N) is chosen, this position is the one where the greatest number of positive and negative NHW model events can be found There are in the two plots, respectively 23 cases covering 87 pentads, and 21 cases covering 78 pentads[31]

The positive case bears a strong resemblance to the Dole (1982) positive composite at the same position, that is, a strong positive central cell, resulting in a blocked North-Atlantic circulation, with an indication of downstream and equatorward wave-like propagation, henceforth called the EMA, *i e* Europe/Middle-East/Africa, pattern A weaker negative anomaly south of the main centre completes the Atlantic dipole pattern. There finally seems to be a hint of a north/south oriented chain of extrema that includes the two Atlantic, and weaker Greenland and NSU centres. No other global scale features of importance seem to be present

Turning to the negative composite, the picture is quite different. There is again an indication of the EMA downstream and equatorward wave-train, but much more is happening elsewhere The NSU and especially the Greenland centres are here very important centres There also seems to be some dipole-like events taking place in the Northeastern-Pacific and two negative extrema are found over Sudan and Korea Thus, the picture we get around 30^0N is of four negative anomalies fairly evenly separated in longitude The geographic centre around which these negative extrema

[31]Removing the pentad portions corresponding to build-ups or demises, the events, strickly speaking, last a total of 360 and 320 days, respectively.

are distributed is closer to the NSU extrema than the North Pole Still the Atlantic dipole is the strongest by far. Its negative centre is associated with a zonal flow over Europe, while the positive centre enhances a northward meridional circulation, *i e* *blocks* the North-Atlantic flow, in marked contrast with what Dole (1982) found

It is not at all clear that the sum of all the different extrema found in Fig. 11b represents a unique and consistent circulation pattern, or rather a mean of several types For example, the Pacific extensions could be (and they in fact turn out to be) the signature of a few double blocking events It is also possible that not every Atlantic negative centre is associated with a Greenland positive centre The events where they would not be thus associated would then resemble negative images of the positive events found in Fig 11a

Dole's (1982) negative composite, while still more global in nature than his positive composite, still resembles the latter to a further extent than is the case in the CCC simulation. The main difference between model and observations, as they are presented by Dole, is the strength of the Greenland positive centre in the model negative composites It could be that the model Greenland positive centre is a reflection of the tendency of the GCM for a more northerly jet stream Indeed, we have already established the model's tendency for more northerly low- as well as high-frequency eddies, namely in the Atlantic It is now also known that, at least in the NH atmosphere, high-frequency eddies are associated with the acceleration/deceleration of the time-mean jets (mainly along their northern flanks) while the low-frequency eddies seem to be linked to their decelerations (at the jet exit)[32]

The NMC (1965-79) observation composites of positive and negative NHW Atlantic events at (18^0W, 52^0N), as determined from our criterion, can be found in Figs 12a and 12b This centre position is chosen as it is our closest grid point to the Atlantic position used by Dole at (20^0W, 50^0N) It should be pointed out that it is not the position where

[32]See either Hoskins *et al* (1983), Lau and Holopainen (1984) or our fourth chapter dealing with this subject

the maximum number of persistent events is to be found. This latter is rather at (36^0W, 52^0N). The composites respectively represent 92 and 94 pentads.

Notice that both composites differ from Dole's This can be seen in that we now have a series of relatively weak centres of alternating sign, weakening with distance from the primary centres Even more interesting is the fact that the path of these secondary centres lies along the total circulation and not across it, as seems to be the case in Dole's work. There still is an EMA wave-train downstream of the anomaly, but it is now greatly reduced. The two observation composites still remain close mirror images with respect to one another, thus contrasting the model composites Another point to notice is that we only find very weak secondary dipoles over the Pacific in the observation composites. This feature was very prominent in the simulation This is surprising since, according to Treidl *et al.* (1981), double Pacific/Atlantic winter blocking events are frequent enough and we would have expected them to somehow show up in our composites Finally, apart from the previous discrepancies, the qualitative agreement is now good between our model and observation composites.

We have also investigated modelled and analysis composites obtained from events occurring at slightly different positions[33] to get an idea of the stability of the propagating-like patterns This is important inasmuch as we have taken care with our locality criterion to consider the possibility for the events to travel Two general comments can be made. Firstly, more than 80% of the model positive events identified at the downstream position were already included in the upstream composite and, secondly, the model events found at the former position tend to occur later than their corresponding upstream events. More precisely, twice as many will either start and/or end later than the reverse situation. The same comments stand when considering the negative composites

[33] Namely, (9^0W, 52^0N) for the model and (36^0W, 52^0N) for the observations Note that while these positions are close to the original ones, neither of them were included by the locality criterion when determining the first composite sets

derived from the observations. The downstream events are thus a subset of the upstream events and also tend to occur later. There are occasions when this last comment does not hold, for example when events retrogress before disappearing However, this simply does not seem to be a general rule, even when positive events are considered It may be that the dissipating and possibly retrogressing events no longer satisfy the amplitude criterion

Let us now turn our attention to the new model composites, corresponding to respectively 53 and 69 pentads, Figs 13a and 13b, and start with the positive case By choosing this second position, we now select model positive anomalies for which the centre of the blocking-like dipole occurs closer to the exit region of the North-Atlantic jet The downstream equatorward structures weaken very slightly, while the poleward structures strengthen, a new centre near Korea being added to the chain The negative centre south of the main positive one in Fig 13a is also considerably more important Turning to the negative composite, the Greenland and NSU secondary centres are not as important as before The Pacific itself is not as active The equatorward wave-like string of extrema is still very much present The negative model composite, Fig 13b, is again different from the first one we saw The Greenland and especially the NSU secondary extrema are not as important The same is apparently true for the Pacific dipole, as if double events are not as frequently associated with these further downstream cases This negative composite no longer resembles a northerly version of the positive, as in the first set of composites Neither is the global aspect as prevalent and the only really globally organised feature retained from the previous set of model composites is the LMA wave-like pattern, still very much present

The second set of observation composites, from respectively 86 and 121 pentads, is presented in Figs 14a and 14b, in the same order as before These are even more different than the first set from the Dole composites The features added with respect to the latter are of the same type as in our first composite set, but stronger, namely very clear poleward or rather, Northern Eurasia wave-like patterns in both composites. The patterns in fact ressemble the well established Eurasian teleconnections[34] The EMA wave-like pattern is either very weak, as in the positive case, or missing entirely, as in the negative case.

Notice that a pair of extrema are present over the Eastern-Pacific/North American Rockies region of the NMC positive composite, the negative extremum being stronger than the positive. This could be related with Dole's (1987) comment on the fact that the Pacific negative anomalies are often related to increased ridging over the North American west-coast This extrema pair would then be the signature left in the Pacific of certain double blocking events As we commented earlier, a much weaker but similarly positioned extrema pair can be also seen in our first NMC positive composite, Fig. 12a. We find this type of left-over circulation only in the model negative mid-Atlantic composites, Figs 11b and 13b But these residue of Eastern-Pacific events differ markedly in the NMC observations and in the model, as do indeed the corresponding total flow themselves Instead of the single oceanic negative extremum, the model presents us with a significant dipole structure with an added anomalous ridge over Alaska

There are certainly a few points worthy of notice as we conclude this sub-section It has been shown that the model and atmosphere have the same qualitative behavior with respect to their mean NHW Atlantic events. More precisely, as the event centre position shifts in relation to the underlying mean flow, the downstream *response* to the event also shifts. In every case, this response resembles a set of wave-like and sign alternating extrema whose amplitude decreases with distance from the main centre The path of this downstream wave-like response seems to be that of a great circle initially tangent to the mean flow One difference between simulation and atmosphere is in the strength of these downstream patterns the atmosphere's are generally stronger

There is always a secondary extremum of opposite sign associated with the primary pattern but its importance depends on the event's posi-

[34]As an example, compare with the EU2 November teleconnection patterns in Barnston and Livezey (1987)

tion, again in relation to the mean flow A tentative relationship between position in space and position in the life cycle of the events was also established, at least for certain types of observation and modelled events Finally, the negative mean events tend to display more global patterns than the positive events, especially in the model There seems to be more than one type of circulation going into the making up of the latter composite. The differences between Figs 11a and 11b illustrate this point very clearly.

2.4.3 Composites vs individual events

One could wonder at this point to what extent the NHW composites discussed in the previous pages reflect the reality of the individual events that make them up. A visual inspection of the time means of each of the simulated and observed individual events (not shown) occurring at our NH Atlantic secondary positions was performed to establish this. The positive cases are considered first.

What we find is that, practically all of the major patterns found in both observed and simulated data sets seem to satisfy the aforementioned ***Rex criterion***, that is to say, they are North-Atlantic blocks The downstream chains of sign-alternating and amplitude-decreasing anomalies is also a generic feature to the class of positive events At the same time however, the situation that holds in the observed Pacific region is not quite as clear The negative extrema found there could indeed be the left-over signal from double-block events. But then, the corresponding positive extremum can be found at either northerly or north-easterly positions and these two possibilities seem to cancel each other out. The resulting composite is smaller than either But this is a rather minor point and to a large extent, the positive composites would indeed represent most of the significant aspects of its individual events

Consider now the individual negative NHW Atlantic cases Model and analyses are not as similar as in the positive events Again, a large number of events consist of NHW blocks. The persistent and large-amplitude negative centres we identify are then either the southerly cell of a dipole structure, as is mainly the case in the model, or the upstream cyclone of a northern Europe blocking episode, as in the analyses. The reverse situations also exist That is, there are a few observed negatives corresponding to Greenland blocking and still fewer model negatives corresponding to European blocks. The large number of model dipole events with relatively northerly positions is consistent with some of the other discrepancies already noted between both data sets The Greenland medium- and low-frequency activities and the northerly extensions of the geographical distributions of positive events are amongst these We have already pointed out the importance of the NSU centre in the model composite This turns out to be a large downstream extremum very often associated with the Greenland blocks The EMA pattern identified in the negative model composite is itself again associated with these Greenland blocks. As for the observations' NSU centre, it seems to be associated with European blocks, as a downstream negative centre. A connection between mid-Atlantic and NSU negative anomalies also holds for the observations

On the other hand, not all negative events can be included in these blocking situations A significant number in both data sets simply correspond to persistently enhanced zonal circulations, very high zonal index situations over a large part of the North-Atlantic and Europe There does not seem to be any particular global pattern consistent v occurring in conjunction with these zonal events Thus, the contritutions of these particular subsets to the observed and modelled negative composites is to enhance the main negative centres

We have to conclude that both the observed and modelled negative composites are somewhat misleading in that each of them include several, quite different types of events Retrieving a single explanation for the ensemble's existence is probably impossible and the attempt could only lead to confusion A sub-classification is certainly required Still, essentially all of the features found in these composites were traced to real features in certain of the individual events, so that these constructs are not altogether useless.

2.4.4 Other model composites

We end this chapter with a quick review of some of the other interesting model composites. The discussions will be shorter than fo the NHW Atlantic cases as much of what was found there applies here as well An example of this is the sensitivity of the composite patterns to the position of the anomaly in relation to the corresponding total circulation. It was indeed verified that the model composites of NHW Pacific anomalies may change significantly with relatively small changes in the anomaly centre position Another recurrent feature is the preferred patterns found in the composites Again, wave-like structures are very often found downstream of the principal extrema The NHW model composites for positive and negative Pacific events having a centre position at (162^{0}W, 35^{0}N) are presented in Figs 15a and 15b, corresponding to, respectively, 15 cases covering 49 pentads and 13 cases covering 43 pentads A second position ten degrees closer to the dateline was also used (not shown but discussed) to determine the robustness of the composites With this very slight geographical shift, the changes found in the features making-up the composites were more quantitative than qualitative, but they were still noteworthy.

Let us first consider the negative composite in Fig. 15b. The most striking features are the two dipole structures found over the oceans And indeed, the corresponding total circulation depicts a situation consistent with a model North American west-coast block that would be frequently accompanied by a second block over the Atlantic This is (not too surprisingly) the converse of what we found for the model negative Atlantic composites. A weak wave-like structure is also seen downstream of the main negative extremum When we consider the composites of negative anomalies with centres at the secondary Pacific position (not shown), the two Atlantic extrema as well as the one over Alaska are weaker, the weak downstream wave-like string of anomalies remains nearly identical and the Korean relative extremum is stronger and better identified

The positive NHW Pacific events, Fig. 15a, are discussed next. The main feature is the somewhat PNA-like pattern that is made of the primary positive extremum, the negative Rockies and positive North American eastern seaboard extrema, all very clearly present in this case. Other weaker wave-like features are also present either following lines emanating from the main positive centre towards Eurasia or along 30^0N over the same land mass. We again have a secondary extremum over or near Korea, as in the previous negative composites But now, no obvious circulation type dominates over the Atlantic basin When we investigate the other Pacific positive composite (again not shown), it displays an even more clearly defined PNA pattern This is as if these positive PNA-like anomalies, viewed as the model's response to an unspecified forcing, were somehow *enhanced* as their centre approaches the position chosen by Wallace and Gutzler (1981) in their teleconnection study The model behaves a lot like the atmosphere in this respect At the same time, it should be stressed that the sea-surface conditions experienced by this version of the CCC GCM are specified and are those derived from climatology. As such, these simulated PNA patterns are definitively not a response to an anomalous (external) forcing Note that this (internal) view is supported by Frederiksen (1989) in a case study of an observed Pacific blocking event

The last types of events we consider in our study of composite anomalies are the positive and negative SHS streamfunction anomalies downstream of New Zealand, Figs 16a and 16b, corresponding respectively to high and low zonal index flows over the region. The number of cases, respectively six and 13, and the total number of pentads, 20 and 49, that are used in these composites are more limited than what was used in the NH so that care should be taken not to stress too much the significance of the results, and this especially for the positive composite.

This SH anomaly centre is again immediately downstream of a major centre of high-frequency transient activity, as were the two other sets of NHW composites in the Atlantic and Pacific oceans. The negative, anti-cyclonic composite, Fig 16b, displays a single very clear wave-like pattern that starts with the main extremum and extends eastward and equatorward. Nothing of a more global nature is present, so that this pattern could tentatively be labelled as a relatively pure example of a "local" anomaly.

This is not at all the case for the positive composite, Fig. 16a, whose overall features are much more hemispheric. The first thing to notice is the quite important zonally symmetric pattern of negative anomaly values in the Arctic and positive values at mid-latitudes This is very similar to the dominant mode of monthly variation in the SH high latitudes as reported by Szeredi and Karoly (1987) In addition, this composite can be seen to display strong zonal wavenumber four, as well as wavenumbers one and two, anomaly components Finally, there are no equatorward wave-like patterns to be found in this mean of positive anomaly events

Either by accident or because these SHS events are "purer", perhaps due to the simpler SH orography, the two composites we have briefly investigated for events occurring there clearly display the two main types of mean anomaly structure. In retrospect, it would indeed seem that the features found in the composites we have displayed often take on either a global or local nature. The local type of events, another example of which are the NHW (anti-cyclonic) positive events, are mainly characterized by downstream wave-trains quite reminiscent of barotropic energy propagation as presented by Hoskins and Karoly (1981) At this stage, nothing can be said as to whether these wave-like structures are standing, propagating or even significant features. They are surely recurrent. On the other hand, the global or rather hemispheric type of events remind us of the resonant planetary wave-number amplification mechanisms such as proposed by Tung and Lindzen (1979a) and others (Chapter 1).

2.5 Conclusion

Model and NMC analyses have similar anomaly distributions in time and space even though the model transient activity is markedly weaker than in the NMC data set Model positive and negative anomalies, at least in the Northern Hemisphere winter, seem to be of quite different types (local *vs* global, respectively), again in agreement with what Dole (1982) concludes from his NMC analyses. There are some interesting and consistent differences in the situations pertaining to the two sets of events One of these is the greater number of more northerly events in the model and the fact that there exists an accompanying extension of the high-frequency model transient activity in those regions The NMC analyses do not display this type of transient northerly extension

There is also a real need for a better classification of events than that of the simple scheme used up to now Indeed, we saw that certain composites may be made up of several quite different kinds of events And furthermore, it is not clear whether considering the resulting composites in any quest for physical explanations to persistent anomalies is at all meaningful This problem of separation of types will be addressed in the next chapter

Chapter 3
Variance analysis

3.1 Introduction and Methodology

We have seen in the last chapter that the preferred modes of variations to be found in both model and atmosphere turn out to be more complex than what can be determined from direct averages or other slightly more involved compositing techniques We discussed how, for instance,

both the model and atmospheric mean negative mid-Atlantic anomalies are made of several types of quite different synoptic events The fact that this is true could also have been inferred by considering the apparent confusion found in the means themselves, as each of the different event types contribute to the overall mean, either cancelling and/or emphasizing one another.

Once this has been realized, the use of standard composites when attempting to determine the underlying physics associated with these persistent events is to be highly discouraged. There are fortunately several other and, at the same time, better means to identify the basic features associated with persistent events Several relatively simple statistical methods have been proposed in the last few years that attempt to extract salient information from complicated data sets Meteorologists and climatologists have thus started to use one or another of these, depending on the hypothesis underlying their work and/or their specific kind of data Examples of these methods range from the *Principal Interaction Patterns* (i e PIPs) of Hasselmann (1987), to *Canonical Correlations*, as presented by Nicholls (1987), to the study of the *Phase/Coherence patterns* of Lau and Nath (1987), to finally *Rotated Empirical Orthogonal Functions* (i e REOFs), as used by Horel (1981, 1984) and Barnstom and Livezey (1987), amongst others

3.1.1 Methodology. Overview

The main tools retained in the present chapter are the oblique-real and oblique-complex versions of the REOF method We will only expound here what turns out to be the most relevant set of properties of an REOF analysis A more complete discussion of these properties and of certain other important aspects of the mathematics involved can be found in Appendix A[35] As neither the time nor the space components of the analysis results are constrained to be orthogonal, and since we choose to let the latter geographical patterns carry the data's specific variance information, these should more properly be called *primary patterns*, but we will henceforth refer to them as REOFs

Our approach is different from that of the last few authors mentioned (e g Horel or Barnstom and Livezey) Indeed, it seems that since Horel has presented his procedure to the meteorological community in his 1981 paper, most of the relatively few climate diagnostics papers that deal with REOFs have followed him in using the VARIMAX orthogonal rotation. The other referenced paper on the subject, by Barnstom and Livezey, also makes use of this specific algorithm. What is implied by this choice is discussed in Appendix A

The most striking aspect of REOFs and what makes them so useful is their ***stability***. Let us explore what this means in the present context Given that there exist a relatively small number of distinct states (or modes) that account for most of the timewise or spacewise variance found in a data set containing many independent realizations of these states, the REOFs will tend to reflect these individual states In addition to this, halving the time series or the spatial domain does not necessarily destroy or even change the REOFs beyond recognition. On the other hand, a careful selection of the times and area where a certain state is more important will certainly highlight this state in terms of a specific REOF, or at most, a small set of them[36] Obviously, a mode has to be present in both of the chosen spatial and time frames in order that the analysis can pick it up, so one should still seek to have the largest amount of data possible

---

[35] A basic description of the real and complex EOF models is given, as well as a discussion on EOF selection rules We end with a definition of certain relevant EOF rotations and their properties.

[36] The latter depends on the nature of both the specific mode and the rotation See Appendix A for more details.

A last comment should be made on this spatial domain requirement. The rotation algorithms we have used all work under the hypothesis that the physical modes contained in the data can be isolated either in time or in space The choice is left to the user We have chosen to try to isolate them in space One consequence of this choice is that a hypothetical global signal may or may not be picked up by this type of analysis, depending on its relative importance In any event, the domain has to be at the least large enough to contain a significant part of the spatial signature of the modes we expect to identify, but not necessarily any larger.

3.1.2 First analysis step

Perhaps surprisingly, it seems that the most sensitive parameter in the analysis is the actual number of EOFs to retain before rotation This number has to be determined in a more or less subjective fashion, depending on the underlying data set. Thus, it should be *intuitively* clear that more *complex* data sets will require a larger number of modes than *simpler* ones to adequately describe them This turns out to be true in a REOF analysis One should note that the reverse problem also stands. Indeed, care has to be taken to choose a value that is not too large, even slightly so At the point this starts to happen, the rotation algorithm will tend to break up some of the patterns into their sub-patterns. The method chosen to determine this measure of complexity is twofold.

In a first step, the EOFs are ordered in terms of the persistence characteristics of their respective *principal components* (PCs) We use a statistical selection rule geared for persistence[37], as opposed to randomness. As our interest lies with persistent types of events, only the most persistent (EOF,PC) pairs are now kept North *et al* (1982) comment on the problem of discriminating between EOFs associated with close eigenvalues They point out that such groups of EOFs cannot be

[37]See Appendix A

considered independently as the information they contain is randomly spread throughout the group members To account for this, we reject all EOFs from groups in which any member fails the statistical selection rule.

3.1.3 Second analysis step

In a second step, the rotation is attempted with several different numbers of retained EOFs, e g the first five, ten or fifteen components. At this stage, a new set of composites is invoked to help us For each REOF pattern, we choose the time intervals at which the data project in a persistent and strong fashion on this component and average these time intervals together This is done separately for the positive and negative phase of the modes Thus, positive and negative composites are obtained for each REOF pattern A number of retained components that is too small will yield a composite set for which the members cannot all be interpreted in terms of simple synoptic events In other words, there would not seem to be a simple link between the REOFs and their underlying composites The key words here are *interpreted* and *simple* This is where we have to refer to the data set and our knowledge of what can be found in it In this study, this means examination of individual events, occurring at different positions or times of year As a simple example, the relation between a composite and its REOF could be as direct as one reflecting the other within an amplitude factor

Choosing a number of retained components that is too large can result in two problems Several REOFs can be identified to the same composite and/or we can end up with patterns that do not relate to their composites at all[38] The first problem is inherent to the different rotation algorithms, as they all attempt to isolate (i e. breakup in time or in space) the information contained in the EOF model of the original data set This recalculation of the REOFs (with different numbers of EOFs) is then refined until an optimum value is determined for which the two problems do not arise As we will shortly see, this number does not

[38] This often happens with REOFs that explain too little of the total variance They may be persistent but do not seem to be important

have to be the same in our simulated data and in the corresponding observations

The end result is a set of patterns that are not orthogonal, i e that are oblique, in the rotated dimension (space or time, whereas the EOFs are orthogonal in both) and that may not be quite orthogonal in the other. The approach retained here is to rotate the spatial components, giving patterns that have a nearly orthogonal (or independent) timewise behavior and for which the spatial patterns are no longer constrained to be orthogonal These latter patterns will tend to be spatially isolated, or at least of a more regional nature than the original EOFs Note that this is not necessarily the case for the time components

3.1 4 Real and complex analyses

We conclude this section with an explanatory comment on the real and complex versions of the analysis In the present context, the primary version is the real one The complex calculations are used only as a check for the real calculation The real REOF analysis can only correctly identify stationary patterns Travelling patterns will always be broken up into two or more patterns and the relationship between these *aliased* patterns need not be at all obvious This is not the case in the complex version of the analysis (i e CREOF) in which the real and imaginary part of the CREOF provide for the quadrature information needed to describe travelling patterns.

However, the cost associated with the CREOF analysis is not at all negligible The complex analysis method is not as straightforward as the real one, having to rely on a pair of digital filters in the production of the complex data sets, the imaginary parts of which are Hilbert transforms of the real parts An undesired aspect of this filtering step is that it removes, strictly as a side effect, the very lowest frequencies As an example, the version we used of these filters start to remove information at periods longer than 36 days (in the case of model data) This may or may not be acceptable, but it certainly has to be kept in mind Furthermore, the computing requirements involved in this complex calculation are at least twice as big as in the real version and, since the phase between the real and imaginary parts of a complex REOF is arbitrary, the resulting patterns are not as clearly defined Finally, both methods give nearly identical results when the modes are stationary Thus, it has been found sufficient to verify in a few relevant cases that the most important modes produced by the CEOF analysis are indeed stationary Therefore, unless it is otherwise mentioned, we always consider the results of the real analysis It is to be understood that the modes we present are at worst only quasi-stationary

3.2 Covariance matrix and data selection

As in the preceding chapter, we consider the data as sets of consecutive pentads (five-day averages) of the data when circulation anomalies are present The covariance matrix for which the EOFs are eigenfunctions are then constructed from the slowly varying model and atmospheric components We have already commented on the fact that the principal modes we consider among all these functions are not travelling, but rather, stationary This is not to say that there are no such atmospheric travelling modes as can be found by another CEOF analysis It is only that the nature of the phenomena in which we are interested and the several steps we feel are required for this study have all but eliminated them

Several authors have done REOF analyses on such data sets as NMC heights[39] A major design difference between their work and ours lies in their simpler selection rule for the EOFs themselves They all use a rule of the *dominant variance* type, whereas we use a *time history* selection rule[40] Note that this type of rule assumes implicitly that the different samples are statistically independent, and this is why, in an attempt to satisfy this hypothesis, we consider pentadic data As well, because of our particular choice of selection rule, we do not at the onset require our signal to be confined to the very strongest EOF modes The other type of selection rule assumes that this signal has to *dominate* the whole variance information This choice of design has enabled us to identify and remove several components that, if kept, would have seriously compromised our results As a consequence, we eventually reject more of the total variance than if we had used a *dominant variance* rule.

It was also found during the testing phase of our work that some of the largest modes that we were rejecting displayed certain of the characteristics associated with travelling features This is not too sur-

---

[39] For example, see Hsu and Wallace (1985) on Multi-level data and Kushnir (1987) with CEOFs.

[40] See Appendix A

prising as the persistence test we apply is of a local nature and any travelling wave will thereby be penalized to the extent that it removes itself more or less rapidly from the testing domain.

3.2.1 Time selection

Calculations have been done either restricted to winter circulations or with the whole data sets and, since the data sets are themselves deseasonalized, the results of the two calculations agree to a large extent This not too surprising as the winter season is itself the most often sampled season In any event, the full year calculations have been retained as they do not imply an artificial seasonal cutoff and they maximize the number of persistent events We have commented in a previous section on the effect of data selections This is relevant in the present context in the following way If we retain moments in time at which no significant persistent event is taking place, has taken place or is about to take place, the signal corresponding to those events that we know occur will be partly masked by other types of events On the other hand, a too careful selection may only highlight a single type of event at the expense of all others. We have thus chosen a loose time selection based on the event identification rule presented in section three of the preceding chapter. But this criterion is applied now over the whole year instead of a particular season as it was done before.

In Chapter 2, we presented the spatial distributions of anomalies satisfying a fixed amplitude/duration criterion. If we consider instead the two dimensional anomaly distributions at a fixed position (*e.g.* the mid-Atlantic), obtained by varying both of the criterion thresholds (not shown), we find a distinct relative minimum at around the nine-day duration level, for a wide range of amplitudes Both of the model and atmospheric versions of these distributions display a single rather homogeneous pattern for durations shorter than nine days, but in the same respective amplitude ranges. These shorter duration events clearly belong to the class of synoptic events we specifically want to eliminate in the present context. Thus, events are constrained by definition to last at least nine days. This minimum duration criterion is the same as that used in Chapter 2

Anomalous persistent events can be found at any vertical level but we have verified that the (analysed or simulated) events have an equivalent-barotropic three-dimensional structure Indeed, applying appropriately scaled versions of the anomaly criterion at either 85 kPa, 50 kPa or 20 kPa, we will essentially extract the same time segments out of the full time series The time-mean events found at these different pressure levels display equivalent-barotropic relationships between each other. This is one of the known characteristics of persistent events and should not surprise anyone.

The horizontal structure of the events can then be well defined using a single pressure level. Again for the sake of comparison with other studies and unless specified otherwise, the 50 kPa data set is retained We thus consider the time covariance matrix of the anomalous 50 kPa streamfunctions.

3.2.2 Space selection

We have shown that the Atlantic basin was one of the most, if not the most, active region in terms of persistent events and this in both model and atmosphere We have also discussed at length the relatively low amplitudes attained by the model persistent events with respect to the observed ones Assuming that the physical mechanisms underlying the events are the same in both model and atmosphere, and that the reduced level of transient activity found in the former has its root elsewhere, it makes statistical sense to use different amplitude thresholds for the CCC and NMC data sets. Using streamfunction amplitudes of respectively 0.80×10^7 and $1.2\times10^7\ m^2s^{-1}$, the relative frequency of days when persistent streamfunction anomalies take place is then nearly the same in both types of data so that the statistical weights given to the events are then quite similar

Considering the above, we retain roughly 36% and 43% of all observation and modeling data, respectively. This means that roughly 40% of all pentads contain anomalies that are in their onset stage, in their mature stage or in their demise stage. This value is rather large and it highlights the fact that persistent events, as we define them, do not seem so rare. If, instead of only looking for Atlantic events, we had considered events occurring at any of the three primary anomaly positions as identified in Chapter 2, this percentage would have been even larger. As it is, it compares favorably with the number of blocking days obtained by Treidl *et al.* (1981) by completely different methods. But this proportion, obtained from yearly data, is two- to three-times bigger than the 16% Dole (1986) finds as the total of all positive and negative events, using his (ten-day, 100 gpm) criterion on the NMC NH winter data alone. Admittedly, Dole does not consider the onset and demise stages of the events, but his amplitude threshold is also not as selective as the one used here for our own NMC data set. This relatively low hit percentage for the Dole anomaly criterion is quite surprising, considering the slight modification by which our criterion was obtained from his. It is also interesting to note that Dole's anomaly percentage rises to 36%, a value equivalent to ours, when he considers low-pass filtered data (with a cutoff at around the ten-day periods). This is in fact the data he uses in his own EOF study.

3.2.3 Normality

We have already mentioned that a compositing technique is used in the process of determining what REOF set is most significant with respect to the total circulation. The times used in a particular composite are those when the anomalous circulation projects strongly onto the corresponding REOF. The *rotated principal components* (RPCs) associated with REOFs have zero mean and unit variance. They contain the timewise normalized importance of the REOF at any particular moment. The projection threshold value that is used, 1.28, corresponds to the 90% probability of the Gaussian $N(0,1)$ distribution.

Whether or not the RPCs are normally distributed (*i.e.* whether the preceding threshold extracts roughly 10% of the data) is indeed quite debatable A quick test for normality applied to both simulation and atmospheric data, using the Cramer-Von Mises W^2 statistic (Stephens, 1974), only establishes that the first RPC is almost certainly (at the 99% level) non-normal and the others probably not either (at lower significance levels) Be that as it may, the threshold value mentioned above is still used In order for a pentad to go into the making of an REOF composite, its RPC has to exceed this value for at least two consecutive pentads This ensures that the projections that go into the composites are as persistent as the events themselves

Even though the RPCs may not be normally distributed, we cannot reasonably hope to extract more than 10% of the data with this selection method of computing the composites The fact that we use the whole year instead of restricting ourselves to only winter conditions permits us to be as restrictive and still obtain stable composite fields For example, using the 1 28 amplitude threshold, each model composite is typically made of 30 to 40 pentads This means that from 150 to 200 days go into each model composite, *i e* about 6% of all anomalous cases The particular threshold is unimportant in itself as is the actual imposed duration. What is important here is that we correctly and unambiguously identify the circulation patterns associated to the REOFs In that sense, the n mber of cases that go into each composite has to be large enough to eliminate small inter-case variations but not so large as to include cases that have little relevance to the particular REOFs

The time-history EOF selection rule discussed earlier generally tries to eliminate components having a behavior in some way similar to that of a white noise process A few test were actually run in which this white noise requirement was replaced by red noise The results (not shown) agree with those of Dole (1986), in that the first few EOFs were indeed discarded by the modified selection rule As these same EOFs are eventually kept and contribute heavily to the final REOFs, this indicates that the REOFs themselves have a strong red noise "flavor"

3.3 Model persistent NH Atlantic modes

3.3.1 Overview

We now present the result of the variance analysis on the model streamfunction. A few of the basic statistics associated with the REOF patterns, such as the variance they each explain and some of their important correlation characteristics, or the number of pentads included in their composites, can be found in Tables 3 and 4 The REOFs are given names in the first line of Table 3 and the naming convention is based on a short-hand of their respective regions of importance The data set used in this section consists of the anomaly pentads of the northern Atlantic 50 kPa streamfunction in which a persistent positive or negative mid-Atlantic event is taking place We consider an area covering 36% of the Hemisphere centred at about (15^0W, 55^0N) where the Siberia/Pacific and near-equator regions are ignored. The number of model EOFs retained before rotation is six, the same as in the observations, to be discussed in Section 3 4. Note that, in an earlier series of calculations spanning the whole Hemisphere (not shown), the corresponding numbers were both found to be between 10 and 15, the model number being slightly less than the one that holds for the observations. The complex version of the analysis was only used during this earlier hemispheric series of calculations

There is an additional analysis step that has not been discussed yet. It certainly was not obvious at the onset that it would be required, but experience has shown that it is, particularly for the model data. This step concerns the values of the anomalous surface averages. These do not have any dynamical meaning and they are indeed generally set to zero when we calculate global streamfunctions However, while the average values are still meaningless when the domain is reduced to either a full Hemisphere or a relatively large section of one, they are then no longer constrained to be null and thus make contributions to the anomalous variance in time. This added variance happens to be of the same order in both our data sets. This is not too dramatic in the observations where it turns out to be a good deal smaller than what the anomalies themselves contribute.

On the other hand, due to the relative weakness of the model anomaly signal and to the EOF analysis method itself, this surface mean variance, if it is not previously removed, completely contaminates the model analysis. How does it achieve this? The first part of the answer is that the EOF analysis, by its very definition, attempts to load the first eigenfunction with as much signal as it can. This means that the surface average variance, being large with respect to other model signal, is largely included in this eigenfunction along with the variance of several other signals. If, for example, the seasonal signal were still included in the data at that very moment, which it certainly is not, it would indeed replace this surface average component in the first EOF, being itself much stronger than any other individual model feature. The very high correlation of the model PC(1) with the time series of surface averages, ~90%, shows this clearly. Simply removing the first EOF is the obvious but unsatisfactory solution since we then loose the relatively important and physically meaningful part as well In addition, a few other EOFs are also contaminated at the onset, admittedly to a smaller extent For the sake of comparison, only the twelfth or thirteenth observed EOF is affected by this problem. The solution we retain is to remove these surface averages from both simulated and observed data sets, before doing the actual analysis, as is done for the seasonal cycle.

The fact that we now consider positive and negative events together means that the total time-mean pattern that is subtracted before calculating the covariance matrix is very small compared to any of the anomalous events that go into it. As a consequence, the variance patterns we find will be related to the anomalies themselves rather than to deviations from the mean positive or negative anomalies, as would be the case if we only retained one or the other.

Limiting the domain area to the Atlantic Hemisphere is important in the present context of regional rotation algorithms as it relates to one of the results of the previous chapter. Indeed, we then commented upon the more local patterns associated with the persistent anomalies found in that area, if only with regards to positive anomalies. On the other hand, this domain limitation does not really change any of the main results but, at the same time, allows for their more concise presentation In fact, the large scale modes that are eliminated by this reduction describe phenomena that are important over regions other than the North-Atlantic, modes such as the PNA and the WP patterns (Wallace and Gutzler, 1981)

TABLE 3.

General information on the model NH Atlantic REOFs 1 to 6. The second row gives the percentage of retained variance explained by each REOF The third row mentions which EOF contributed to the REOF, the main ones with a bold-italic typeface The fourth row tells us which REOFs are connected to each other in terms of their temporal evolution The last two rows contains the number of days retained in each phase of the composites

	1 GRN	2 ATL2	3 ATL1	4 EUR	5 NSU	6 WA
Variance %	27 3%	18.7%	14.4%	14 2%	13 5%	11 9%
from EOF #	***1***,4,6	***2***,3,5	***1***,2,***6***	***3***,6	***4***,5	4,***5***
Max Correl	3.+31%	5·+15%	1:+31%	5:+17%	4.+17%	5 -9%
+ Composite	260	165	110	180	200	180
- Composite	155	155	125	190	175	190

The short-hand used to name the individual modes in Table 3 is mainly self-explanatory. It is probably sufficient only to mention that ATL1 and ATL2 refer to the monopole and dipole mid-Atlantic modes, respectively, while GRN refers to the Greenland mode. It is interesting to note that each of the first six EOFs make important contributions to at least one of the REOFs and that none of them contribute to only one REOF. In building this table, EOF(i) is said to contribute to REOF(j) if the $T_{ij}=T(i,j)$ component of the rotation matrix is larger than 25% and this contribution is strong when T_{ij} exceeds 80%.

The goal that underlies the current section on model results and the next one on observations is to present the persistent modes of atmospheric variations (simulated or otherwise) as given by the REOF analysis and more importantly to show how these modes can help us in understanding the evolution of the full system. This will be attempted through the description of the relationships displayed between these REOFs at any stage in their respective life cycle The extent to which these life cycles are realistic will give us a measure of the usefulness and success of the REOF analysis method as a whole.

Table 4.

General information on the model analysis procedure. The first row gives us a measure of the time dependance of the REOFs The next two rows contain the surface average of the regional variances before and after the EOF selection algorithm has been applied The last row also mentions the number of EOFs retained for rotation and the number of EOFs that account for 90% of the total variance.

Time Correlation Determinant	0 882
Total Hemispheric Variance	$4\ 050 \times 10^{13}$
Retained Variance (6/22)	2.177×10^{13}

3.3.2 Significant correlation

The values quoted in the tables for the maximum linear correlations r, among the different time components of our REOF model, should somehow be put into (statistical) perspective. How small a value should we consider? Indeed, a value that is said to be *significant* will be expected to depend on the length N of the time series to which it applies What is then needed is an N-dependent correlation threshold to which a certain statistical significance can be assigned. Essenwanger (1986, pp.273, 279) provides us with a few approximate ways of doing this. He first states that when two time series (the RPCs in the case of interest to us) are normally distributed[41] ***and*** their regression line is linear, the null hypothesis $\{ H_0 .\ r=0 \}$ can be tested with Student's t parame-

[41]We have already briefly discussed this aspect and concluded that the RPCs are probably non-normally distributed.

ter. In fact, under the previous two hypotheses, t and r are related through the following relationship:

$$t_r = r \sqrt{\frac{N-2}{1-r^2}} \qquad (3.1).$$

Thus, H_0 is accepted at a certain significance level α when $t_r < t_{1-\alpha}$ and the corresponding number of degrees of freedom is N-2. In the present circumstances, this number of degrees of freedom can be considered for all practical purposes to be infinite. A satisfactory first order approximation to (3 1) can be substituted, namely that $r_\alpha = t_\infty / \sqrt{N}$, where r_α is now the absolute value of the desired correlation threshold at the level of significance α and t_∞ is the two-tailed asymptotic value of $t_{1-\alpha}$ for infinite N

The second test presented by Essenwanger is based on an application of Fisher's z-transform and does not involve a linear regression line hypothesis. It merely requires that the population of correlation coefficients be not too close to ±1. This condition is quite easily satisfied in our data sets, as this value is then closer to ±0. It turns out that

$$z_r = \frac{1}{2} \ln\left(\frac{1+r}{1-r} \right) \qquad (3.2)$$

has a nearly Gaussian distribution with specified mean $\bar{z}_r$ and standard error ϵ_r, both being related to the number of pairs in the correlations It is thus possible to test z_r for departures from normality. But in fact, the correlations we find are small enough and the number of degrees of freedom large enough that the test deriving from (3 2) can be simplified to verifying whether $\|r\| \geq a_\alpha \epsilon_r$, where a_α is here the preselected (two-tailed) Gaussian value at the significance level α and $\epsilon_r \approx 1/\sqrt{N}$. H_0 will then be rejected at the α significance level when this is the case. It is also noteworthy that under these circumstances, we obtain nearly the same answers in this test as we do in the previous one.

The appropriate number of degrees of freedom to be used in these tests has to be at least as large as the number of persistent synoptic events identified by the anomaly criterion, 190 for the model and 110 for the observations, and smaller than the total number of pentads retained for the REOF calculations, *i.e.* respectively 616 and 367. If we consider the large scale decorrelation times in the atmosphere (and in the model) to be of the order of 10 to 15 days, values of 300 and 190 would seem adequate. Thus, in the case of model data, H_0 can be rejected with *10%*, *5%* or *1%* chance of mistake if $\|r\|$ is respectively larger than *9.5%*, *11.3%* or *15.0%*. Accordingly, the minimum absolute value of model correlations we will be considering is *9.5%*. Anything smaller will be deemed insignificant. The other thresholds will also be useful. They will essentially provide us with a scale with which we will be able to assign a relative importance to the correlation values we find.

3.3.3 Mode correlation

Most of the major patterns mentioned in the preceding table are significantly cross-correlated. The only exception is the West-Atlantic REOF(6). The highest correlation value is between the Greenland dipole and Atlantic monopole patterns. This and other high correlations should not be unduly surprising considering the small number of modes retained here and the relatively large amount of variance they each explain. Indeed, from Table 4, we note that the first six model REOFs account for 54% of the (surface averaged) time variance.

These high correlations can be explained by the fact that there really is no reason why only one mode can contribute to the life cycle of a normal event at any one time. What we have identified here are the *simple* modes, in the sense discussed in Appendix A, Section 5. Any simulated or observed situation will then be made up of one or more of these modes. As we have done here in the case of a successful rotation, each of these simple modes can now be identified as an individual and physically meaningful type of situation.

This discussion may *a priori* give the reader the impression that every mode is going to be linked, in some significant fashion or another, to all the others. This is far from true, a fact that can be gathered from the value of the determinant of the 0 lag correlation matrix, 0.882. To appreciate the significance of this number, consider that the mean value of this statistic from a large ensemble of pseudo-random input situations[42] is found to vary from 0 916 to 0 977 depending on whether we have individual sample sizes of 200 or 600 The asymptotic value for the infinite sample size (or fully independent case) is 1.0 The other extreme situation we should consider is one in which at least one of the RPCs is completely explained by the remaining others This gives us a zero correlation determinant value The value of 0 882 is thus much closer to what we would get from an experiment made up of independent samples than to the corresponding value from a deterministic one

The variance that remains unexplained by any of the REOFs corresponds to motions of smaller scales (in time and/or space). As such, these motions can be considered, at best, as corrections upon the primary large scale patterns (so that they still contain some kind of low-grade *physical* signal), and at worst, as random perturbations of these same larger scale patterns (in which case, we absolutely have to eliminate them). Thus, the interpretation of variance of the higher order EOFs in terms of physically meaningful processes may be essentially impossible in the present context. In fact, their inclusion in the REOF analysis procedure would only serve to mask the essential nature of the first six modes

3.3.4 Transformation scatter diagrams

In Section 5 of Appendix A, we also mention a prerequisite condition for assuming success in rotating a set of EOFs. Indeed, Richman (1986) describes a graphical procedure by which a given rotation T can be evaluated. The full set of scatter plots of every normalized *primary patterns* (and not the loading factors) with respect to every other is examined and the extent to which points gather near the axes

[42]Where the RPCs are replaced by $N(0,1)$ pseudo-random deviate vectors.

and/or the origin determines to relative high or low quality of the transformation. Let us consider a particular scatter plot of two modes As the rotation algorithms attempt to isolate the hypothetical signal (presently in space), a satisfactory outcome requires a small degree of scattering away from the axes (i e few points at which the two patterns are simultaneously large), indicating a clear modal separation, and a relatively large concentration near the plane origin (i e several points at which both patterns are small, providing for a buffer zone), indicating that the modes are indeed spatially isolated Cases where this is not found denote either a lack of *simple structures* (an expression coined by Thurstone (1947)) in the data set or the use of an inappropriate rotation algorithm in this analysis step An unsuccessful rotation will have a tendency to spread the information all over the scatter plane in a seemingly random distribution.

We have thus made a quick attempt to quantify this *closeness* concept, as applied to scatter diagrams, using a series of Monte-Carlo simulations. For example, we can calculate the percentage P_{10} of points that lie within ± 0 10 of the x and y axis, the data along each of them being normalized. For illustration purposes, Fig 17 displays the first four of the model scatter plot series This set of four should be considered as representative of all the others One question we could want to ask is "What is the probability of these diagrams occurring randomly?" A closely related question is "What is the probability of this percentage P_{10} being found randomly?" We chose to answer the latter question.

As our goal is to evaluate the complete transformation and not only a small part of it, we consider the full set of scatter plots and the average P_{10} is the quantity we will test for Its value is 30 4% for model data[43]. By comparison, a scatter plot of two vector samples of $N(0,1)$ deviates would be expected to give us from probability theory (on the average) 15% of the points within the same bounds After repeating this experiment a very large number of times, we find that 30.4% is a

[43] P_{10} is equal to 20.6% for the corresponding six unrotated EOFs

very extreme value. Indeed, 99.99% of the pseudo-random deviate vector experiments, with each vector containing the same number of points as the REOFs, produce smaller P_{10} values than this. If we separate the points near the origin from those away from it, but still close to one of the axes, the same conclusion holds for both subsets. This indicates that the patterns are both more isolated and more separate than would occur randomly and that the rotation is indeed acceptable.

In fact, the conclusion stands as long as the distance away from the axes is small enough. Replacing 10% by 25% does not change the result significantly, but replacing it by 50% does. In the latter case, there are still too many points near the origin, but the number of those away from there become indistinguishable from what we find in the random simulations. This is not surprising as the area of the plane we are testing is then an appreciable portion of the total area within a standard deviation of the origin. Accordingly, the procedure is then only testing for points close to the origin. In other words, for a distance threshold that is too big, the distinction between points that are near or far from any axis is statistically irrelevant.

Coming back to Richman (1986) and considering the full set of model REOFs scatter plots (not shown) in a fully subjective manner, we would probably say that, using his terminology, the model rotation displays a moderate to weak amount of *simple structure*.

3.3.5 Spatial representation

Let us now turn to the spatial representation of the modes themselves. Figures 18 (a to f) and 19 (a to f) present the two opposite phases of the first to the sixth model REOFs. The former set is called the positive or first phase and the latter, the negative or second phase. Members of the positive set will at least display a main positive extremum over their region of importance. The negative set follows suit. As in Section 2.4, the underlying stippled and clear bands correspond to the total streamfunction composite, but this time made up of all pentads that strongly project onto the chosen phase of a particular

REOF pattern, itself displayed with heavy contour lines The contour intervals are the same as in the preceding set of surface figures

We have also inspected the means of the individual events that go into the total streamfunction composites, as was done in the previous chapter and for the same reason, that is, to gain an idea of the representativeness of the composite with respect to the events that make them up. While none of these maps will be shown at this time, we will certainly use the insight gained from their inspection when commenting upon the total fields

At first glance, it seems obvious that all of the patterns described by Figs 18 and 19 fall into two distinct classes, high and low zonal index situations, at least over their principal region of interest In the mid-Atlantic region, low zonal index cases are illustrated by the positive REOF(1, 2 and 3) (Figs 18a, 18b and 18c, respectively), while the high zonal cases are represented by the negative REOF(1 and 2) (Figs 19a and 19b, respectively) The positive REOF(1) is by far the most frequent case found in this sample of model realizations, as can be seen from Table 3 and it highlights the model Greenland blocking events. This mode is clearly derived from the negative Atlantic anomaly cases discussed in Chapter 2 Note the downstream NSU negative and the larger lower latitude mid-Atlantic negative extrema The other two mid-Atlantic low zonal index modes resemble the more normal mid-latitude Atlantic blocking situations as described by mono- or dipolar anomaly patterns Both of them display downstream secondary patterns as well as lower-latitude secondary patterns, as was the case for the model positive Atlantic anomaly

All of these cases, and especially the positive REOF phases, mimic quite closely the individual events that make up their total circulation composites This is one of the main reasons why we tend to believe that the analysis method is successful in producing a *basis* for the persistent anomalies of the model Thus, the first three REOFs are the dominant model modes we could expect from the discussion of Chapter 2. One surprising aspect is the splitting of the mid-Atlantic blocking events into two families In view of the high in-phase correlation between members of the (3,1) REOF pair, this may or may not be an artifice of the analysis method We again tend to believe that this separation has a real physical basis The high correlation can simply be explained by certain events that either have larger latitudinal extent or take place *between* the two REOFs The in-phase correlation of the (4,5) REOF pair can be similarly explained These are by no means average situations or else they would show up as modes in themselves The last important correlation, involving the (2,5) REOF pair, is only a first indication of the model's tendency to link the mid-Atlantic and NSU regions as discussed earlier

The most important result of this section is that we can now identify a few of the other important types of persistent circulations patterns that can occur simultaneously with mid-Atlantic positive and negative anomalies The two most obvious are the European and NSU low zonal index types of situations described by the positive REOF(4 and 5) There are relatively large numbers of pentads that project significantly onto one or the other of these modes Their inclusion in any of the previous anomaly types could be quite misleading Please note that we again have an in-phase relationship between the mid-Atlantic and NSU regions in both of these latter anomaly modes

The opposite phases of the European and NSU blocks would seem to indicate high zonal index circulations And indeed a few of the individual pentads that identify with these REOFs are precisely that. On the other hand, not all of them can be so easily categorized The same comment stands with respect to the negative phases of the first three modes. The events that go into these modes cannot be unambiguously ascribed to only one type of circulation For example, some of the negative REOF(3) are in fact reflections of a positive REOF(1) situation As well, negative REOF(2) pentads can be associated to positive REOF(4) pentads. This simply means that negative mid-Atlantic centres of anomaly can be associated with either positive Greenland centres or with positive European centres. Thus, the difference from previous analysis methods is that we now have means to discriminate between those negative anomaly situations by way of the other REOFs.

3.3.6 Lag correlations

We have not yet discussed the patterns associated with REOF(6) beyond mentioning that it is the only REOF not significantly correlated with any of the other five This sixth REOF portrays a West-Atlantic dipole situation In an attempt to establish that the WA pattern is indeed part of the evolving large-scale circulation, we have calculated the lagged time-correlation from -5 to +5 pentads between every pair of PCs to see if there were any indications of linked life cycles

Let us first define the short-hand notation ***(i,j) is significant at k lag*** means that REOF(*i*) and REOF(*j*) are significantly correlated when the former lags the latter by ***k*** pentads The value ***k*** can be either positive (lag) or negative (lead) Only for the purpose of this calculation, moments in time at which no significant persistent events[44] are taking place have been included in the series but with zero coefficient values These moments do not contribute in any way to the correlations but their inclusion precludes us from making spurious connections between events that may not have been originally adjacent in time The time series used here thus have length equal to the number of pentads in the original data set We have also calculated the composites of the onset and demise of the significant events that project onto each phases of the REOFs These will again not be displayed, but we will comment on the information they contain, when appropriate.

The length of time over which the lagged auto-correlations remain significant tells us the characteristic duration of the different types of events described by the REOF patterns It also gives a time frame in which cross-correlations should be considered. In all but one case, there is a sharp cutoff after five days, from about 50% to 10→15%. The lagged auto-correlation of REOF(1) drops more slowly and is still 17% at 15 days, when none of the other correlations remain significant The

[44]As defined by our standard anomaly criterion.

typical time scale associated to the REOFs is then ~20 days for REOF(1), ~10→15 days for REOF(2) and ~5→10 days for REOF(3, 4, 5 and 6). Lag 1 correlations can thus be considered for every pair of modes as all modes display memory on that time scale. Unless clearly explained through an indirect connection (i.e. involving a third mode), a lag 3 or longer correlation should never be considered. The lag 2 situations will be marginal in that very strong correlation values will be needed to retain them as significant. Finally, whether the larger lag correlations are grouped in time (i.e. the (i,j) pair is significant at lags k_0-1, k_0, k_0+1, and so on) or are found for an isolated lag time will also have to be taken into account. The former will be given much more credence than the latter as it hints to a dynamically evolving situation.

What we find is that there are indeed a few significant series of correlations. Namely, REOF(6) seems to significantly lag the first three REOFs by one and two pentads. The correlation extrema are respectively +13%, +21% and +10%. The signs indicate that positive WA anomalies would follow positive Atlantic basin anomalies. This is consistent with the known behavior of blocking events to eventually drift northwestward as they become isolated from the main circulation. The northward component of this drift as well as the fact that ATL2 mode is the closest geographically to WA could explain the higher values for the (6,2) pair. The composites of the decline phases of all these types of blocking anomaly verify this drift.

Lagged correlation of the (5,1) and (6,5) pairs are also found to be significant, although not as strongly for the latter. In the former, REOF(1) leads at one and two pentads. The zero lag correlation is not significant. The maximum correlation, at lag 1, is -19% and the sign indicates that negative NSU anomalies tend to follow positive Greenland anomalies, a fact that is verified by comparing the composites made up of the negative NSU anomaly build-ups and the positive GRN anomaly declines. The (6,5) pair displays both positive and negative significant lag times. But again, the zero lag values turn out to be nonsignificant. REOF(6) leads REOF(5) with -13% at five days and then lags with (a barely significant) +9% at five days. The latter again corresponds to a westward drifting of the NSU (positive) anomalies. The first part is a little harder to explain. We can note that REOF(6) displays a second dipole pattern downstream of the principal one. This secondary dipole is both weaker and of opposite phase. What seems to obtain (and the NSU positive anomaly composite verifies this) is that this second patterns will have a tendency to build up into the NSU REOF(5) pattern. The presence of a strong Northwest-Atlantic precursor of opposite phase is quite interesting as it is not at all what Dole (1982) describes as a NSU anomaly precursor with his own NMC compositing

Finally, the (3,4), (3,5) and (4,5) pairs all display lag 0 and 1 significant correlations The (3,4) and (3,5) maxima, +14 and +15%, are at lag 1 while the (4,5) maximum, 17%, is found at lag 0 All of these lag 1 values could again be interpreted as examples of westward propagation of positive anomalies toward the end of their life cycles There is another possibility with respect to the (3,5) pair Both negative anomaly composites for the REOF(3) onset and REOF(5) demise resemble a Greenland block. We have already commented on the (5,1) and (3,1) correlations involving the same type of events In view of this, the (3,5) connection is also probably due in large part to the model's propensity to link negative Atlantic and NSU anomalies to positive Greenland anomalies as discussed in the previous chapter

It should be clear from this section that although the correlation values we discuss here may appear to be generally small in absolute terms, the proportionally large data base we retain is what makes them statistically significant This in turn points out the need in this type of analysis for a careful but by no means exclusive data selection algorithm Let us now turn to the results of the REOF analysis of the anomalies of the observed NH Atlantic geostrophic streamfunction

3.4 Observed persistent NH Atlantic modes

3.4.1 Overview

We will use in this section the same data as in Chapter 2, namely the NMC analyses of the NH geopotential at 50 kPa valid from March 1965 to February 1979 We also consider exactly the same spatial domain as in Section 3 3, and the analysis proceeds as before except where specifically noted. Due to their shorter duration, the correlation thresholds we use for the NMC PCs are ***11.9%***, ***14.2%*** and ***18.7%*** at the ***10%***, ***5%*** and ***1%*** significance levels, respectively Tables 5 and 6 contain some of the basic information derived during this NMC REOF calculation and can be read in the same fashion as the corresponding model Tables 3 and 4, respectively The mode naming convention used in the fifth table is also the same as in Section 3.3 The spatial distributions of the positive and negative phases of the NMC REOFs one to six are respectively displayed in Figs 20 (a to f) and 21 (a to f), the sign being again that of the REOF main pattern. The underlying total circulations that are displayed in these figures are now given by the 50 kPa composites of the geopotential height itself

TABLE 5.

General information on REOFs 1 to 6 from the NH Atlantic NMC geostrophic streamfunction. Table organisation is the same as in Table 3

	1 GRN	2 ATL2	3 EUR	4 NSU	5 ATL1	6 WA
Variance %	21 4%	19 5%	17 3%	14 6%	13 9%	13 2%
from EOF #	1,*2*,5	1,2,4,5	1,*4*,6	*3*,5	1,3,5,6	1,5,***6***
Max Correl	3 -21%	4.+15%	1 -21%	2 +15%	6 +20%	5 +20%
+ Composite	170	100	105	130	110	90
- Composite	80	135	100	135	85	80

We have recalculated the P_{10} statistic with the rotated NMC data. The result, 30 $1\%^{45}$, is again extremely unlikely to be found at random.

Compared to the model data, there are about 2% fewer values near the origin and about 2% more near the axes, but away from the origin. Roughly speaking, this means that the observed patterns can be expected to be very slightly larger on the average than the model patterns were shown to be.

By far the most recurrent NMC individual pattern is the positive REOF(1) Greenland block, even though the geographical position at which we apply the selection criterion happens to be southeast of that. The second most frequent pair of modes are the positive and negative REOF(4) NSU patterns The negative REOF(2) mid-Atlantic high zonal index circulation is itself about as frequent as the two previous ones And although fewer pentads project onto the other modes, the least well represented still have a respectable 80 days going into their composites The actual percentage of all retained anomalous days that go into one or another phase of a particular REOF ranges from 9% to 4%. These percentages are roughly comparable to the ones that apply to the corresponding model REOFs

From Table 6, the value of the (lag 0) correlation matrix determinant, which provides us with a measure of the independence of the REOF set as a whole, is again such that the NMC REOFs can be considered to be weakly mutually uncorrelated (as a set, if not exactly independent). We will now consider the instances where this is not the case.

3.4.2 Correlations and spatial patterns

Notice first that each REOF is found to be significantly correlated (at 0 lag time) with at least one other. In particular, the (1,3) and (6,5) pairs display very strong correlations In the former, the value is negative so that it relates opposite phases of the two REOFs. Let us now consider this pair Some features of the total circulation composites are sufficient to explain the high correlation values. In the first place, the negative EUR and positive GRN patterns (Figs 21c and

[45] The un-rotated result is now 22.3%.

20a, respectively) both describe Atlantic ridges at about 30^0W, the latter being much more intense than the former. Similarly, the negative GRN and positive EUR patterns (Figs 21a and 20c, respectively) again both describe ridges but now along 20^0E, the latter also being more intense than the former Thus, a REOF corresponding to positive anomaly patterns over either Greenland or Europe finds common aspects with the negative phase of the other REOF. It should also be noted that the positive phases of these two REOFs let us distinguish between the strong negative mid-Atlantic anomalies associated with two very different types of atmospheric circulations.

Table 6.

General information on the observation analysis procedure To be interpreted as Table 4

Time Correlation Determinant	0 921
Total Hemispheric Variance	$6\ 841 \times 10^{13}$
Retained Variance (6/21)	3.955×10^{13}

The second highly correlated pair associates the Atlantic monopole (Figs 20e and 21e) and WA patterns (Figs 20f and 21f) of the same sign What connects these two patterns so strongly is not immediately obvious, especially if we consider only their positive phases A good indication is instead provided by the two negative composites of the corresponding total circulation which both describe a high-latitude Atlantic ridge, upstream of the REOF(5) and downstream of the REOF(6) main patterns The individual events (not shown) that make up these negative composites do indeed verify this relationship We find several events for which the means display strong East-Atlantic and Eastern North America negative extrema, more often than not in conjunction with a Greenland positive extremum These events would project strongly onto the negative phases of both REOFs Surprisingly enough, we also find a few instances of double positive extrema for the events that go into the composites of the positive REOFs, but not as many as in the negative REOF cases and this, particularly for REOF(6)

Another element we can gather from this examination of individual events is that the negative anomaly events associated with a particular REOF do not fall into a unique type of circulation, be that for negative REOF(5) events or for negative REOF(6) events. Indeed, a few may correspond to Greenland blocks, and then again, others correspond to mid-Atlantic blocks, to name but two differing types of negative REOF(6) events. In fact, upon examination, the negative phases of the other REOF(1, 2 and 4) also have the same non-uniqueness problem to varying degrees. The least affected mode is REOF(3) where most events projecting upon the negative phase describe a circulation structure similar to an Atlantic-NSU double block situation, while the positive phase events resemble a nicely defined European block

The above points out that, as was found for the model REOFs, the composite means obtained from negative anomaly events are ambiguous Again, one has to wonder about results that concern event life cycles or their underlying physical mechanisms. These results are often obtained when all negative anomalies are considered together, that is, without a prior attempt to distinguish between the different types of circulation these negative anomalies can reflect To be sure, using a much more stringent selection rule than what is applied here may alleviate the problem somewhat (at the same time, eliminating most events) However, we would probably end up studying a very particular type of composite anomaly.

On the other hand, this ambiguity does not seem to apply in general to the anomaly sets that make up the composites of the positive REOF. From an examination of their individual member events, those latter sets of anomalies are more homogenous in morphology and can thus be said to define certain circulation families. Each family then essentially represents enhanced ridging over its mode's main geographical pattern Not surprisingly, in view of its very nature, the only real exception to this is REOF(6) where the positive anomaly cases would generally describe situations of increased zonal circulation.

What are the typical time scales that can be associated with these empirical modes? An answer is provided by their lagged auto-correlation statistics. We find large (*i.e.* ~50%) values for all REOFs at lag 1. As well, all of them, except for REOFs 2 and 5, remain significantly auto-correlated to ten days, the largest value being found for REOF(1) at 24.8%. But none is correlated at 15 days, although REOF(1) comes close. It is thus obvious that all modes evolve along a five- to 15-day time scale, a range that brackets the minimum duration value in our anomaly criterion. In terms of individual modes, the most persistent REOF(1) can be assigned a ten- to 15-day time scale while the least persistent REOF(2 and 5) can be assigned five- to ten-day time scales.

3.4.3 Lag correlations

Does this REOFs model offer any insight on the evolution of the atmospheric modes that it holds? We will now discuss the links we find between the observed REOFs through their time lagged correlations. As we did for the model in Section 3 3, the onset and demise composites of the events that project significantly onto each phase of the NMC REOFs will often be considered in the following discussion, but they will not be displayed

The most persistently related set, even if not the most strongly, appears to be the (1,4) pair of REOFs, the Greenland and NSU patterns. The correlations remain significantly large for lag times of -2 to +2 pentads. The pair displays two extrema, the +1 value which is +17% (in-phase) and the -1 value at -18% (out-of-phase) It is interesting to note that the zero lag correlation, 3%, is not at all significant, a fact that could indicate the existence of two distinct connections between the REOFs. Accordingly, we consider the positive and negative lags separately. The out-of-phase negative lag, where the Greenland anomalies lead the NSU anomalies of opposite sign, would be consistent with either polarity of the REOFs. For example, the negative REOF(1) displays a weak downstream pair of extrema and a corresponding weak ridge in its composite circulation that are nearly colocated with the positive REOF(4) main pattern, itself describing an intense NSU ridge. The composites of the demise of the negative REOF(1) and the onset of the positive REOF(4) bear this out even more clearly. The negative REOF(4) pattern, a NSU trough, also holds within its own composite an attenuated flavor of the positive REOF(1) Greenland block and this is again evident in corresponding onset and demise composites. This five-day lag could thus present us with either a NSU blocking precursor or a Greenland positive anomaly follow-up

The situation is not as clear for the positive lag times, where the REOF(1) patterns lag the REOF(4) patterns of identical phase. This associates positive NSU anomalies to positive Greenland anomalies and vice versa. Whereas the lag 0 patterns gave us a least an inkling of what was going on in the previous case, here only the demise and onset composites supply us with an interpretation in terms of synoptic situations And what they suggest is that the positive Greenland anomalies sometimes follow positive NSU anomalies in a general easterly motion of these large scale patterns. Insofar as their composites can tell us, there does not seem to be any particular links between the negative anomalies

The strongest observed correlation at any lag time is found for the (6,5) pair at lag 1. This maximum, +27%, applies to lag 1. We have already discussed the strong value at lag 0 and the conclusion was that the negative cases were mainly responsible for it. The onset and demise composites tell quite another story The anomaly patterns found in the demise of the positive REOF(5) and the onset of the positive REOF(6) (*i.e.* positive WA following positive ATL1) are very similar, much more so than the reverse phase composites. That is not to say that the previously proposed mechanism involving negative extrema does not stand There is indeed sign of it in the latter pair of lagged composites. But this signal is decidedly weaker than the one accounted for by the positive events

There are two other pairs of significantly correlated REOFs in this set yet to be discussed They are the (2,4) and (2,1) pairs at lags 0, 1 and 2 and lags 1 and 2, respectively. Both have their maximum at lag 1, +23% and -17%. Let us first consider the (2,1) pair. This out-of-phase relationship involves the demise of the positive REOF(1) and the onset of the negative REOF(2). This is quite clear from the composites of each of these events, as these two composites bear strong resemblances to one another This is not the case for the composites of reverse signs The situation described here is a westward movement of the decaying Greenland positive extremum, accompanied by a drifting and amplification of the negative extremum towards the northeast.

The (2,4) correlation in which an ATL2 pattern follows an NSU pattern is a little harder to explain, as was the case for the (1,4) in-phase lag 1 case. The same explanation can be invoked here as was then, *i.e.* an easterly drifting (or maybe re-establishing is more appropriate) of large scale patterns of positive sign. However, something else now seems to be involved as well The lag 0 correlation, +15%, is significant so that there also is some degree of co-evolution present. The events included in the lag 0 composites make this quite clear Indeed, we find several instances of either double troughs or double ridges, one of them over the NSU and the other over the mid-Atlantic. This is reflected in the total circulation composites by the fact that an important ridge over one region is accompanied by a smaller one over the other. And, the same holds for troughs. On the other hand, most of the demise and onset composites do not tell us very much The only one that contains a recognizable set of patterns is the onset of the positive REOF(2) What shows up there is a clear positive REOF(2) pattern with a rather amplified NSU positive extremum. This again points to a lagged connection involving positive anomalies between two regions, the earlier anomaly being situated downstream of the latter's position.

3.5 Conclusion

It is very interesting to note the extent to which both the CCC and NMC analyses of variance parallel each other. To be sure, the differences noted in the second chapter are still much apparent, if only in the amount of variance explained by the six NMC modes with respect to the six CCC modes. But even then, both REOF sets account for nearly the same relative percentage of their respective total variance, *i.e* 57% and 54%.

The most striking similarity resides in the modes themselves There is indeed a clear parallel between the model and observed REOFs. The same circulation patterns are identified by both even though their relative importance may not be quite the same As an example, in view of the northerly bias already displayed by the more classic model analysis carried out in Chapter 2, the fact that the proportional importance of the GRN pattern is significantly larger in the model than in the observations is not surprising However, this pattern is the one that explains the most variance in both data set

Some significant lag-correlations were found in both analyses. As an example, a few situations described WA follow-ups to mid-Atlantic events Another recurrent situation seems to indicate a strong negative GRN anomaly as precursor to NSU blocks. There are several other examples. There are also, certainly, points in which the model and observations do not agree. But these seem to be minor when compared to those points for which they do

One aspect for which there certainly is an agreement concerns the negative anomaly phases of the REOFs. These were found in most instances to be ambiguous in that, quite often, more than one type of circulation managed to project strongly onto them. On the other hand, it seems that the positive REOFs did not display any of this behavior There is only one, nearly successful, case of a negative anomaly mode, the one depicted by the negative ATL2 REOF We were not quite able to find an empirical mode that could be said to *uniquely* represent a negative mid-Atlantic "block". This type of circulation anomalies may just not be frequent enough compared to the other types of persistent anomalies and is thus not identified by the REOF analysis. However, the instances when this circulation pattern is in effect, in either of the observations or the simulation, are obviously included in the negative ATL2 REOF. And indeed, upon verification, the individual negative events that strongly project onto this REOF are mainly of this type, but even then, not all of them were

---

Chapter 4
Transient forcing

4.1 Introduction

We have seen in the previous chapter how a REOF analysis can, under certain circumstances, provide us with the primary modes of persistent model and atmospheric variations. Once these modes have been identified, the next step is to attempt to understand the mechanism by which the corresponding events are either initiated, sustained or terminated. Several hypotheses were indeed presented to that effect in the theory review of Chapter 1 In retrospect, all of them are derived from simplified or low-order models of the atmosphere and, as yet, very few have been satisfactorily tested on more complex data sets such as those provided by either GCM simulations or by observations. One noteworthy example of such a verification is that of Mullen (1987) (hereafter called M87), also discussed in the first chapter.

Turning back to our second chapter, recall that one of the main results dealt with some of the differences found between the model and atmosphere with regards to high frequency[46] storm-tracks and how these differences were reflected in their respective persistent anomaly distributions. Namely, the CCC GCM seems to have a more northerly region of Atlantic synoptic activity than is found in the NMC (1965-79) analyses of geopotential heights At the same time, the model also displayed a distinct Greenland extremum in its positive anomaly distributions, a feature not present in the corresponding observations Furthermore, while both the observed and simulated REOF(1) derived in Chapter 3 were Greenland dipoles, the variance explained by the GCM mode was significantly larger. These facts seem to point to a possible causative link between the *HF* transients and persistent anomalies. This link, as proposed by Green (1977) and Shutts (1983), is the one that was studied by M87 in a diagnostic study, following Lau and Holopainen (1984) (hereafter LH84), using normal composites of both simulated and observed block-

[46]We will henceforth use the shorthand *HF* to denote *high frequency*

ing events. Shutts reasons that eddies embedded in a deformation field (here the *HF* transients evolving in a diffluent jet stream) are (on average) strained into filaments and thus, by energy conservation constraints, energy should appear at progressively lower wavenumbers This mechanism implies that an anticyclonic forcing (due to these *HF* transients) is found immediately upstream of the block, in fact, at a position that is in quadrature to the ridge itself.

We propose in the current chapter to investigate this same link, but to distinguish between different moments in the life-cycle of the events and to make use of an REOF decomposition of the data sets before attempting any composites The diagnostic tool that will be used are the E-vectors as presented by Trenberth (1986) (hereafter referred to as T86), a recent extension of the concept of Eliassen-Palm vectors (*i.e.* the so-called *E-P flux vectors* of Edmon *et al.* (1980)) to the case of time-mean deviations[47].

This E-vector analysis will be restricted to certain specific cases of NH Atlantic anomalies, that is, to the same type of events as the ones presented in Chapter 3.

[47] A first version of this concept is presented by Hoskins *et al* (1983), hereafter referred to as HJW.

4.2 E-vector theory

We will now briefly present the E-vectors themselves, what they mean and in what context are they applicable. The first (quite general) assumption in their derivation is that the set of governing equations for the atmosphere are the hydrostatic primitive equations This seems quite appropriate as this is precisely the set of equations used by the CCC GCM. The vertical coordinate used by T86 is $Z=ln(p_0/p)$ where p is pressure and $p_0=100\ kPa$, but this can be replaced by pressure itself without any particular problem An entropy form of the first law of thermodynamics provides us with an evolution equation for the temperature T. Other frequent approximations, such as quasi-geostrophy (as in M87) and/or horizontal non-divergence of the eddies (as in HJW), need not be made at this stage. The starting equations are thus the horizontal momentum and thermodynamic equations

$$\left.\begin{aligned} & D\,\underline{V} + (f + u\tan\phi/a)\cdot\vec{k}\times\underline{V} + \nabla_h \Phi = \underline{\mathcal{J}} \\ \text{and}\quad & D_h\,\Phi_p + \sigma\,\omega = -\left(\frac{\alpha}{c_p} D\,Q\right) = \mathcal{S} \end{aligned}\right\}\quad(4.1)$$

along with the hydrostatic ($\Phi_p=-\alpha$) and continuity equations, as well as the perfect gas law ($p\alpha=RT$). Here, D denotes the total four-dimensional Eulerian derivative and D_h is simply equal to D without its vertical portion The same distinction holds with regard to the gradients ∇ and ∇_h. This three-dimensional gradient operator ∇ on the sphere is defined as

$$\left(\frac{1}{a\cos\phi}\frac{\partial}{\partial\lambda}\ ,\ \frac{1}{a\cos\phi}\frac{\partial}{\partial\phi}\cos\phi\ ,\ \frac{\partial}{\partial p}\right)\ .$$

Q is the entropy and σ is the (time-dependent) static stability. All horizontal vectors of variables such as $\underline{\mathcal{J}}$ and $\underline{V}$, respectively the horizontal friction and wind, are denoted by underscores As well, a is the earth radius and ϕ and λ are respectively the latitude and longitude. The local 3-dimensional orthonormal vector basis is denoted by $(\vec{\imath},\vec{\jmath},\vec{k})$. The other symbols have their usual meteorological meaning

The next step is to expand all of the variables into their respective time means (over a specific sample) and deviations therefrom, *i.e.*

$X = \overline{X}+X'$, and time-average the previous set of equations. The last step is to re-write the resulting products of time deviations in flux form (using the continuity equation). The time-averaged momentum and thermodynamic equations are then respectively,

$$\left.\begin{aligned} &\overline{D}\,\underline{\overline{V}} + (f + \overline{u}\tan\phi/a)\cdot\vec{k}\times\underline{\overline{V}} + \nabla_h(\overline{\Phi} + K_E) = \underline{\overline{\mathcal{I}}} + \frac{1}{\cos\phi}\cdot \\ &\left[\nabla\circ\cos\phi\left(\frac{1}{2}\left(\overline{v'^2} - \overline{u'^2}\right), \overline{-u'v'}, \overline{-u'\omega'}\right),\right. \\ &\qquad\left.\nabla\circ\cos\phi\left(\overline{-u'v'}, -\frac{1}{2}\left(\overline{v'^2} - \overline{u'^2}\right), \overline{-v'\omega'}\right)\right] \end{aligned}\right\} \quad (4.2)$$

and

$$\left.\begin{aligned} \overline{D}_h\,\overline{\Phi}_p + \overline{\sigma}\,\overline{\omega} = \overline{\mathcal{J}} + \overline{\omega'\Phi'_p}\left(\frac{R}{c_p} - 1\right)/p \\ - \nabla\circ\left(\overline{u'\Phi'_p}, \overline{v'\Phi'_p}, \overline{\omega'\Phi'_p}\right) \end{aligned}\right\} \quad (4.3),$$

where K_E is the time-mean kinetic energy of the horizontal transient eddies As well, $\overline{D}$ and $\overline{D}_h$ now only contain the advective components (but by the mean winds $(\overline{u},\overline{v},\overline{\omega})$ and $(\overline{u},\overline{v})$) of the original D and D_h.

The reader will no doubt have recognized in the right side of equation (4.2) that the horizontal portion of the first vector to be operated upon by ∇ is very nearly the E-vector of HJW. In fact, the major difference is an extra *1/2* factor to be found here T86 shows that with this modification, the (barotropic) relative group velocity of the transient waves, $C_g-\overline{v}$, is parallel to this horizontal vector Another advantage of the present formulation is that we now have an explicit expression for the $\overline{v}$-tendency as well as for the $\overline{u}$-tendency associated with the transients. The approach of HJW gives us only the latter $\overline{u}$-tendency. This is relevant in the present context as we know the mean meridional wind $\overline{v}$ to be locally more important in the situations that are of interest to us than is generally the case[48] One possible explanation for this difference could very well be the existence here of an appropriately large eddy forcing of this component

[48] Compare an Ω-block situation with the usually more zonal circulation.

The goal of the E-vector approach is to isolate all transient forcing of the mean momentum in such a way that, in the absence of such forcing, the mean wind profile would remain fixed. This is not the case in the system described by (4.2) and (4.3). Assuming that the transient eddy part of (4.2) is null, there still exists the possibility of (indirect) transient forcings of mean momentum through the mean thermodynamic equation forcing of $\bar{\Phi}_p$. To account for such a possibility, a mean residual wind $V^* = (u^*, v^*, \omega^*)$ is defined which satisfies the continuity equation and corresponds to the circulation remaining once the geostrophic and hydrostatic balances have (nearly) taken place. Thus, following T86, we define (using the hydrostatic equation):

$$u^* = \bar{u} + \frac{1}{f}\frac{\partial}{\partial y}\left[\bar{\Phi} + K_E\right] + R\frac{\partial}{\partial p}\left[\frac{\overline{u'T'}}{\bar{\sigma} p}\right]$$

$$v^* = \bar{v} - \frac{1}{f}\frac{\partial}{\partial x}\left[\bar{\Phi} + K_E\right] + R\frac{\partial}{\partial p}\left[\frac{\overline{v'T'}}{\bar{\sigma} p}\right]$$

$$\omega^* = \bar{\omega} - R\frac{\partial}{\partial x}\left[\frac{\overline{u'T'}}{\bar{\sigma} p}\right] - \frac{R}{\cos\phi}\frac{\partial}{\partial y}\left[\frac{\overline{v'T'}}{\bar{\sigma} p}\cos\phi\right]$$

so that (4.2) and (4.3) become, respectively,

$$\bar{D}\,(\underline{\bar{V}}\cos\phi) + f\cdot\vec{k}\times(\underline{V}^*\cos\phi) + 2\,\vec{j}\,K_M\sin\phi = \bar{\underline{\mathcal{F}}} + \left[\nabla\circ\vec{E}_u,\ \nabla\circ\vec{E}_v\right] \qquad (4.4)$$

and

$$\bar{D}_h\,\bar{\Phi}_p + \bar{\sigma}\,\omega^* = \bar{\mathcal{S}} + \left[\frac{\partial}{\partial p} + \left(\frac{R}{c_p} - 1\right)/p\right]\cdot\overline{\omega'\Phi'_p} \qquad (4.5)$$

where $K_M = (\bar{u}^2 + \bar{v}^2)/2$ is the kinetic energy of the horizontal mean flow and $\vec{E}_u$, $\vec{E}_v$ are the so-called u and v E-vectors. These are respectively the same two vector expressions found in the second and third line of (4.2) (without their $\nabla\circ$ operator), to which are added the following vertical components:

$$\left[-\frac{fR}{\bar{\sigma} p}\ \overline{v'T'}\cos\phi\right]\ (\text{for } \vec{E}_u) \quad \text{and} \quad \left[\frac{fR}{\bar{\sigma} p}\ \overline{u'T'}\cos\phi\right]\ (\text{for } \vec{E}_v).$$

Notice that, apart from the $\overline{(\omega'T')}$ covariance contribution, which vanishes in the quasi-geostrophic limit, there is now no transient eddy forcing of the mean flow in this modified thermodynamic equation (4.5) and the essential part of this forcing is then directly contributed by the two E-vectors, found in the new momentum equation itself. This implies that, except for the eddy vertical flux of heat, the usual indirect forcings, arising through secondary circulations, are thus explicitly accounted for by this formulation. We should also mention that the momentum equation (4.4) has been re-written in terms of $(U,V)=(u,v)\times\cos\phi$ since this is the appropriate continuous expression for the horizontal wind when using latitude/longitude coordinates on the sphere.

As T86 comments, the definition of the residual circulation that is used here is based upon the usual quasi-geostrophic approximation of the more general geostrophic balance equation and, as such, it is not quite appropriate for planetary scale waves. As well, all terms involving ω' are dropped by T86 in his final expressions for $\vec{E}_u$ and $\vec{E}_v$. This may in part explain the large imbalance he finds in a point-wise budget calculation of his $\overline{u}$-momentum equation[49] On the one hand, the vertical speed ω is a notoriously ill behaved field when derived from any type of observed (initialised or not) quantities This is obviously not the case with modelled fields Furthermore, the usual scale analysis of atmospheric waves (most often applied to planetary scale waves) predicts that the terms involving the vertical speed (or, for that matter, its time-deviation ω') should be small. On the other hand, a ***synoptic*** scale analysis of these same terms shows that they cannot be ignored so easily. Since we intend to study the influence of the high-frequency transients, which are precisely of synoptic scale, we feel that the ω terms should at least be evaluated in the case of the observations and fully considered in the model analysis Accordingly, we will construct ω fields by vertically integrating the horizontal divergences provided by both the model and observed data sets. These integrations will be carried out from the top down and will assume a *no-vertical-wind* condition at the top.

We have chosen to display the tendency $(\partial\overline{\psi}/\partial t)_{tr}$ of the time-mean horizontal streamfunction $\overline{\psi}$ due to the eddy transient as it combines the relevant information of the $\overline{u}$- and $\overline{v}$-tendencies in a single relatively smooth function This former field is easily obtained from the latter

[49]See his Appendix B.

two. Indeed, if Δ is the Laplacian,

$$\left(\frac{\partial \overline{\psi}}{\partial t} \right)_{tr} = \Delta^{-1} \left[\vec{k} \circ \nabla_h \times \frac{\partial}{\partial t} (\overline{u} , \overline{v})_{tr} \right]$$

where $(\partial\overline{u}/\partial t)_{tr}$ and $(\partial\overline{v}/\partial t)_{tr}$ are directly related through (4.4) to the (three-dimensional) divergence of $\vec{E}_u$ and $\vec{E}_v$, respectively. We can thus distinguish between contributions of the horizontal (barotropic) and vertical (baroclinic) components of the E-vectors. These will be labelled $(\ )_{trh}$ and $(\ )_{trv}$, respectively.

It will be very important, while viewing any of these $\overline{\psi}$ tendency fields, to remember that their absolute amplitudes are of themselves quite arbitrary and that one should instead consider the results of the $(\vec{k}\times\nabla)$-operator on these fields, which are quite meaningful, as they relate to the (rotational) wind tendencies. This means that a strong horizontal gradient of $(\partial\overline{\psi}/\partial t)_{tr}$ will be more important than a large absolute value.

Before proceeding to the analysis itself let us discuss some of the mechanics involved.

4.3 Practical considerations

4.3.1 Multi-level observations

The first practical consideration has to do with the observed data set. Up till now, we have (mainly) used a 50 kPa NMC set of NH geopotential analyses spanning the period of March 1965 to February 1979. This single-level data set is no longer sufficient and we have had to turn to one of the newer multi-level data sets The NMC eight-year daily (00 GMT) analyses, valid from December 1977 through November 1985, of temperature, vorticity and divergence have been retained in the present chapter The data are available at 12 mandatory pressure levels from 5 kPa to 100 kPa

Trenberth and Olson (1989) discuss at length the problems associated with this data set The main one for our purpose has to do with missing data. Altogether, nearly 10% of the data are found to be missing. The earlier NMC geopotential analyses used in our study suffered from the same problems, but to a smaller extent, i e roughly 2 5% No timewise (very extensive) blocks were found missing in the earlier data set[50], so that linear interpolation in time was thought to be sufficient to fix the problem This cannot be relied upon for the newer set Indeed, for the eight years period over which the data are valid, there are six blocks of missing data, each lasting at least six days and two of them lasting for 18 and 23 days, in July 1982 and April 1983, respectively

Thus, we have had to re-consider the fashion in which the annual cycle is removed, as doing a time-Fourier analysis across such extensive blocks of interpolated data is clearly unacceptable if its purpose is only to determine exactly a few specific components. The beginning and the end of the interpolation periods would then be unrelated and could result in unpredictable results in Fourier space The box method in which each day of the year is one such box was used instead The *annual*

[50]Only one block lasted four days, while none of the others exceed two days

cycle is then made-up of the mean of each of these boxes. Only the days for which the data were actually available are considered.

It can be easily shown[51] that removing this box-like *annual cycle* corresponds to the removal in time-Fourier space of the annual period and all of its sub-harmonics. As the current set is eight years long, this means removing every eighth harmonic. This is more severe than the procedure we used up till now and it may partly account for the fact that this data set has the weakest anomalies of all of the observed data sets we have used throughout this thesis. Indeed, when statistics such as those found in Table 1 of our second chapter are calculated, we find that these observations are now only 20 to 30% more active than the model, in terms of NH channel kinetic energy. In accordance with this, the anomaly criterion has also had to be re-scaled downward so that the amplitude threshold of the observed anomalies has been reset to 1.1×10^7 m^2/s On the other hand, the duration threshold part of our criterion has not been changed. A total of 192 pentads (i e 33% of this data set) were found to satisfy either the positive or negative versions of the criterion. This percentage of retained pentads is only very slightly smaller than the corresponding one for the earlier observations.

Returning to Trenberth and Olson (1989), their quality analysis reveals that the NH analyses, poleward of 20^0N, are largely free of the main biases and spurious trends If they restrict themselves (as we did) to 00 GMT fields, they then find only three obviously erroneous global analyses, roughly 1% of the data we used As an example, a maximum of 13 6% of suspect or clearly bad analyses is reported for the year 1984, but nearly all of them concern tropical or SH problems. As the diagnostics we aim to produce will be restricted to the NH Atlantic, we feel confident in using this data set as is, once the obvious holes have been accounted for.

---

[51]See Appendix B.

4.3.2 Spatial derivatives and smoothing

Let us now consider the method used for calculating the derivatives associated with the E-vectors. Such highly differentiated quantities always involve a large part of error as each successive differentiation increases the importance of smaller and smaller scale waves for which our knowledge can be quite inadequate. In an attempt to alleviate this problem somewhat, we consider exact horizontal derivatives (such as those provided by a surface spherical harmonic expansion of the data) and fourth-order precise vertical derivatives (as provided by the Numerical Algorithm Group's (NAG) E01BAF cubic spline routine). This minimizes the introduction of errors by the analysis. Both model and observations were projected onto a T20 (i.e. triangular 20) spherical harmonic truncation.

The errors found in the initial analyses are still present, though, and even the streamfunction tendency has to be lightly smoothed so as to remove excessive noisiness. Also, this latter field essentially contains a T40 level of information as it is the result of the product of T20 arrays. A *(r=2, n_0=20)* version of the spectral smoother proposed by Sardeshmukh and Hoskins (1984) is used to effect this smoothing. This results in fields containing the same spectral range as the original T20 data, but without the usual Gibbs phenomenon that would accompany a simpler truncation to T20 of the result itself.

The minimum size of horizontal domain we could consider, because of our choice of spherical harmonic basis functions, was the Hemisphere, even though we only wanted results over a smaller area such as the NH Atlantic window of Chapter 3. The original data were provided as global fields so that care had to be taken in producing the corresponding consistent hemispheric fields. This means that data equatorward of roughly 20^{0} latitude were eventually discarded by the process of rendering the fields either symmetric (temperature, geopotential and divergence) or anti-symmetric (vorticity) with respect to the equator. Poleward of 30^{0} latitude, the resulting fields were essentially unmodified.

The last spatial consideration concerns the vertical domain used in the diagnostic procedure Briefly, we did not retain the 100 kPa level as we wanted results pertaining to the free atmosphere, at or above 85 kPa, the next level upward. Thus, vertical means (if either shown and/or only discussed) will represent averages from 5 kPa to 85 kPa.

4.3.3 High-frequency cutoff

As we mentioned at the beginning of this chapter, we seek to determine the influence of *HF* transient eddies on certain particular mean circulation flows. The frequency cutoff used to define these *HF* transients is the same as in Chapter 2, namely, periods shorter than one week. We have thus had to isolate the *HF* components of our data sets This was done through time-Fourier analysis, retaining only the components contributing to the *HF* range. One immediate problem is that this procedure requires continuous data so that we decided to "fill in" the missing observations by linear interpolations. So, care had to be taken also to exclude from the re-constructed (and filtered) data time levels corresponding to any of the previously discussed large blocks of missing observations

To be sure, a Fourier analysis of such (interpolated) data means that the complex coefficients of individual frequencies may be imprecise, but, as we currently only require a very broad-band knowledge of the information[52], the procedure is nevertheless deemed acceptable Again, the model data set does not at all suffer from this.

There is a second point concerning this frequency separation that needs to be brought to light. We will very shortly use these *HF* data sets to construct several composites Implicit in this is a discontinuous sampling of the total time-series, highlighting certain types of events. The (model and observed) sets used to build the covariance statistics from which the E-vectors are defined will thus not be the same as the ones in which the frequency separations were done Now, we know

[52] For which band, we have a large number of correct realizations at each frequency.

from elementary Fourier analysis[53] that the total variance of a specific variable X is the sum of the squared amplitudes of all of its frequency components. Thus, we can effectively make distinctions between contributions to the total variance by either specific frequency components or by specific frequency bands. The different frequency contributions are separate and it is quite meaningful to consider them in isolation. However, this only arises because the basis functions used to do the Fourier expansions are orthogonal over the whole time-series. This is no longer the case with the sampled data sets.

As a consequence of the time-sampling, the sample means $\overline{X}$ that define a composite will in fact contain contributions from all frequencies, as well as from the complete time series time means X_0. As the sample becomes more extensive, $\overline{X}$ will be expected to converge to X_0. However, for smaller samples, it is possible to consider a breakdown of $\overline{X}$ into several distinct (and non-zero) sample-means, each one corresponding to a different frequency range. Thus, we find that

$$\overline{X} = X_0 + \overline{(X_S)} + \overline{(X_{LF})} + \overline{(X_{HF})} \qquad (4.6),$$

where the new subscripts S and LF refer to the seasonal and low frequency components of X. All of the preceding applies immediately to the variance/covariance calculations. This implies that, as well as considering the usual sample-mean of HF-eddy quantities (of the type $\overline{(X'_{HF}X'_{HF})}$, which is then equivalent to taking the HF contributions to the total mean), the HF sample-mean of unfiltered fields (of the type $\overline{(X'X')}_{HF}$, where interactions between different frequency ranges are permitted) will also contribute to the variance/covariances of the composite events. For large samples, we expect the latter contributions to be very much smaller than the former. In view of this, the former type of statistics is more important (and unless mentioned otherwise our results are derived from them). We have nevertheless evaluated the latter type of quantities in certain cases of model data.

---

[53] In fact, from Parseval's equation.

4.4 Tendencies due to high-frequency transients eddies.

4.4.1 Observed positive ATL2 events.

Let us now turn to the E-vector analysis itself. We first consider the observed data set. As a preliminary step, the same REOF analysis discussed in the previous chapter has to be redone, but now, with this shorter eight-year set The different modes thus identified parallel the ones in the earlier observations That is not to say that the REOFs are identical This is not the case Rather, it is possible to establish functional equivalences between the two sets of empirical modes This is a good example of the *stability* feature of the REOFs themselves, as discussed at length in Appendix A.

We have chosen to concentrate our analysis effort upon a single type of circulation and thus, to extract time levels at which the anomaly flow projects strongly onto the observed positive ATL2 mode (that we denote by +ATL2), a mid-Atlantic dipole blocking situation. As it turns out, this is the most important REOF of the present anomaly data set (at least in terms of explained variance, *i.e.* 22%), whereas it was second to the GRN mode in both of the longer 1965-79 geopotential analyses and in the 20-year model data set

We also separate the onset, mature and demise periods of each of these +ATL2 events, thus obtaining three different composites. This is done in the following manner. As in Chapter 3, we make use of an amplitude/duration criterion applied to each of the rotated principal components (RPC) in order to identify the individual events (by their respective pentads[54]) to be included in the corresponding REOF composites. Note that the amplitude part of this criterion is not quite as restrictive as the one to be found in Chapter 3, namely the RPC pentad value has only to be larger than 1.036[55], rather than the previous 1.28 This is only changed to account for the shorter time spanned by this particular data set. The model amplitude threshold is not modified and the

[54]Remember that our REOF analysis applies to five-day mean data.
[55]This only the cumulative *N(0,1)* value for the 85% probability level.

minimum duration of an event is again set to two pentads in both data set. Using this type of criterion, we thus identify pentads in which strong +ATL2 events are present[56]. At this point, we now reconsider the individual days that go into these particular pentad periods. The onset and demise parts of the composite are then the averages of all the first and last three days of each of these (disjoint) retained periods, respectively. Finally, the average of the middle days, those that are left-out by this procedure, define the mature part of the composite. The tendency analysis is itself carried out upon each of these three parts of the composite event.

The only real difference between the observation and model calculations is that, in the latter, we always consider the streamfunction tendencies obtained both with the $(\omega' V')$ covariance contributions, while in the former, these contributions may not be included. Note that this only applies to the mature situations. As we shall shortly see, our single case illustrates the relative importance of these usually neglected terms.

Figures 22 (a, b and c), 23 (a, b and c) and 24 (a, b and c) each contain $(\partial\bar{\psi}/\partial t)_{tr}$, $(\partial\bar{\psi}/\partial t)_{trh}$ and $(\partial\bar{\psi}/\partial t)_{trv}$, in that order, for the onset, mature and demise parts of the composite event, respectively. As before, the underlying stippled fields are the corresponding total composite streamfunctions $\bar{\psi}$. The labelled tendency contour intervals are in units of 10^6 (m^2/s)/day, while the unlabelled $\bar{\psi}$ contours are evenly spaced, every 2×10^7 m^2/s. As well, the a and b parts of Fig. 25 contain the mature $(\partial\bar{\psi}/\partial t)_{tr}$ and $(\partial\bar{\psi}/\partial t)_{trv}$, respectively, when the [illegible] covariance terms are not retained. Most tendency fields have an extremum at or around 25 kPa so that this level is the one chosen for display purposes.

Do the three $\bar{\psi}$ composite found in Figs. 22, 23 and 24, [illegible] present us with any realistic (or even semi-complete) [illegible] of a blocking event? It is very clear from [illegible]

---

[56] Nine events lasting a total of 60 days are [illegible] for the full data set.

(Fig. 22) that a significant mid-Atlantic block is already the major feature in the onset streamfunction composite. This agrees with the rapid growths of this type of event in its initial period, as documented by Dole (1982). This composite block grows substantially toward its mature stage (Fig. 23) Finally, while the demise composite (Fig 24) still displays relatively weak mid-Atlantic westerlies, it also shows no strong ridging activity, so that the block is then effectively gone.

We now address the $\overline{(\omega' \underline{V}')}$ problem. Comparing Figs 23a and 25a, the total tendency maximum is more localized in the former than in the latter. Furthermore, this extremum is then also stronger, 8.03×10^6 m^2/s, and in a quadrature position to the event itself, while in the latter case, we find an value of 6 21×10^6 m^2/s at a position 30 degrees longitude further upstream. The corresponding vertical components, presented in Figs 23c and 25b, are at first glance very similar, as for example, the major horizontal gradient, between the Québec positive and West-Atlantic negative extrema, is smaller by only 0.55×10^6 m^2/s in the former figure[57]. This overall pattern is indeed present in both cases and can be associated to a strong baroclinic deceleration of the time-mean jet stream[58], mainly along its northern flank and just upstream of the block, as synoptic events grow at the expense of the time-mean flow.

The largest differences can be found over the general area of the block itself and, in particular just upstream of it. There, the North American anticyclonic tendency is essentially cutoff in Fig. 23c as compared to what can be seen in Fig. 25b. Instead, a distinct cell of anticyclonic forcing is now apparent and it combines with the barotropic tendency over the block, Fig. 23b, rather than cancelling it. The upshot is that the vertical momentum covariance terms seem to reinforce the barotropic tendencies over the block, while reducing their baroclinic counterparts over or near the upstream continental coast. One result of this is a better horizontal separation of the tendencies

[57] This same gradient is reduced by 1 5×10^6 m^2/s in the case of the onset composite.

[58] As found by LH84, for general wintertime flows, and by M87, in blocking events.

due to all the vertical components and this, along the lines of more distinct near and far-upstream behaviors, thus taking into account the changing nature of the flow between these two regions. Another point worth mentioning is that nowhere are the tendencies due to the (ω, V') terms the dominant ones, but rather, they seem to act as (qualitatively important) corrections. In that sense, we are at least as interested in their qualitative nature as we could be in their exact quantitative nature (if this latter were known with any confidence at all). This is why we choose to keep them in this version of the analysis.

Coming back to the horizontal tendency due to the *HF* eddies in the mature composite, Fig. 23b, this field displays a pair of north-south extrema over the time-mean jet stream, resulting this time in the acceleration of the latter as the *HF* eddies (barotropically) give energy back to the time-mean flow[59]. In the present situation, this acceleration is not at all strong enough to compensate for the previous (baroclinic) deceleration of the time-mean jet stream. We can see, as well, a very clear anticyclonic forcing immediately upstream of the block, as required by the (barotropic) theory of Shutts (1983) and as indeed found by M87. Note that this latter forcing is not found in calculations done with the complete data, when no prior event sampling occurs, so that it indeed seems relevant to the blocking problem.

The next question we choose to address is "What are the main differences (if any) in the tendency terms between the onset, mature and demise stages of the composite event?" The onset and mature composites are compared first. The obvious difference is the larger values we find at the onset of the composite event. Indeed, both of the barotropic acceleration and baroclinic deceleration, which are again centred along 70°W, are significantly stronger. The same holds, as well, for the onset anticyclonic quadrature forcing. An interesting point to mention is that this latter feature is larger due to the vertical component tendency. This was certainly not the case in the mature composite. In effect, at this earlier phase of the blocking event [illegible]

---

[59] As in either of ML84 or [illegible]

transports would be major contributors to the required forcing of the event, the horizontal *HF*-eddy momentum transports providing weaker support.

This conclusion is quite different from that of M87, who concludes that the tendencies induced by the heat transports act instead to dissipate the temperature anomaly with the blocking pattern and that (barotropic) processes associated to the latter are predominant in forcing the upper level flow At this moment, we can only point to the differences between his analysis procedure and ours The main ones is that M87 solves for the (quasi-geostrophic) geopotential tendency over the whole composite event. Thus, it is for example quite conceivable that the tendencies due to the *HF* transients change significantly as the events go through their full life-cycle.

As for the demise stage tendencies, since the block has by that time mainly disappeared, we would expect the results of this tendency analysis to resemble those of LH84 and indeed they do, except that the tendency due to the *HF*-eddy heat fluxes is still very much stronger than the tendency due to the eddy momentum fluxes, which has by then markedly decreased. M87 comments that using the eddy heat transports in an E-vector type of approach does indeed produce larger tendencies than is found by the Lau and Holopainen tendency approach. The quadrature forcing term itself is all but gone The eddy associated baroclinic deceleration is now oriented zonally, indicating that the eddies are no longer deflected northward, as is clearly the case in the earlier composites, so that the eddy straining mechanism hypothesized by Shutts would also be absent.

An example of the vertical averages of the horizontal and vertical component of these tendencies is provided in Figs 26a and 26b, respectively, which apply for the mature stage of the events As expected, the tendency due to the (barotropic) *HF*-eddy momentum fluxes does not display any tilt with height, as the vertical average extrema occur at the same position as the 25 kPa extrema. And again, as expected, the same cannot be said for the tendency due to the (baroclinic) *HF*-eddy heat fluxes. Notice that the quadrature forcing that is quite evident at the 25 kPa level is not at all apparent in this latter figure which, as T86 comments, is simply the difference between eddy heat fluxes at the bottom and at the top of the domain, the former level largely dominating the latter. Thus, what is very clear here is the stormtrack deflection brought about by the block, as the *HF* eddies continue to flow on a path that passes to the north of it.

4.4.2 Modelled positive ATL2 events

We discuss next the model E-vector analysis of model +ATL2 events. The standard RPC criterion that we had used in Chapter 3 extracts 16 events that last a total of 165 days. Each of these 16 events can be considered to project strongly and persistently onto the model +ATL2 mode. As in the previous sub-section, Figs. 27 (a, b and c), 28 (a, b and c) and 29 (a, b and c) each contain the 25 kPa $(\partial\bar{\psi}/\partial t)_{trs}$, $(\partial\bar{\psi}/\partial t)_{trh}$ and $(\partial\bar{\psi}/\partial t)_{trv}$, in that order, for the onset, mature and demise model composite events, respectively. And again, the underlying stippled fields are the corresponding total composite streamfunctions ψ. The units and contour intervals used here are also the same as those used for the NMC tendencies.

As well as for the NMC analyses, the three successive composites provide us with a large part of the total life-cycle of the composite model event. The first one, Fig. 27, presents an already full-blown mid-Atlantic dipole event which manages to intensify in the second composite, Fig. 28, and has nearly disappeared in the last one, Fig. 29.

The onset, mature and demise tendencies will now be presented in that order, and, at the same time, compared to the "corresponding" observed fields. As we could have expected, there are several large quantitative and even qualitative differences [illegible] these are obviously due to model deficiencies [illegible] see, while others may simply arise because of [illegible] errors [illegible] have to keep in mind that the high-order [illegible] that are calculated here somewhat strain the quality of the observation [illegible] the model and observed +ATL2 modes no longer match as exactly here as they did when we used the older, but more extensive, 1965-79 NMC analyses.

The model onset total tendency due to *HF* transients and, in particular, its vertical component, respectively Figs 27a and 27c, are two such fields in which the major differences with the observations are probably caused by a model inadequacy We can see a very strong zone of jet stream (baroclinic) deceleration immediately downstream of Greenland, over Scandinavia. The usual West-Atlantic/North American deceleration zone is still present, but is less intense, though geographically more extensive, than other one The Scandinavian baroclinic zone is very clearly the result of the (erroneous) model tendency for a very high latitude extension of its mid-latitude stormtrack Synoptic events thus have a second chance to grow at the expense of the time-mean flow

The *HF*-eddy heat fluxes do not seem to sustain the main anticyclonic event at all If anything, they do quite the opposite. On the other hand, the tendency due to *HF*-eddy momentum fluxes, Fig 27b, displays a very clear quadrature anticyclonic forcing The North American barotropic acceleration we generally had in the NMC cases seems to be nearly absent The only present aspect of it is the rather northward acceleration found upstream of the model ridge, but even that is much weaker. Strictly in terms of the amplitudes of the different tendencies, we certainly could have expected smaller model values, as we had already found the model *HF* transients to be themselves smaller than the observed ones However, it would seem that this problem is linked more to the momentum fluxes than to the heat fluxes, as the tendencies associated with the former are relatively weaker than those of the latter, and that especially when comparing to the corresponding observed quantities. In fact, the most important barotropic forcing is the quadrature forcing which is itself directly associated with the block maintenance

In general, these comments still hold for the model mature composite, as the barotropic and baroclinic tendencies, respectively Figs 28b and 28c, display the same biases However, it should now be noted that the latter can be seen to exactly oppose the blocking circulation itself, as for example, in the middle of the block, the tendency due to the *HF*-eddy fluxes would accelerate the flow northward, opposing the time-mean southward flow. The zones of maximum (baroclinic) activity of Fig. 28c also extend too far north. Finally, the block itself is essentially maintained by the quadrature (barotropic) forcing due to the *HF* eddy momentum fluxes, which has now increased in strength from that of the onset composite.

The situation changes dramatically in the demise composite. Remember that in the corresponding observations, the quadrature forcing disappeared and the baroclinic tendency simply picked up, without changing its essential draining nature on the time-mean zonal momentum. In the model case, the quadrature forcing, Fig. 29b, weakens only slightly. ***However,*** the baroclinic tendency, Fig. 29c, which is also picked up, is now such as to completely destroy the blocking circulation, which has by that time indeed lost much of its strength and may have even started to drift with the flow. In particular, the tendencies found in Fig. 29c would tend to establish a southerly flow, eliminating any meridional flow associated with the block. The (still weaker) barotropic component seems to be generally better organized than it was in the other model composites and now tends to accelerate the time-mean flow over much of the mid-northern latitudes.

The vertical averages of the barotropic and baroclinic tendencies due to the *HF*-eddy fluxes are found in Figs. 30a and 30b, respectively, for the case of the mature model composite. The average of the former is clearly an attenuated version of its corresponding [illegible] field, while the later again reflects the [illegible] eddy heat fluxes, except that the contours, compared to those of the corresponding observed vertical average, are more uniformly bound together [illegible] the more extensive northerly baroclinic [illegible] eddies.

We end this section with a [illegible] of some of the other *HF* terms that may contribute to the tendency [illegible] those arising through [illegible] posed by equation (4.6). We have already mentioned that these extra terms should be small for large sample sizes and this indeed turns out to be the case, at least where the (larger) model sample is concerned. The resulting tendencies (not shown) are at best organized along the very small scales and seem to have little to do with the larger scale circulation. The spatial distribution of the individual wind tendencies (which are again not shown) indeed reveal a series of small scale, sign-alternating, extrema along the sample-mean wind track, a series which is quite reminiscent of the individual synoptic events themselves. The upshot is that, as we are essentially interested in the large scale patterns, these contributions to the small scale total forcing are irrelevant to us. This would certainly not have been the case had we been studying tendencies of synoptic scale events.

4.5 Conclusion

What can we conclude from these calculations? First, with respect to the *HF*-eddy transient forcing of blocking events, the required quadrature forcing always seems to accompany diffluent (or even diverted) flows in both model and observations. That does not prove that the transients are solely responsible for the events, but it does does show consistency with the simulation of blocking flows in simpler models such as those of Shutts (1983) or Haines and Marshall (1987).

Secondly, the model forcing are generally weaker than the ones derived from the NMC analyses, which is again consistent with less intense transients of the model. However, there are nevertheless several instances of strong *HF*-eddy transient forcing in the model, but these are not as widespread as in the observations. Examples of this are the (probably erroneous) high latitude (baroclinic) forcing of the onset composite and, more interestingly, the mid-Atlantic (again baroclinic) "anti-blocking" forcing found for the demise stage of the composite event.

The quadrature forcing seems relatively more important in the model data set than in the observed one, but in both data sets, it also varies with the intensity of the block. Again, with respect to this forcing, a major difference between the two data sets is that it seems to be a purely barotropic phenomenon in the model, while both the barotropic and baroclinic components of the *HF*-eddy transient forcing make contributions to it in the NMC analyses. In fact, the baroclinic component can be seen to be the major contributor in the observed onset composite. This would agree well with the old idea of thermally forced (or initiated) blocks[60], something that studies such as M87 have not been able to verify. In fact, M87 seemed to imply the reverse. One thing is very clear and that is that the forcing associated with the *HF* E vectors varies substantially within the life-cycle of this type of event. The

[60] Hoskins and Sardeshmukh (1987), in a case study of a winter 1986 blocking event, show a series of isentropic potential vorticity maps that somewhat support this idea.

model baroclinic component do not appear to be involved in the block maintenance (in the sense of a quadrature forcing at least), but, on the other hand, it seems clearly related to its demise, something which is not obvious in the observations.

Part of these differences may have arisen because we '.ad to relax our selection criterion for the compositing of these eight-year NMC analyses, so as to obtain more stable statistics. A larger data base would certainly have helped as is witnessed by the good agreement between the model and the older (but longer) 14-year observations in the variance analysis of the previous chapter There is indeed a correspondence between the model and observed versions of the ATL2 mode, but it is no longer as good as before

Finally both data sets show the same physical general interactions between the time-mean flows and their corresponding *HF* transient eddies As an example, over the storm tracks, the latter baroclinically extract energy from the former and and at the same time, give back part of that energy in a barotropic manner (*i e* by wave-wave interactions) This agrees with earlier results such as in HJW and LH84.

Chapter 5
Overall conclusion

Throughout this thesis, we have tried to gain a better understanding of the important atmospheric events we call blocks. We have used both simulated and observed data for that purpose and several climatologies have thus been established. A first strong conclusion that can be drawn, relating to these different climatologies, is that their differences are more of a quantitative than a qualitative nature. We have found the simulated and observed anomaly climatologies to be quite similar as to preferred time and space scales. The objective anomaly criterion that is used seems to identify most, if not all, significant persistent events. It is shown, in agreement with older studies, that blocks are ***not*** rare phenomena. The time-mean averages of atmospheric flows is thus made-up of very different situations. One immediate consequence of this is that the meaning (or usefulness) of such averages is questionable. In particular, the winter mid-Atlantic circulation seems to spend nearly half of its time either in the onset, mature or demise stages of blocking events.

Note that the most severe quantitative disagreement between the observations and model data occurred in conjunction with the best qualitative agreement. Indeed, the older NMC analyses, while displaying the most active transients of all data sets (the GCM displaying the least), produced nearly the same preferred REOF anomaly modes as did the CCC model. This is the second noteworthy conclusion of our thesis. These modes are the major ones during persistent mid-Atlantic anomaly events, whether they be positive or negative. That is not to say that they are all mid-Atlantic modes themselves. Some of them are not. These latter are the modes that may be found in conjunction with any of the phases of mid-Atlantic events. Their relation to the main mid-Atlantic modes have been studied through lag-correlation statistics, as well as the relationships between the main modes themselves, and significant sequences have been produced. Altogether the CCC and NMC dominant modes of variation, such as the REOFs can represent them, proved to be remarkably similar. The REOF analysis method has thus been shown to be useful in identifying the underlying physical signals associated with large-scale atmospheric anomalous circulations.

As for the theories that have been proposed to explain blocks, most, if not all, rely on such severe simplifications of atmospheric dynamics that it is difficult to extend them to more complete systems or to observations However, several means have at the same time been produced by which data could be tested as to the relevance of a few of these theories. The *high-frequency* (*HF*) transient forcing of Shutts (1983) has been chosen for our purpose. This is because, throughout Chapters 2 and 3, systematic differences in the modelled and observed *HF* transients were reflected in every persistent event statistics. In Chapter 4, an E-vectors diagnostic gives us the longer time-scale tendencies associated to these synoptic time-scales.

Making use of our REOF analysis results, we considered the composites of the onset, mature and demise phases of a particular type of event, namely the mid-Atlantic dipole blocks, as represented by the positive ATL2 REOF modes. These diagnostic calculations have shown that both the model and the atmosphere display forcing fields that agree with Shutts, at least in the onset and mature stages of the +ATL2 blocks. An interesting result is the change (or non-change) in the nature of the *HF* forcing (or of its individual components) as the composite event goes through its life-cycle Thus, as an example, both model and observed baroclinic components grow, (or at least change their respective nature) toward the end of the event, in such fashion has to oppose or destroy it. This opposition is not observed at the onset of the event, when these components have a positive effect on the event's growth. Mullen (1987) only considers the complete events and thus only concludes as to the importance of the barotropic forcing, a component we find to be consistent throughout the +ATL2 event life-cycle. Finally, note that even though there certainly exist other important forcings that apply to these events, we find that the $\bar{\psi}$ tendencies due to the *HF* eddies are generally quite large[61].

[61] Such as to build the anomalies within a day or two

As it could have been expected, the strengths and weaknesses of each type of data, whether it be model of observations, shows through the results we have obtained in our endeavor Consider the observations. The data sets we have used seem to have been either old (but extensive) or recent (but short) On the one hand, the older data have given us very stable statistics, but some of the known deficiencies of the data gathering systems responsible for their production can never be remedied. These deficiencies can eventually cast doubt over results that are obtained with this type of data On the other hand, the newer sets have benefited from the better observing networks, as well as from the more appropriate analysis tools of the post-FGGE years However, there is only as of now a limited number (at least in terms of time span) of these, when compared to the older observations

As for the simulated data, it also has its own set of problems The most obvious is the presence of some biases in the model climatology. We have taken pains to point these out, as far as they seemed relevant to our problem The model's low level of transient activity, as well as its northward extension of the climatological mid-Atlantic storm track, are probably the aspects that were brought up most frequently Furthermore, these difference between the analyses and simulation climatologies have been considered at every step in our work However, the simulated time-span of this data set, 20 years, is certainly one of its more interesting qualities, as well as the overall very good agreement between the climatologies[62] This permitted the use of very selective objective and statistical techniques, techniques that had to be relaxed somewhat for some of the later observations

[62]This is certainly true for the first-order statistics. Our problems mostly concern the second-order statistics.

Appendix A
REOF methodology

A.1 Introduction

This Appendix presents the method used to describe the original data sets in terms of a simpler set of fields, such as to retain as much as possible of the evolutionary information contained in the data. The basic data reduction is done with empirical orthogonal functions (EOFs). These functions have been widely used in meteorology in the past few years so that an in-depth derivation is not necessary at this time. In fact, we only go so far in this introduction as to be able to explain the particularities of the approach used in the analysis Both real and complex EOFs are discussed. Once determined, a certain subset of the EOFs is rotated (producing REOFs) so that the space and time domain dependencies inherent in the EOF approach are minimized. Two rotation algorithms are used, the orthogonal VARIMAX and oblique PROMAX. The relevant strengths and weaknesses of these methods of analysis are presented. The main references for this section are the following· Richman (1986) deals with real EOF models and especially their rotations; Preisendorfer *et al.* (1981) present several statistical selection criteria for EOFs; and finally, Horel (1984) reviews the complex EOF models (CEOFs) and gives several interesting examples of the VARIMAX complex rotation (RCEOFs). They are referred to as R86, PZB and H84, respectively

A.2 Real EOF models

The basic equations and definitions used throughout the Appendix and much of Chapter 3 are presented in this sub-section. Let us consider a $(N \times n)$ data matrix $Z = \left\{z_{ij} \; . \; i = 1, \; \ldots, \; N; \; j = 1, \; \ldots, \; n\right\}$ where i indexes the cases and j indexes the variables. The case means have been previously removed from Z. Two valid examples of the most widely used type of data matrix Z are the 50 kPa ψ time anomalies in our GCM climate simulation and the same data normalized by their timewise *root-mean-square (rms)*. The variables are then the ψ values at different positions and the cases consist of values at different times. We call this the *time-variance* approach. The analysis could also be carried out with an alternate presentation where the cases correspond to spatial positions and the variables to differing times. We would then make use of the *space-variance* approach. It is interesting to note that when both the case and variable means are removed at the onset, the two approaches give essentially identical results. The reason behind this is discussed in the sequel.

The real EOF model representation[63] of z_{ij}, which we denote by z'_{ij}, is

$$z'_{ij} = \sum_{m=1}^{r} f_{im}\left(a_{jm}\right)^{t}, \quad i = 1, \ldots, N, \; j = 1, \ldots, n, \; r \le n \qquad (A.1)$$

where f_{im} is called the ith score of the mth principal component (PC) and a_{jm} is the corresponding loading factor of that PC on the jth variable. The t superscript denotes the matrix transpose. The normalized loading factors are the EOFs, which then have unit (spatially integrated) variance. Equation (A.1) becomes

$$Z' = F\,A^{t} \qquad (A.2)$$

in matrix notation. The (row×column) dimensions of A and F are then $(n \times r)$ and $(N \times r)$.

In practice, the EOFs are a subset of the eigenvector of the correlation or of the covariance data matrix

$$\Phi = (Z^{t}\,Z)/N$$

and they depend on the specific nature of the z_{ij}'s. In most instances, Φ will also be either the time covariance or spatial covariance matrix depending on how the variables and cases are respectively defined. The loading factors are then its eigenvectors multiplied by the positive square root of their respective eigenvalues α_{η}. These eigenvalues are

[63] Often also called a Principal Component Model.

in fact the amount of variance or the correlation percentage *explained* by the corresponding eigenvector. That is to say that the loading factors matrix A carries the variance or correlation information contained in the right side of equation (A.2). The PC matrix is then defined by[64]

$$F = Z\,A\,(I/\alpha).$$

This simply means that the PC matrix F is the normalized projection of the original data matrix Z onto the EOF matrix.

If we now consider the alternate (covariance or correlation) matrix Φ' derived with Z' instead of Z, we find that with the previous definitions of A and F, the eigenvalues/eigenvectors of Φ' are precisely the ones selected by the EOF model of equation (A.1). In this sense, Z' is a filtered version of Z, the former retaining a selected portion of the latter's variance structure.

Every variable is given the same weight in the calculation of the total variance. This may or may not be appropriate in certain circumstances. When, for example, these variables represent a field in space, their respective importances should, in some fashion, be proportional to the area they represent. The total variance one attempts to explain with the EOF model is then the real spatially-integrated value. There are at least two methods to obtain this. One of them is to use an underlying equal-area grid as in Barnston and Livezey (1987) The data generally have then to be interpolated to such a grid, since none of the widely-used data set make use of them. An easier alternative method is to pre-multiply the individual variables by the square root of their corresponding area weights. The matrix A will then contain the "real" weighted variance information.

The covariance matrix Φ is by construction positive definite and symmetric[65] so that its eigenvalues are all positive real numbers The

[64] Throughout this Appendix, let it be understood that expressions of the type αI stand for the $(r{\times}r)$ diagonal matrix such that $(\alpha I)_{mm} = \alpha_m$, I being the $(r{\times}r)$ identity matrix The same applies to (I/α) and $\sqrt{\alpha} I$

[65] Indeed, $X^t \Phi X = X^t Z^t Z X = (ZX)^t (ZX) \geq 0$, $\forall\, X$, an arbitrary column vector of dimension $(n{\times}1)$ If X is chosen to be one of the eigenvectors of

sum of all eigenvalues is the trace of Φ, *i e* the total (or space integrated) space/time variance/correlation, depending on the type of data used to build Φ. Again by construction, the EOFs as well as the PCs are orthogonal. Also, because of their (quadratic) definition, the EOFs are indeterminate to within a sign change

These relationships can be summarized in the following set of equations.

$$\left.\begin{array}{l} A^t\ A = \alpha I \quad \text{and} \\ N\quad \Phi'\ A = A\ N\alpha I = \left(Z'^t Z' \right) A = \left(F\ A^t \right)^t F\ A^t\ A \\ \qquad\qquad = A \left(F^t\ F \right) \alpha I, \\ \text{so that } F^t\ F = NI \quad \text{and} \quad A\ A^t = \Phi' \end{array}\right\} \quad (A\ 3)$$

Most authors seem to use the correlation approach[66], *i e* they use the z_{ij} containing the original data divided by their timewise *rms* values, which then have unit variance in time This may be quite appropriate when, for example, the data consist of geopotential fields Then the correlation matrix is the only one that can contain useful information on patterns extending over a wide latitude band The amplitude information itself is then lost The covariance of the streamfunction ψ is not affected by this deficiency and its amplitudes, being directly related to the transient energies, may be more interesting physically than the previous correlations. Since the data set we use is precisely this ψ field, Φ is here defined to be the covariance matrix The factor loadings are then related to the variances or amplitudes of the data and not to their correlations Note finally that the loading factors or their corresponding EOFs and PCs are generally ordered by the decreasing amount of variance they explain, *i e* the first EOF is associated with the largest eigenvalue, α_1, the second EOF to the second largest, α_2, and so forth

---

Φ, this implies that the corresponding eigenvalues are also positive

[66] Note that if the data consist of several physically different types of measurements the correlation approach has to be employed

The main interest in an EOF model is that it can be shown that it is the optimum fashion in which to reproduce the variance structure of a data set[67] That is to say that a large percentage of the total variance can be accounted for by a relatively small number of mutually orthogonal components. Furthermore, the goal of the EOF model is precisely and only this: to obtain the smallest set of functions that all together explain the largest proportion of the total variance of a data set. This means that choosing $r \ll n$ in equation (A.1) is a reasonably good approximation and in practice, r is often chosen to be less than 10% of n. No other orthogonal set of function will manage this as efficiently.

There is an interesting consequence to the EOF unicity When the case and variable means have been removed prior to processing, the *time-variance* and *space-variance* approaches mentioned at the beginning of the Appendix will effectively commute. Then, up to within a multiplicative constant, the PCs of one approach are the EOFs of the other, and vice versa.

There is no *a priori* physical meaning to the EOF patterns and no reason either that there should be, in general, any such physical meaning. There are in fact several problems inherent in any endeavor to assigning such meaning to specific EOFs. R86 discusses a few of these problems. We briefly present some of the most important

1) It turns out that the shape and size of the space domain on which the EOFs are defined may impose a certain predictable pattern progression to the EOFs themselves, this being essentially due to their spatial orthogonality constraint. R86 calls these *domain shape dependence* and *sub-domain stability*, respectively A good parallel to this situation is the shape progression evident in most complete basis set of functions such as the Legendre polynomials on the real interval [-1,+1] or complex exponentials on the unit circle The EOFs can indeed be considered as another basis set with which to *optimally* represent a field on a *specific* domain. An enlightening example of the second problem is given by R86 where halving the domain produced two new sets of

[67]See, for example, Chapter 8 of Morrison (1976), where the model is derived using the fact that each successive EOF explains a maximum of the residual variance

EOFs, the union of which had very little to do with the set derived on the full domain

2) The extent of the time domain is itself important. Halving the time series can also produce two very different sets of PCs. This is related to the asymptotic convergence rate of the PCs, which can be fairly slow. In certain circumstances, especially when the *real* eigenvalues turn out to be very close to one another, the PCs may not converge at all

On the other hand there exist certain situations where the EOFs are precisely the normal modes of the physical system under study. North (1984) shows that this is the case for systems governed by linear Hermitian operators, driven by stochastic forcings uncorrelated in space and time. Smith (1987) extends the result to linear non-Hermitian operators (which include damped systems). He even establishes certain relationships between EOFs and a still slightly more general system's normal modes, through its covariance and cospectra

The relations between EOFs and the normal modes of a system are interesting but it may not be possible to establish similar relationships in more realistic situations. The lack of stability inherent in the patterns produced by the PC model is also quite bothersome. For these reasons, the direct physical interpretation of EOFs, except possibly for the first one, seems unadvisable. The model can still be very efficiently used as an optimum basis set, instead of other more classical expansions, and researchers such as Schubert (198[illegible]) [illegible] that there are ways around some of the interpretation problems mentioned above. R86 and Horel (1981) propose that the EOFs be rotated. We will come back to what this means after discussing the complex EOFs and certain statistical selection rules applicable to [illegible].

A 3 Complex EOF models

[illegible]

travelling sine wave is treated.

Example 1. Let us consider the continuous case so that we now have $z(x,t) = \sin(kx - \omega t)$. The symmetric covariance matrix Φ becomes

$$\Phi(x, y) = \frac{1}{2\pi} \int_0^{2\pi} \sin(kx - \omega t) \sin(ky - \omega t) \, dt$$

$$= \frac{1}{2} \cos k(y - x) ,$$

so that the eigenvalue problem then reduces to finding $(\alpha, q(y))$ pairs such that

$$\int_0^{2\pi} \cos k(y - x) \; q(y) \, dy = \alpha \, q(x) \; , \; \forall x \in [0, 2\pi].$$

Clearly, the only two such functions are then $q_1(y)=1/\sqrt{\pi} \sin(ky)$ and $q_2(y)=1/\sqrt{\pi} \cos(ky)$. These two EOFs explain the same amount of variance, $\pi/2$, but they are in quadrature. The PC corresponding to the EOFs clearly shows the link between the two components. This is a very simple situation where the two patterns are evidently linked to one another.

The following can even be used as a fairly good guide· situations where two EOFs approximately explain the same amount of variance and display this type of quadrature relationship are probably the signal of some travelling (or at least not evolving *in situ*) event and the two EOFs should then be linked. There are obviously other cases where the two extreme patterns may not be so easily linked, more so when quite a few components are retained as will invariably happen in our climate data. There is thus a need to be able to reliably identify the standing as well as the travelling patterns The complex EOF model provides a means to do this.

In this new case, the original data set is transformed so that the covariance matrix not only contains the amplitude information but also the phase information. What is needed is a quadrature image of the data. A Hilbert transform provides for just that. The ideal Hilbert transform will introduce no amplitude change but will shift each of the spectral time components by $\pi/2$. Now, suppose that $\tilde{z}_{ij}$ is the Hilbert transform of z_{ij} then

$$Z^c_{ij} = z_{ij} + i\,\tilde{z}_{ij} \qquad \text{where} \quad i = \sqrt{-1}\ ,$$

can be used to define a new complex covariance

$$\Phi = ((Z^c)^t)^* \, Z^c ,$$

the asterisk denoting complex conjugation. From then on, the complex procedure parallels the real case. Φ is now Hermitian instead of symmetric. This matrix is still positive definite and we again have a set of real positive eigenvalues, α_m. The fundamental difference is that their corresponding eigenfunctions, as well as their own associated PCs, are now complex, the real and imaginary fields providing for the two extreme situations of the (possibly) travelling patterns. Note that standing patterns are then characterized by the real and imaginary parts of the CEOF being equal to within a real multiplicative constant. The data reconstruction equation (A.2) then becomes

$$Z = Real\ (Z^c) = Real\left[\, F^t\ A^t \,\right] \qquad \text{(A.4)}$$

where the dimension of the complex A matrix is $(n \times r)$ and that of the complex F matrix is $(N \times r)$. The sign indeterminacy present in the EOFs becomes a phase indeterminacy in the CEOFs, for exactly the same reason.

> **Example 2.** As an example of CEOFs, we reconsider the previous travelling sine wave case. We will now find only one eigenfunction, the real and imaginary parts of which contain the sine and cosine functions produced by the real EOF model. In fact, extending the continuous notations to the complex case we find that [illegible] where [illegible]
>
> [illegible] and [illegible]
>
> The CEOF [illegible] and the corre[illegible]

sponding unique eigenvalue is $\alpha = 2\pi$. Notice that information on the spatial and temporal phases (and phase speeds) is now directly available from the CEOF model.

It should be noted that all of the problems discussed in the case of real data carry over to the complex case, so that here again a supplementary analysis step is required before any interpretation of the results is attempted. Luckily, as we shall see, the main rotation algorithms can also be adapted to the CEOFs

The only aspect of all this not covered completely in H84 deals with the complexification of the original data. Let us consider a Fourier expansion of the original data so that

$$z_{ij} = \sum_{k=-N/2}^{N/2} a_k(j) \cos(2\pi i k/N) + b_k(j) \sin(2\pi i k/N) \ , \ i = 1,2, \ \ldots \ , N$$

The analytic Hilbert transform of z_{ij} is then

$$\tilde{z}_{ij} = \sum_{k=-N/2}^{N/2} b_k(j) \cos(2\pi i k/N) - a_k(j) \sin(2\pi i k/N) \ , \ i = 1,2, \ \ldots \ , N$$

It is thus quite possible to construct $\tilde{z}_{ij}$ from the Fourier transform of the z_{ij}. Barnett (1983) does not recommend this procedure because of some of the problems in doing Fourier analysis on short (sampling) and/or noisy and/or discontinuous (Gibbs phenomenon) data sets Rather, he proposes the use of one of a family of digital Chebychev filters[68]. The main advantage of these filters is the following. Their amplitude response is very flat for the greater part of the frequency spectrum, even in the case of low order filters of this type, *i e* filters making use of a relatively small number of points. In addition, the same low order filters can still produce sharp frequency cutoffs, especially when compared to the more classical tapered filters. The only remaining problem is that we now have to operate on the original data as well, but with a second filter, one having as close as possible to the same amplitude response as the digital filter, but producing no

[68]See Hermann (1969)

phase shift. This is so that the real and imaginary parts of Z_{ij} be nearly analytic Hilbert transforms of one another. We now discuss how this second filter can be built from the first Chebychev filter.

Suppose that the coefficients[69] of the $(2K-1)$ Hilbert filter are the anti-symmetric[70] h_k for $k = \pm 1, \pm 3, \ldots, \pm(2K-1)$ so that we can define

$$\tilde{z}_{ij} = \sum_{k=-2K+1}^{2K-1} h_k \; z_{(i-k)j}$$

$$= \sum_{k=1}^{K} h_{2k-1} \; (z_{(i-2k+1)j} - z_{(i+2k-1)j})$$

Note that, as is always the case in such digital filters, $(2K-1)$ points are lost at each end of the time series. Moreover, there still is a trade-off between the sharpness of the frequency cut-off and this number of lost data points. We will come back to this before the end of the section.

Let us first consider the transfer function $Tr(h,\omega)$ of this first filter h, where the frequency ω goes from $-\pi$ to π. This function is simply the response obtained by applying the filter to a simple complex exponential function, i.e. $z_{kl} = e^{ik\omega}$. So, using the properties of h_k,

$$Tr(h,\omega) = \sum_{k=-2K+1}^{2K-1} h_k \, e^{-ik\omega} = -2i \sum_{k=1}^{K} h_{2k-1} \; \sin\,(2k-1)\omega$$

A plot of the amplitude of this last function, for $0 < \omega < \pi/2$, can be found in Fig. A1 (full curve), for the case where $K=10$. Note that, as we can see from the previous expression, this transfer function is symmetric about $\omega=\pi/2$, so that it again goes to zero at π, and it is also anti-symmetric about $\omega=0$. Since the filter we seek should not produce any phase shifts, we want that filter to be a symmetric filter, but also having much the same amplitude response as that found in Fig. A1.

---

[69] Again, see Hermann (1969) for tables of these coefficients.
[70] Note that $h_{2k} = 0$ and $h_{-k} = -h_k$.

The derivative of $Tr(h,\omega)$ with respect to ω seems to have some of the properties we want the transfer function of our second filter to display It is indeed quite flat, if maybe not quite as flat as $Tr(h,\omega)$, over much of the same spectrum range and it is a symmetric function. But, notice that its amplitude value at zero frequency is at a maximum instead of at a minimum. To correct this, we normalize this derivative by its value at zero frequency and subtract the new function from unity. The result is still symmetric, still quite flat but is now at a minimum at zero frequency The amplitude of this final function is the second (dashed) curve found in Fig A1 What we now have is the following transfer function $Tr(s,\omega)$

$$Tr(s,\omega) = \sum_{k=-2K+1}^{2K-1} s_k \, e^{-ik\omega} = s_0' + \sum_{k=1}^{K-1} 2s_{2k} \quad \cos 2k\omega \; .$$

This is then the transfer function of a symmetric[71] filter, the coefficients (s_0', s_{2k}, $k=1,\quad ,K-1$) of which are then defined, in accordance to the preceding discussion, in the following fashion

$$s_{2k} = -\frac{(2k+1)}{Sum} \left| \, h_{2k+1} \right| \; , \; s_0' = 1 + s_0 \text{ and } Sum = 2 \sum_{k=0}^{K-1} (2k+1) \; h_{2k+1}$$

To recapitulate, the normalized derivative of the transfer function of the original Chebychev filter is the transfer function of this second one. Now, since it is symmetric and positive definite, the new filter does not produce phase shifts and its output is such that it forms an Hilbert transform pair with the output of the first filter

In any event, the responses of these two filters are dependent on the number of points we can afford to loose. The two filters presented in Fig. A1 would cost 2×(2K-1)=38 timesteps if we chose to use them To place this into a more practical context, this cost can indeed be considered quite small if, for example, we intend to apply these filters to our model data set, which contains close to 10000 time samples (i e 20 simulated years) On the other hand, their frequency cutoffs are such

[71]Note also that $s_{(2k+1)} = 0$.

that periods longer than 19 and 2[illegible] days, respectively, would then be missing (in part or in full) in the resulting real and imaginary parts of the newly constructed complex data. As we want to investigate persistent atmospheric and modelled phenomena, an implicit low-frequency filtering of this order is not at all acceptable. The amplitude responses of these two real and imaginary filters, once they have reached unity, deviate from it by only three and one percent, respectively.

We do have other alternatives to the previous filters. Hermann (1969) gives the filter coefficient of a wide range of Hilbert filters. The (K = 35) filter is the highest grade filter he provides. Using this filter and its corresponding real filter, we stand to loose a total of 2×69 timesteps, but the low-frequency filtering now stops at (more tolerable) periods of 36 and 41 days for the real and imaginary parts of the modelled complex data, respectively. These two new filters are also two orders of magnitude flatter than their (K = 10) counterparts.

A.4 An EOF selection rule

By their very nature, the higher order EOFs, those explaining very little of the total variance, tend to acquire noise-like features and they or their associated PC may indeed be indistinguishable from random processes. It is thus important to select only the EOFs (or CEOFs for that matter) containing significant information. There are several ad hoc criteria that attempt to do this. The so-called Guttman criterion whereby any EOF explaining less than the typical variance of an individual variable is dropped, is one of those. [illegible] equivalent criterion could be used to retain all of the most important EOFs until their cumulative explained variance reaches a sufficiently large percentage, say 90% or 95%, of the total.

While it is probably [illegible] the Guttman criterion, [illegible] EOFs are free of random [illegible] selection rules of EOFs [illegible] tails. These rules are [illegible] sumption made in the first one, the *Dominant-Variance Rules*, is that a non-random signal will account for a larger proportion of variance than will a random one. The eigenvalue curve will then show some kind of a break when one type of behavior stops and the other starts. This turns out to be a much more severe or rigorous set of rules than the Guttman criterion, even though what the user is given by both is essentially a cutoff value.

The second set of selection rules, the *Time-History Selection Rules*, assumes that the time behavior should be tested instead of the variance. From PZB, pp. 112

> "(· ·) it is not enough to look only at the variance of the data set, some examination of the time variations producing the variance must be made; for it is possible that somewhere in all the fury that signifies nothing, there may be a quiet voice that is saying something informative. (· · ·)"

Indeed, we see no obvious reason why the (EOF or CEOF) model components containing physical information have to explain the largest amount of total variance.

Some type of random behavior is selected and the EOFs or PCs, depending on which carries the time dependencies, are then tested against them. Let us assume henceforth that the PCs are to be tested. PZB generally suppose their random *fury* to be white noise processes, but we have also assumed them to be red noise in certain cases discussed in Chapter 3.

We use PZB's selection *Rule* ***Q***, modified according to their own suggestion. The following paragraphs present some of the theoretical basis for this selection rule. The rule assumes that a PC can be separated as $f_m(t) = \zeta_m(t) + \epsilon_m(t)$, where $\zeta_m(t)$ is the (physical part of the) signal and $\epsilon_m(t)$ is white noise drawn from a Gaussian $N(0,1)$ for each t. This rule is applied with the null hypothesis that $f_m(t)$ is itself a random sample from a one dimensional Gaussian population, i.e. there is no (physical) signal. Under this hypothesis, the serial correlation function $r_m(\ell)$ of $f_m(t)$ will be distributed in a known fashion. In fact, if

$$r_m(\ell) = \frac{\sum_{t=\ell+1}^{N} r_m(t)\; r_m(t-\ell)}{\sum_{t=1}^{N} r_m^2(t)}$$

then, the $r_m(\ell)$, $\ell = 1, \ldots, k \ll N$ turn out to be uncorrelated and

$$Q_m = N(N+2) \sum_{\ell=1}^{k} (N-\ell)^{-1}\, r_m^2(\ell)$$

is approximately distributed as a χ^2-variate with k degrees of freedom This follows from the fact that, for all practical purposes and under the null hypothesis, $r_m(\ell)$ is normally distributed with zero mean and approximate[72] variance $1/N$ If Q_m is sufficiently large, the underlying PC is deemed to display un-random characteristics and the null hypothesis is then rejected

This selection algorithm can be easily adapted to the complex domain If a complex PC displays random behavior, one or both of its components, the real and imaginary, will also do so The procedure will then test these latter separately and the null hypothesis has to be rejected for both of them in order for the PC to be retained for further analysis

In addition to *Rule Q*, a variant of the Guttman criterion is also applied to the data, namely the variation previously suggested at the beginning of this sub-section This can be considered as a very poor man's *Dominant-Variance Rule* so that both types of rules are then taken into account

We now turn to the next part of this appendix, dealing with loading factor linear transformations or rotations

[2]See Priestley, p. [illegible] for more details on this

A.5 EOF (or CEOF) rotations

It is probably worthwhile to recapitulate some of the material covered up to now in this appendix. We have seen that the EOFs or their associated factor loadings are the most efficient basis to represent the variance contained in a data set. On the other hand, those same patterns are nothing more than a basis set. It is usually quite inappropriate to assign physical meanings to any of the individual fields in that set, except maybe in a limited way, to the first one[73] As an example of the problems inherent in this endeavor, let us just mention that the mutual orthogonality constraints, imposed by the EOF model on both the PCs and the EOF themselves, ensures that the variable patterns display quasi-predictable shape progressions. Several other problems have also been noted. It may still be tempting to use the eigenfunctions in some kind of physical interpretation. When would this be possible? We generally hope that the physically understandable structures underlying the variance of the data set are in some fashion simple ones. And also, that there are a limited number of them When these two conditions hold, there may be statistical techniques whereby the researcher can obtain the desired simple structures from an equally limited set of EOFs.

With this in mind, let us consider the review article of R86 where the author discusses in some detail EOF rotations, their underlying theory and applications. H84 does not go as deeply, limiting himself to the more widely used VARIMAX algorithm, but he extends rotations to the complex models Fortunately, his example is sufficiently comprehensive that it can be used to adapt other (perhaps more appropriate) rotation algorithms from the real to the complex realm We will proceed to discuss (again briefly) the basic assumptions behind rotations, their strengths and some of their pitfalls, especially as they relate to the algorithms we use.

The basic assumption made in this type of analysis is that there exist, contained in the data, some *simple structures*[74], a combination of

[73] As it is the only one not constrained by any orthogonality constraints.

which manages to explain a great deal of the total variance. A second assumption is that these structures can be obtained by linearly combining a subset of the loading factors derived from the covariance matrix of the data set. The total variance explained by the set of modified functions is constrained to be the same as that of the original set of empirical functions. The loading factors are thus used as the original basis set with which to re-construct the physical signal contained in the *simple structures*.

From the preceding paragraph, it may already be evident that the loading factor selection principles are critical to this simplifying process. If functions containing very little "physical" information are retained at the selection step, the variance they explain will be spread out over a wide range of new structures, masking their simplicity. In the present context, remembering the discussion on the EOF selection rules in a previous section, we seek non-random signals. The physical events in which we are interested are indeed known to be strongly persistent. For these reasons, it is quite out of the question to use the complete EOF set, and some preliminary selection algorithms have to be employed, such as those already discussed.

Let us now reconsider the EOF model of equation (A.2) and how it can be modified while still retaining its informational content. There are in fact an infinity of other (F,A) pairs satisfying this model equation. Indeed, let T be any non-singular $(r \cdot r)$ matrix (often called a rotation). Then, if we define $\tilde{A}=AT$ and $\tilde{F}=F(T^t)^{-1}$, then

$$Z' = F\,(T^t)^{-1}\,T^t A^t = (F\,(T^t)^{-1})\,(A\,T)^t = \tilde{F}\,\tilde{A}^t$$

and also

$$\Phi' = \tilde{A}\;\tilde{S}\;\tilde{A}^t, \qquad (A.5)$$

where $\tilde{S}=(T^tT)^{-1}$. When T is normalized in a manner such that the diagonal elements of $\tilde{S}$ are all ones, the latter matrix is in fact the correlation between the column elements of [illegible] between the new or after[illegible]

---

*An expression coined by Thurstone [illegible] who developed a set of five geometric criteria to help ensure that the new structures be more easily interpretable.

native principal components. In the case of the original EOF model, this correlation matrix is the identity matrix and the last expression in (A.5) is then the rotated equivalent to the last expression of equation (A.3) Using the matrix $\tilde{S}$, we can derive a general expression for the variance accounted by the new rotated components, *i e* by the columns of $\tilde{A}$. Indeed, it can be very easily shown that

$$Trace(\ \Phi'\ ) = Trace(\ \tilde{A}^t\ (\tilde{A}\ \tilde{S})\ )$$

and that the diagonal elements of the right-hand matrix are in fact the contributions of the individual components to the total variance When $\tilde{S}$ is the identity matrix, the rotated components are orthogonal and the total variance is then the sum of the individual variances.

These new matrix expressions, $\tilde{A}$ and $\tilde{F}$, contain the same information as the original EOF model and indeed, can be used to represent the data as efficiently as the original A and F matrices. What distinguishes the new model from the old? The first point is that the original model components are indeed unique, but only in that both the principal components and loading factors form orthogonal sets, *i.e.* A and F are two orthogonal matrices This means that the different PCs and EOFs are mutually un-correlated. This property is not preserved by any of the non-trivial T transformations, as the $\tilde{A}$ matrix is then no longer orthogonal[75] Some form of orthogonality is preserved when T is itself orthogonal, as the $\tilde{F}$ matrix then remains orthogonal, so that the new PCs are still un-correlated. We have already discussed how the orthogonality inherent to the EOF model hinders its interpretability In view of this, the loss of this property may be quite acceptable, and perhaps even desirable. $\tilde{A}$ is called either the *PC loading matrix* or the *primary pattern matrix* depending on whether T is orthogonal or not.

The second point is that the transformations T can be chosen such as to provide an algebraic approximation to the classic *simple structures* criterion set, *i e* the $\tilde{A}$ matrix is somehow simpler than the origi-

75Since $\tilde{A}^t\tilde{A} = (AT)^tAT = T^t\ (\alpha I)\ T \neq \beta I$, where both αI and βI are diagonal $(r\times r)$ matrices, as in equation (A 3).

nal *A*. R86 examines several packaged algorithms that do just that He shows that all of them work quite satisfactorily when strong simple structures are inbedded in the data, but that the non-orthogonal, *i e* oblique, packages will consistently give more reliable answers than the orthogonal[76] ones. The reliability of all of the packages is reduced in the cases when the strength of the structures is either moderate or weak. In the moderate cases, it turns out that only the oblique algorithms still provide useful answers. Finally, in the weak cases, none of the rotation packages perform well and rotation should not really be considered when one has reasons to believe that this situation prevails In the cases of interest to us, that of moderate to strong persistent events, this latter should not occur.

There is an obvious question that has not yet been considered and that is "What then is a *simple structure*?" Let us now do so As a first (and useful) approximation, simpler here means more regional In the case of the spatial EOFs produced by the time-variance approach, this will indicate that the algorithms search for a combination of regional patterns explaining most of the time variance over their limited geographical area. When, for example, the cases and variables consist of the monthly means of the 50 kPa streamfunctions, the rotated EOFs bear a striking resemblance to the so called teleconnection patterns, as documented by Horel (1981) A problem may occur when some of the real underlying features, the ones "hidden" in the data, extend over the whole space domain The rotations may then attempt to represent the full pattern into a few recognizable but disjoint sub-patterns

An alternative approach is to rotate the EOFs of the *space-variance* approach. These are then timewise EOFs obtained by replacing the Z matrix by its transpose $Z''=Z^t$ in equation (A 2) The transformation will output patterns that are isolated in time rather than isolated in space The associated transformed PCs contain the spatial distributions and these latter are no longer constrained to be regional Depending on the type of rotations, though, they may still be mutually orthogonal, in

[76] The only orthogonal transformation retained by R86 is the most widely used VARIMAX

which case interpretation can still prove to be difficult. Again, this is not the case with oblique transformations. As an example, with data consisting of (timewise) persistent events, the rotated PCs could then reproduce the several normalized[77] types of events.

There is yet another aspect of *simple structures* analysis that needs to be stressed. The fewer patterns that are important locally (in time or in space, depending on the nature of the EOF model), the better. Ideally, a single pattern would explain nearly all of the variance over its specific space/time region. A situation where several regional patterns are necessary to explain this variance is by definition not a simple one and the hypothesis under which the rotation algorithms operate does not really hold The validity of the results is then open to question. Either another type of transformation is required or no transformation should be attempted. In view of this, care has to be taken to check the extent to which the transformed data conform to a certain ideal of simplicity. That is why R86 suggests that all of the primary patterns (or loading factors) be examined in pairwise graphical fashion, using scatter plots of one primary pattern versus another. The coordinates of the points contained in each plot are then the amplitudes of the patterns that we want to compare, and each point in turn corresponds to an individual variable.

One is then able to establish the extent to which the variables project on more than one pattern, *i.e* their ***simplicity*** or lack thereof As more or fewer of the points tend to gather along one of the axes of the scatter plots, the transformation can also be deemed more or less successful Conversely, plots presenting thinly spread out clouds of points are the sign that the rotation did not succeed in identifying the possible *simple structures*. In the latter case, the effect of the transformation may not be any different from applying any other randomly chosen matrix T to the original loading factor matrix A

Everything we have so far stated with respect to the rotation of

[77]Indeed, the surface mean of each PC is then constrained, by construction, to be one

real loading factors also applies to their complex equivalent. H84 gives indications on how to modify the (*VARIMAX*) IMSL source routine OFROTA so that it works in the complex realm. This is a fairly simple task as the routine essentially maximizes a quantity depending only on the squared amplitudes of the rotated loading factors The transformation matrix remains real Since the transformation output of the *VARIMAX* algorithm is orthogonal, we may wish to use another (oblique) transformation R86 establishes that the better of the real domain packaged rotations seems to be the (*PROMAX*, $K=2$ or 4) algorithm This is done by the IMSL source routine OFPROT Here again the modifications from the real to the complex cases are fairly straightforward, and we discuss them next

The name *PROMAX* comes from the fact that the method uses a mixture of *PRO*crustes target rotation and one of the more common orthogonal rotations, for example, vari*MAX* or equi*MAX* The point is that the orthogonal rotation (hopefully) provides nearly the right answers. The Procrustes step is then viewed as a type of correction The method solves the following equation for T, in a least squares fashion,

$$B = AT + E \text{ such that } \frac{\partial}{\partial T} Trace\ (E^t E) = -2A^t B + 2AT = 0 \qquad (A\ 6)$$

We can then obtain from this that $T = (A^t A)^{-1} \quad A^t B$

A is as before and the target B as well as the residual E are $(n \times r)$ matrices How B is found illustrates the manner in which *simple structures* can be approximated algebraically The matrix B is essentially derived from the loading factors of the orthogonal rotation part of the *PROMAX* algorithm Let $A'=(AT')$ be one such (orthogonally) rotated loading factor matrix, i e. T' is itself an orthogonal (varimax or equimax) linear transformation on A The target is then obtained by modifying the patterns found in A' so as to emulate more closely the *simple structure* ideal The large amplitude values of A' are changed by relatively small amounts, while the medium and small values become smaller still For a *PROMAX* with $k=K_0$, each point in a column (or pattern) of A' is multiplied by its own amplitude raised to the power (K_0-1) and then normalized so as not to change the maximum value of the pattern Thus, the sign of a variable pattern is not changed, only its amplitude.

The transformation T that verifies both parts of (A.6) is then the one for which the amplitudes of the column vectors of the residual matrix are at a minimum, i.e $\tilde{A}=AT$ is as good an approximation of B as can be found using linear transformations As a final step, once the PROMAX transformation T has been found, it is normalized so that the auto-correlation of the resultant transformed principal components be unity[78].

The principal required modifications to use this algorithm on complex EOFs are the following:

$$T = \frac{1}{2} \left((A^t)^* A \right)^{-1} \left((A^t)^* B + (A^t) B^* \right)$$ and any other

expression of the type $A\,B$ become $A^* B + A\,B^*$,

where the asterisk * still denotes complex conjugation and A and B are now $(n \times r)$ complex matrices. As we have seen, the algorithm seeks to find an extremum value for a set of squared quantities and thus the theory behind it carries over exactly when these expressions are replaced by the square modulus of the corresponding complex expressions The T transformation matrix is again real.

A.6 Data projection - Alternate data sets

A final note on orthogonal and oblique transformations is necessary We have commented on the fact that for most purposes the oblique rotations should in principle be preferred to the orthogonal rotations On the other hand, there are situations where either an orthogonal rotation or no rotations at all is to be desired rather than an oblique one These arise when the PCs or else the EOFs themselves are to be used as basis upon which to project another data set, either a completely independent set from the one used to derive the EOF model itself or even a simply more extensive set. The orthogonality property then becomes an

[78] That means that if $G=F(T^{-1})^t$, then $(G^tG/N)_{ii} = 1, \forall\, i = 1, 2, \ldots, r$

asset in determining a new set of model parameters. Otherwise, the use of a non-orthogonal basis set in this context can force us to take into account the correlation information between the different spatial or temporal components, inverting a matrix of the same order as the number of basis components.

Let us suppose that we have a new data set W that can be represented as a $(N \times n)$ matrix where, as before, N indices the time variations and n indices the space variations. For a given general r element basis B (one consisting of several meaningful spatial patterns), we seek to find (timewise) projection coefficients H and residuals R, respectively $(N \times r)$ and $(N \times n)$ matrices, such that the following holds

$$W = HB^t + R \quad \text{and} \quad \frac{\partial}{\partial H} \, Trace\,(R^t R) = -2WB + 2H\,B^t B = 0 \qquad (A.7)$$

We then immediately have that $H = WB\,(B^t B)^{-1}$

The part in parenthesis of the last equation is the required correlation matrix information. When the basis elements (i.e. the columns of B) are orthonormal this part reduces to the $(r \times r)$ identity matrix I. In that case, $H = WB$, a result that also obtains when we replace the quadratic condition in (A.7) by a simpler linear condition in which R and H are only required to be mutually orthogonal, i.e. $RB = 0$. When dealing with an REOF model, we have seen that the transformation matrix Γ can provide us with the temporal correlation information, as defined by the matrix $\tilde{S}$ in equation (A.5). But what is needed here are the spatial correlations and those are found in yet another matrix.

There is yet another alternative that combines some if not most of the advantages of both the orthogonal and oblique cases at little extra cost. Let us consider a situation where it would be desirable to obtain the projection matrix H of a particular data set W onto an oblique *primary pattern matrix* $\tilde{A}$. Suppose that we have on hand the transformation matrix Γ. The diagonal matrix (aI) of the variance accounted by each of the original (un-rotated) loading factor matrix A is easily found from the factors themselves. If these two matrices are available, we can make use of the underlying spatial orthonormal basis available here, namely the matrix B of the eigenvectors of the original covariance matrix. Once the projection H' with respect to this basis is known, we only have to remember that $A = B\sqrt{\alpha I}$, so that

$$\left.\begin{aligned} H' B^t &= H' (\sqrt{\alpha I})^{-1} A^t = H' (\sqrt{\alpha I})^{-1} (T^t)^{-1} T^t A^t \\ &= H' (((\sqrt{\alpha I})T)^t)^{-1} (AT)^t = H' (\tilde{T}^t)^{-1} (AT)^t = H \tilde{A}^t \end{aligned}\right\} \quad \text{(A 8)}$$

where $\tilde{T}=((\sqrt{\alpha I})T)$ is the transformation matrix that goes from B to $\tilde{A}$ and $H=H'(\tilde{T}^t)^{-1}$ is the desired projection matrix

As an example, if we were to simply extend in time the original data set Z to a more complete W, the new projection H would under this formulation keep their old values over the Z part of W. The philosophy behind this is that the information on the modes of $\tilde{A}$ is contained implicitly in (αI) and B and any projections onto the latter basis can thus be interpreted as projections onto the former while retaining the orthogonality properties of the latter The lines of the residual matrix R are now orthogonal to the subspace generated by the B column ensemble, so that they are also orthogonal to the columns of $\tilde{A}$, *i e* the REOFs

This concludes the *Methodology* Appendix A Any other required mathematical concept will be discussed in the main body of the text as it arises

Appendix B

Annual cycle filtering

A surprisingly simple result has come to our attention while considering the effect of determining the annual cycle signal by the so-called *box* method. Briefly, with this method, we assign each calendar day to a box. Every datum of a calendar day over the course of a multi-year time series is then added to the content of its box. The final content of each box is averaged to determine the annual cycle.

One of the advantages of this method of defining the mean annual cycle is that it does not require continuous data. This is quite appreciable when dealing with atmospheric observations which frequently have missing time segments. But an apparently little known side-effect of the method has also to be considered. It seems that while effectively (and correctly) identifying the annual frequency components of the time series on which it is applied, the *box* method will as well do so for every sub-harmonic of these same annual components.

When the annual cycle calculated from the box method is subtracted from the original data and if, for example, that data consist of a five-year segment of observations, every fifth frequency components of the resulting *anomaly* data set will thus be put to zero. This can be quite severe if, for example, the *anomaly* energy spectrum happens to be approximately distributed as either a red or white noise process (as often seems to be the case). In either of these situations, we could expect that roughly 20% (i.e. one out of every fifth components) of the anomaly energy would be erroneously eliminated.

To see why [illegible] consider an [illegible] component [illegible] fou[illegible] [illegible] will assume that there are [illegible] the data [illegible]

This assumption only simplifies the proof as [illegible] could as easily have been supposed [illegible] function of [illegible] in which case a cosine [illegible] expansion would then have followed.

$$f(t) = \sum_{i=1}^{N} a_i \sin it, \tag{B.1}$$

where $t \in [0, 2\pi]$ and N/M is an integer

We know, from its definition, that the annual cycle $f_a(t)$, obtained when the *box* method is applied to f, can then be written as:

$$f_a(t) = \frac{1}{M} \sum_{j=1}^{M} f(t + T_j), \tag{B 2}$$

where $T_j = 0, \frac{2\pi}{M}, \ldots, \frac{2\pi(j-1)}{M}, \ldots, \frac{2\pi(M-1)}{M}$ and $t \in [0, 2\pi/M]$. This cycle repeats itself M times from 0 to 2π

Inserting (B 1) into (B 2) and using the usual trigonometric identity for the sine of a sum of angles, we obtain an expansion for f_a in terms of a double sum in i and j of sine and cosine functions. This expression can be formally rewritten as $\sum_{i=1}^{N} a_i g_i(t)$. We can now consider two separate cases. The first is when $i=kM$ for any $k=1,2, \ldots, N/M$. Then

$$g_i(t) = \frac{\sin it}{M} + \frac{\sin it}{M} \sum_{j=2}^{M} \cos (j-1)\, 2\pi k + \frac{\cos it}{M} \sum_{j=2}^{M} \sin (j-1)\, 2\pi k = \sin it$$

since the terms of the first summation are all ones and those of the second are all zeroes

The second case corresponds to all the other values of i, i.e. when $i \neq kM$. Obviously, the g_is are then again made of the same type of expression as in the previous case, except that the two trigonometric summations now have arguments that range from $2\pi i/M$ to $2\pi i(M-1)/M$ with increments of $2\pi i/M$. By simple symmetry reasoning, the first summation can be seen to equal -1, while the second is again zero. For example this result is trivial if $M=2$ and $i=3$. Let us then consider the more general situation where M and i are only supposed to be *even* and *odd* numbers, respectively. The middle of the argument range is then πi for which the cosine and sine values are -1 and 0, respectively. As well, the other terms in the cosine summation are related through

$$\begin{aligned} \cos 2\pi i/M &= \cos 2\pi i\,(M-1)/M = \cos 2\pi i\,(1.0 - 1/M) \\ &= -\cos 2\pi i\,((M/2)/M - 1/M) = -\cos 2\pi i\,(0.5 - 1/M) \\ &= -\cos 2\pi i\,((M/2)/M + 1/M) = -\cos 2\pi i\,(0.5 + 1/M) \end{aligned}$$

so that the first and last values cancel the first values bracketing the middle value. This can be obviously extended to the second and second to last values cancelling the second to middle and second after middle values, and so on. The same type of reasoning takes care of the sine summation. The other valid combinations of M and i are similarly evaluated. The immediate result is that $g_i(t)=0$ if $i \neq kM$.

The function $f_i(t)$ is thus exclusively made of all the Mth spectral components of $f(t)$, which proves the result and ends this appendix.

Bibliography

Austin, J F., 1980· The blocking of middle latitude westerly winds by planetary waves *Quart. J. R Met Soc*, **106**, 327-350

Baines, P G , 1983 A survey of blocking mechanism, with application to the Australian region *Aust Met Mag.*, 31, 27-36

Barnett, T M , 1983. Interaction of the Monsoon and Pacific trade wind system at interannual time scales Part I The equatorial zone *Mon Wea Rev*, **111**, 756-773

Barnston, A G , and R E. Livezey, 1987 Classification, seasonality and persistence of low-frequency atmospheric circulation patterns *Mon Wea Rev*, **115**, 1083-1126

Berestov, A L , 1981 Some new solutions for the Rossby solitons *Izm Atm Oceanic Phys*, 17, 60-4

Berggren, R , B Bolin and C -G Rossby, 1949 An aerological study of zonal motions, its perturbations and break-down *Tellus*, 1, 14-37

Blackmon, M L , S L Mullen and G T Bates, 1986 The climatology of blocking events in a perpetual january simulation of a spectral general circulation model *J Atmos Sci*, 43, 1379-1405

———, Y H Lee and J M Wallace, 1984 Horizontal structure of the 500 mb heights fluctuations with long, intermediate and short time scales *J Atmos. Sci* 41, 961-979

———, 1976 A climatological spectral study of the 500 mb geopotential height of the Northern Hemisphere *J Atmos Sci.*, **33**, 1607-1623

Boer, G.J , 1989 Concerning the response of the atmosphere to a tropical sea surface temperature anomaly. *J Atmos Sci*, **46**, 1898-1921

———, N A McFarlane, R Laprise, J Henderson and J -P Blanchet, 1984a The Canadian Climate Center spectral atmospheric general circulation model *Atmosphere-Ocean*, 22, 397-429

———, ——— and ———, 1984b The climatology of the Canadian Climate Center general circulation model as obtained from a five-year simulation *Atmosphere-Ocean*, 22, 430-473

Ceheleski, P , and K.K Tung, 1987 Theories of multiple equilibria and weather regimes A critical reexamination of baroclinic two-layer models. *J Atmos. Sci* , **44**, 3282-3302

Charney, J G , J Shukla and K C Mo, 1981 Comparisons of a barotropic blocking theory with observations *J Atmos Sci* , **38**, 762-779

——— and J G DeVore, 1979 Multiple flow equilibria in the atmosphere and blocking *J Atmos Sci* , **36**, 1205-1216

——— and P G Drazin, 1961 Propagation of the planetary scale disturbances from the lower to the upper atmosphere *J Geophys Res* **66**, 83-109

——— and A Eliassen, 1949 A numerical method for predicting the Perturbations of middle latitude Westerlies *Tellus*, **1**, 38-54

Derome, J , 1984 On quasi-geostrophic, finite-amplitude disturbances forced by topography and diabatic heating *Tellus*, **36A**, 313-319

Dionne, P , H L Mitchell and J Derome, 1988 On the resonance of an external planetary wave and its interaction with the mean zonal flow *Tellus*, **40a**, 177-187

Dole, R M , 1987 Development of persistent anomalies In the Lecture Notes of the Summer colloquium on the *Dynamics of Low Frequency phenomena in the atmosphere*, Vol 1, NCAR

———, 1986 Persistent anomalies of the extratropical Northern Hemisphere wintertime circulation Structure *Mon Wea Rev* , **114**, 178-207

———, and N D Gordon, 1983 Persistent anomalies of the extratropical Northern Hemisphere wintertime circulation Geographical distribution and regional persistence characteristics *Mon Wea Rev* , **111**, 1567-1586

———, 1982 Persistent anomalies of the extratropical Northern Hemisphere wintertime circulation Ph D Thesis, M I T , 226 pp

Dugas, B and J Derome, 1986 Le maintien du tourbillon des ondes planétaires stationnaires *Atmosphere-ocean*, **25**, 60-81

Egger, J , 1978 Dynamics of blocking highs *J Atmos Sci* , **35**, 1788-1801

Essenwanger, O M , 1986 *General Climatology, 1B - Elements of statis-*

tical analysis. Elsevier ed , Amsterdam/New York, pp.424

Fjortoft, R , 1953· On the changes in the spectral distribution of kinetic energy for two-dimensional, non-divergent flow *Tellus*, **5**, 225-230

Flierl, G.R , 1979· Baroclinic solitary waves with radial symmetry *Dyn Atmos Oceans*, 3, 15-38

———, V.D. Larichev, J C McWilliams and G M Reznick, 1980 The dynamics of baroclinic and barotropic eddies *Dyn Atmos Oceans*, 5, 1-41.

Frederiksen, J.S , 1989· The role of instability during the onset of blocking and cyclogenesis in the northern hemisphere synoptic flows *J Atmos Sci* , **46**, 1076-1092

Frederiksen, J S , 1983 The onset of blocking and cyclogenesis Linear theory *Aust Met. Mag* , 31, 15-26.

Gravel, S , 1989· Periodic and stationary solutions to a forced-dissipated barotropic model of the atmosphere Ph D Thesis, McGill University, YYY pp

Green, J S A , 1977 The weather during July 1976 Some dynamical considerations of the drought *Weather*, 32, 120-126

Haines, K , and J Marshall, 1987· Eddy-forced coherent structures as a prototype of atmospheric blocking *Quart J R Met Soc* , **113**, 681-704

Hartman, D L , and S J Ghan, 1980 A statistical study of the dynamics of blocking *Mon Wea Rev* , **108**, 1144-1159

Hasselman, K., 1988. PIPs and POPs - The reduction of complex dynamical systems using principal interaction patterns and principal oscillation patterns. *J Geophys Res* , **93**, 11015-21

Held, I M , 1983 Stationary and quasi-stationary eddies in the extratropical troposphere Theory Chap 6 of *Large scale dynamical processes in the atmosphere*, B J Hoskins and R P Pierce eds , Academic Press, 127-168

Hermann, O , 1969 Transversal filter for Hilbert-transformation *Arch Elektr Ubertragung*, 23, 581-587

Hirst, A C and E T. Linacre, 1981 Trends in the blocking of high-pressure systems in the Australian region *Search*, 12, 409-11

Horel, J D , 1984 Complex principal components theory and examples

J. Clim. Appl. Meteor., **23**, 1660-1673.

———, 1981: A rotated principal component analysis of the interannual variability of the Northern Hemisphere 500 mb height field. *Mon. Wea. Rev.*, **109**, 2080-2092.

Hoskins, B. J., and P. D. Sardeshmukh, 1987: A diagnostic study of the dynamics of the northern hemisphere winter of 1985-6. *Quart. J. R. Met. Soc.*, **113**, 759-778.

———, I. N. James and G. H. White, 1983: The shape, propagation and mean-flow interaction of large-scale weather systems. *J. Atmos. Sci.*, **40**, 1592-1612.

——— and D. J. Karoly, 1981: The steady linear response of a spherical atmosphere to thermal and orographic forcing. *J. Atmos. Sci.*, **38**, 1179-1196.

———, A. J. Simmons and D. G. Andrews, 197[illegible]: Energy dispersions in a barotropic atmosphere. *Quart. J. R. Met. Soc.*, **103**, 553-567.

Hsu, H. H. and J. M. Wallace, 1985: Vertical structure of wintertime teleconnection patterns. *J. Atmos. Sci.*, **42**, 1693-1710.

Illari, L., 1984: A diagnostic study of the potential vorticity in a warm blocking anticyclone. *J. Atmos. Sci.*, **41**, 3518-3526.

——— and J. C. Marshall, 1983: On the interpretation of eddy fluxes during a blocking episode. *J. Atmos. Sci.*, **40**, 2232-2242.

Jarraud, M., 1986: Sensitivity of the operational ECMWF model to horizontal resolution. ECMWF workshop on *Predictability in the medium and extended range*, March 1986, 109-154.

Kalnay-Rivas, E. and L.-O. Merkine, 1981: A simple mechanism for blocking. *J. Atmos. Sci.*, **38**, 2077-2091.

Karoly, D. J., 1983: Atmospheric teleconnections, forced planetary waves and blocking. *Aust. Met. Mag.*, **31**, 51-56.

Knox, J. L. and J. E. Hay, 1984: Blocking signatures in the Northern Hemisphere: Rationale and Identification. *Atmosphere-Ocean*, **22**, 36-47.

Kuo, H.-L., 1949: Dynamical instability of two-dimensional nondivergent flow in a barotropic atmosphere. *J. Meteor.*, **6**, 105-122.

Kushnir, Y., 1987: Retrograding wintertime low-frequency disturbances over the North Pacific ocean. *J. Atmos. Sci.*, **44**, 2727-2742.

Lambert, S. J., 1987: Spectral energetics of the Canadian Climate Center

GCM *Mon. Wea. Rev*, **115**, 1295-1304.

Lau, N.-C., and M J. Nath, 1987: Frequency dependence of the structure and temporal development of wintertime tropospheric fluctuations - Comparisons of a GCM simulation with observations. *Mon Wea Rev*, 115, 251-271

——— and F O Holopainen, 1984: Transient eddy forcing of the time-mean flow as identified by geopotential tendencies. *J. Atmos Sci*, **41**, 313-328

———, 1981 A diagnostic study of recurrent meteorological anomalies appearing in a 15-year simulation with a GFDL general circulation model *Mon Wea Rev*, **109**, 2287-2311.

———, 1979 The observed structure of tropospheric stationary waves and local balances of vorticity and heat *J Atmos Sci*, **36**, 996-1016

Legras, B and M Ghil, 1985 Persistent anomalies, blocking and variations in atmospheric predictability *J Atmos. Sci.*, **42**, 433-471

Leith, C E, 1983 Predictability in theory and practice Chap.13 of *Large-Scale Dynamical Processes in the Atmosphere*, B.J Hoskins and R P Pierce eds, Academic Press, 127-168.

Lejenas, H, 1987 A comparative study of Southern Hemisphere blocking during the global weather experiment *Quart J R Met. Soc.*, 113, 181-188

——— and H Økland, 1983 Characteristics of Northern Hemisphere blocking as determined from a long time series of observational data *Tellus*, **35A**, 350-362.

McFarlane, N A, 1987 The effect of orographically excited gravity wave drag on the general circulation of the lower stratosphere and troposphere *J Atmos. Sci.*, **44**, 1775-1800.

McWilliams, J C, G R Flierl, V D Larichev and G M. Reznik, 1981: Numerical studies of barotropic modons. *Dyn. Atmos Oceans*, 4, 261-294

———, 1980 An application of equivalent modons to atmospheric blocking *Dyn Atmos Oceans*, 5, 43-66

Malanotte-Rizzoli, P, and P Malguzzi, 1987: Coherent structures in a baroclinic atmosphere Part III Block formation and eddy forcing. *J. Atmos. Sci.*, **44**, 2493-2505

———, 1984: Boundary forced nonlinear planetary radiation *J Phys. Oceanogr.*, **14**, 1032-1046.

Malguzzi, P., and P Malanotte-Rizzoli, 1985 Coherent structures in a baroclinic atmosphere. Part II: A truncated model approach *J Atmos. Sci.*, **42**, 2463-2477.

——— and ———, 1984 Nonlinear stationary Rossby waves on nonuniform zonal winds and atmospheric blocking Part I: The analytical theory *J. Atmos Sci.*, **41**, 2620-2628.

Mitchell, H L. and J Derome, 1983: Blocking like solutions of the potential vorticity equation. Their stability at equilibrium and growth at resonance J Atmos Sci, 40, 2522-2536

——— and ———. 1985 Resonance of topographically forced waves in a quasi-geostrophic model J Atmos Sci., 42, 1653-1666

Morisson, D F , 1976 *Multivariate statistical methods*, 2nd ed , McGraw-Hill, New-York, 415 pp.

Mullen, S L., 1987: Transient eddy forcing of blocking flows *J Atmos. Sci.*, **44**, 3-22.

Mullen, S L , 1895: On the maintenance of blocking anticyclones in a general circulation model. Ph D. Thesis, University of Washington and NCAR Cooperative thesis No 86, 261 pp

Nicholls, N , 1987 The use of canonical correlation to study teleconnections *Mon Wea Rev* , **115**, 393-399.

North, G R , 1984 Empirical orthogonal functions and normal modes *J Atmos. Sci.*, **38**, 504-513.

———, T L. Bell and R.F Cahalan, 1982. Sampling errors in the estimation of empirical orthogonal functions. *Mon Wea Rev* , **110**, 699-706

O'Conner, J , 1963 The weather and circulation of January 1963 *Mon Wea Rev* , **91**, 209-218

Oort, A.H , 1983. *Global atmospheric circulation statistics, 1958-73* NOAA prof paper No 14, U S Government Printing Office, Washington, D C , 180 pp

——— and E M Rasmusson, 1971. *Atmospheric circulation studies* NOAA Prof Pap. 5, 323 pp

Patoine, A and T Warn, 1982 The interaction of long, quasi-stationary baroclinic waves with topography. *J Atmos. Sci.*, **39**, 1018-1025.

Pratt, R.W., 1979: Space-time kinetic energy spectra in mid-latitudes. *J Atmos. Sci*, 34, 1681-1691.

Preisendorfer, R.W., F W Zwiers and T.P Barnett, 1981 *Foundations of principal component selection rules*. SIO Reference Series 81-4, Scripps Institution of Oceanography, University of California, 192pp

Priestley, M B., 1981: *Spectral analysis and time series*, Academic press, London, 890 pp

Rasmusson, E. and J.M Wallace, 1983 Meteorological aspects of the El Nino/Southern oscillation *Science*, 1195-1202

Reinhold, B B, 1989 Comments on "Theories of multiple equilibria and weather regimes A critical reexamination of two-layer baroclinic models" *J Atmos. Sci*, **46**, 1861-1864.

Reinhold, B.B and R T Pierrhumbert, 1982: Dynamics of weather regimes Quasi-stationary waves and blocking *Mon. Wea. Rev*, **110**, 1105-1145.

Rex, D F, 1950a. Blocking action in the middle troposphere and its effect upon regional climate 1 An Aerological study of blocking action *Tellus*, 2, 196-211.

———, 1950b: Blocking action in the middle troposphere and its effect upon regional climate. 2 The climatology of blocking action *ibid*, 2, 275-301

Richman, M B., 1986 Rotation of principal components. *J Climatol*, **6**, 293-335.

Sardeshmukh, P D, and B.J. Hoskins, 1984: Spatial smoothing on the sphere *Mon. Wea. Rev.*, **112**, 2524-2529

Schubert, S.D, 1985: A statistical-dynamical study of empirically determined modes of atmospheric variability *J. Atmos Sci*, **42**, 3-17.

Shutts, G J, 1983 The propagation of eddies in diffluent jet-streams: Eddy vorticity forcing of "blocking" flow fields *Quart J R. Met. Soc*, **109**, 737-761.

Simmons, A.J., J.M Wallace and G W Branstator, 1983. Barotropic wave propagation and instability, and atmospheric teleconnection patterns *J. Atmos. Sci.*, **40**, 1363-1392.

Smith, G.L., 1987: Relations between empirical orthogonal functions and normal modes AMS preprints of the *Tenth conference on probability and statistics in Atmospheric Sciences*, October 1987, held in Edmonton, Canada, 208-11.

Stephens, M A , 1974 EDF statistics for goodness of fit and some comparisons *J American Stat Ass* , **69**, 730-736.

Szeredi, I , and D J Karoly, 1987 The horizontal structure of monthly fluctuations of the southern hemisphere troposphere from station data *Aust Metor Mag* , **35**,

Taljard, J J , 1972 Synoptic meteorology in the Southern Hemisphere Chap 8 of Meteorology of the Southern Hemisphere *Met Monogr* , **13**, 139-211

Trevisan, A and A Buzzi, 1980 Stationary response of barotropic, weakly nonlinear Rossby waves to quasi-resonant orographic forcing *J Atmos Sci* , **37**, 947-957.

Treidl, R.A , E.C Birch and P. Sajecki, 1981· Blocking action in the Northern Hemisphere A climatological study *Atmosphere-Ocean*, **19**, 1-23.

Trenberth, K E., and J.G. Olson, 1988 An evaluation and intercomparison of global analyses from the National Meteorological Center and the European Centre for Medium Range Weather Forecast. *Bull Amer Meteor Soc* , **69**, 1047-1057

———, 1986: An assessment of the impact of transient eddies on the zonal flow during a blocking episode using localized Eliassen-Palm diagnostics *J. Atmos Sci* , **43**, 2070-2087.

———, K.E., and K C. Mo, 1985 Blocking in the Southern Hemisphere *Mon Wea. Rev.*, **113**, 3-21.

Tribbia, J.J., and D.P Baumhefner, 1987: Estimates of the predictability of Low-Frequency variability with a spectral general circulation model. *J Atmos Sci* , **45**, 2036-2317

Thurstone, L L., 1947. *Multiple factor analysis*, The University of Chicago Press, IL.

Tung, K.K. and R S. Lindzen, 1979a A theory of stationary long waves Part I A simple theory of blocking *Mon Wea Rev* , **107**, 714-734

——— and ———, 1979b: A theory of stationary long waves. Part II: Resonant Rossby waves in the presence of realistic vertical shears. *Mon. Wea Rev.*, 107, 735-750.

——— and A.J. Rosenthal, 1985· Theories of multiple equilibria-A critical reexamination. Part I: Barotropic models. *J. Atmos. Sci* , 42, 2804-2819.

van Loon, H., 1956: Blocking action in the Southern Hemisphere Pt 1. *Notos*, 5, 171-8

Wallace, J M and M L Blackmon, 1983: Observations of low- frequency atmospheric variability. Chap. 3 of *Large-Scale Dynamical Processes in the Atmosphere*, B.J. Hoskins and R P Pierce eds., Academic Press, 55-94.

———, and D.S. Gutzler, 1981· Teleconnections in the geopotential height field during the Northern Hemisphere Winter. *Mon Wea. Rev.*, 109, 784-812

Warn, T. and B. Brasnett, 1983 The amplification and capture of atmospheric solitons by topography. A theory of the onset of regional blocking *J Atmos. Sci.*, 40, 28-38.

Wiin-Nielsen, A , 1979· Steady states and stability properties of a low-order barotropic system with forcing and dissipation. *Tellus*, 31, 375-386.

Wright, A D.F , 1974: Blocking action in the Australian region. Tech. Report 10, Bur. Met., Australia, 29 pp.

Figure captions

Figure 1. Northern hemisphere 50 kPa variance of the seasonal cycle of *(a)* the streamfunction ψ in a 20-year simulation of the CCC GCM and *(b)* of the geostrophic streamfunction ψ_g in ECMWF analyses valid from 1980 to 1984. Contour intervals starting from 2.0×10^{13} m^4s^{-2}, with increments of $4\ 0\times10^{13}$ m^4s^{-2}.

Figure 2. Northern hemisphere 50 kPa variance of the low frequency components of *(a)* the streamfunction ψ in a 20-year simulation of the CCC GCM and of *(b)* the geostrophic streamfunction ψ_g in ECMWF analyses valid from 1980 to 1984 Contour intervals for *(a)* starting from $3\ 0\times10^{12}$ m^4s^{-2}, with increments of 6.0×10^{12} m^4s^{-2} and for *(b)* starting from $5\ 0\times10^{12}$ m^4s^{-2}, with increments of $1\ 0\times10^{13}$ m^4s^{-2}

Figure 3. As in Fig. 2, but for the medium frequencies

Figure 4. As in Fig. 2, but for the high frequencies

Figure 5. As in Fig. 2, but for the southern hemisphere

Figure 6. As in Fig. 3, but for the southern hemisphere

Figure 7 As in Fig. 4, but for the southern hemisphere

Figure 8 Northern hemisphere 50 kPa total distribution of positive and negative anomalies, respectively greater and smaller than $\pm1.0\times10^7$ m^2/s and lasting for at least 9 days, of *(a)* the de-seasonalized ψ' from a 20-year simulation of the CCC GCM and of *(b)* the de-seasonalized ψ_g' derived from NMC analyses valid from 1965 to 1979 In *(a)*, contours intervals from 6 events, with subsequent increments of 6; in *(b)*, contours from 10 events, with increments of 10.

Figure 9 As in Fig 8, but for the Northern hemisphere summer. In *(a)*, contours from 4 events, with increments of 4, in *(b)*, contours from 6 events, with increments of 6

Figure 10. Southern hemisphere 50 kPa total distribution of positive and negative ψ' anomalies satisfying the same criterion as in Figure 8, from a 20-year simulation of the CCC GCM The winter data are considered in *(a)* and the summer in *(b)* Contour intervals from 4 events, with increments of 4

Figure 11 Northern hemisphere winter 50 kPa composites of the (de-seasonalized) ψ' anomalies occurring at $(18^0W, 44^0N)$ in a 20-year simulation of the CCC GCM The amplitude and duration that define the anomalies are the same as in Figure 8 The average of all positive events is presented in *(a)* and the negative in *(b)* The shaded contours highlight the corresponding total streamfunction (annual cycle included) Anomaly contour intervals from -1.20×10^7 to $+1\ 20\times10^7$ m^2/s, with increments of $2\ 0\times10^6$ m^2/s The negative contours are dashed The total streamfunction is contoured with increments of $1\ 5\times10^7$ m^2/s

Figure 12 As in Fig 11, but for anomalies of the (de-seasonalized) geostrophic streamfunction ψ_g' derived from NMC analyses valid from 1965 to 1979 and an anomaly centre position at $(18^0W, 52^0N)$

Figure 13. As in Fig 11, but for an anomaly centre position at $(9^0W, 52^0N)$

Figure 14 As in Fig. 12, but for an anomaly centre position at $(36^0W, 52^0N)$

Figure 15 As in Fig. 11, but for an anomaly centre position at $(162^0W, 35^0N)$.

Figure 16. A in Fig 11, but for the southern hemisphere summer 50 kPa

composites of the (de-seasonalized) ψ anomalies occurring at (153°W, 52°S) The total streamfunction is now contoured with increments of 1 0×10^7 m^2/s

Figure 17 Scatter plots of the (normalized) first rotated loading factor with respect to the (again normalized) next four This REOF analysis is done on the modelled positive and negative mid-Atlantic anomalies These four scatter plots each contains 180 points corresponding to the grid points in the geographical window over which the analysis is done

Figure 18 Positive phase of the 50 kPa CCC GCM rotated loading factors, based on the positive and negative (de-seasonalized) ψ' anomalies occurring at (18°W, 44°N), throughout the simulation The shaded contours highlight the time-mean total streamfunction ψ (annual cycle included) of all time levels that strongly project onto this phase of the particular REOF Frames *(a)* to *(f)* correspond to the first, second, , sixth loading factor produced by the analysis, respectively The rotated loading factor are contoured from -1 20×10^7 m^2/s to +1 20×10^7 m^2/s, with increments of 1 5×10^6 m^2/s The negative contours are dashed and the total streamfunction is contoured with increments of 1 5×10^7 m^2/s

Figure 19 As in Fig 18, but for the negative phase of the CCC GCM rotated loading factors

Figure 20 As in Fig. 18, but for the (de-seasonalized) geostrophic streamfunctions ψ_g' derived from the 50 kPa NMC analyses valid from 1965 to 1979 As well, the shaded contours now highlight the corresponding total geopotential height fields (annual cycle included). This total geopotential is contoured from 480 dam to 585 dam, with increments of 15 dam

Figure 21. As in Fig 20, but for the negative phase of the NMC (de-seasonalized) ψ_g' loading factors

Figure 22. Tendency $(\partial\overline{\psi}/\partial t)_{tr}$ at 25 kPa implied by the gradients of the high-frequency u and v *E-vectors*. These latter are calculated for the ***onset*** composite of the ***+ATL2*** type of events found in NMC analyses valid from 1979 to 1986. Frames *(a)*, *(b)* and *(c)* contain the total, as well as the barotropic and baroclinic components of this tendency, respectively. The shaded contours highlight the 25 kPa time-mean total streamfunction ψ corresponding to the *+ATL2* anomalies. The tendencies are contoured from -1.25×10^{7} $(m^2/s)/day$ to $+1.25\times10^{7}$ $(m^2/s)/day$ with increments of 1.0×10^{6} $(m^2/s)/day$. The total streamfunction is itself contoured with increments of 2.0×10^{7} m^2/s.

Figure 23. As in Fig. 22, but for the ***mature*** stage of the events.

Figure 24. As in Fig. 22, but for the ***demise*** stage of the events.

Figure 25. Frames *(a)* and *(b)* correspond, respectively, to frames *(a)* and *(c)* of Figure 23, except that the $\overline{(\omega'\underline{V}')}$ contributions to the *E-vectors* are now neglected.

Figure 26. Vertical average of the ***mature*** stage tendencies implies by the u and v *E-vectors* associated to the NMC ***+ATL2*** events. Frames *(a)* and *(b)* contain the horizontal (barotropic) and vertical (baroclinic) components of this average, respectively. The contour intervals are as in Figure 21.

Figure 27. As in Fig. 21, but for the *+ATL2* events found in a 20-year integration of the CCC GCM.

Figure 28. As in Fig. 22, but for the *+ATL2* events found in a 20-year integration of the CCC GCM.

Figure 29. As in Fig. 23, but for the *+ATL2* events found in a 20-year integration of the CCC GCM.

Figure 30 As in Fig 26, but for the *+ATL2* events found in a 20-year integration of the CCC GCM

Figure A1 Amplitude response functions of the two filters that give us the real and imaginary parts of the complex data set used in the complex REOF calculations The dashed line represents the real filter's response and the continuous line, the imaginary filter's The *K=10* versions of the functions is displayed here

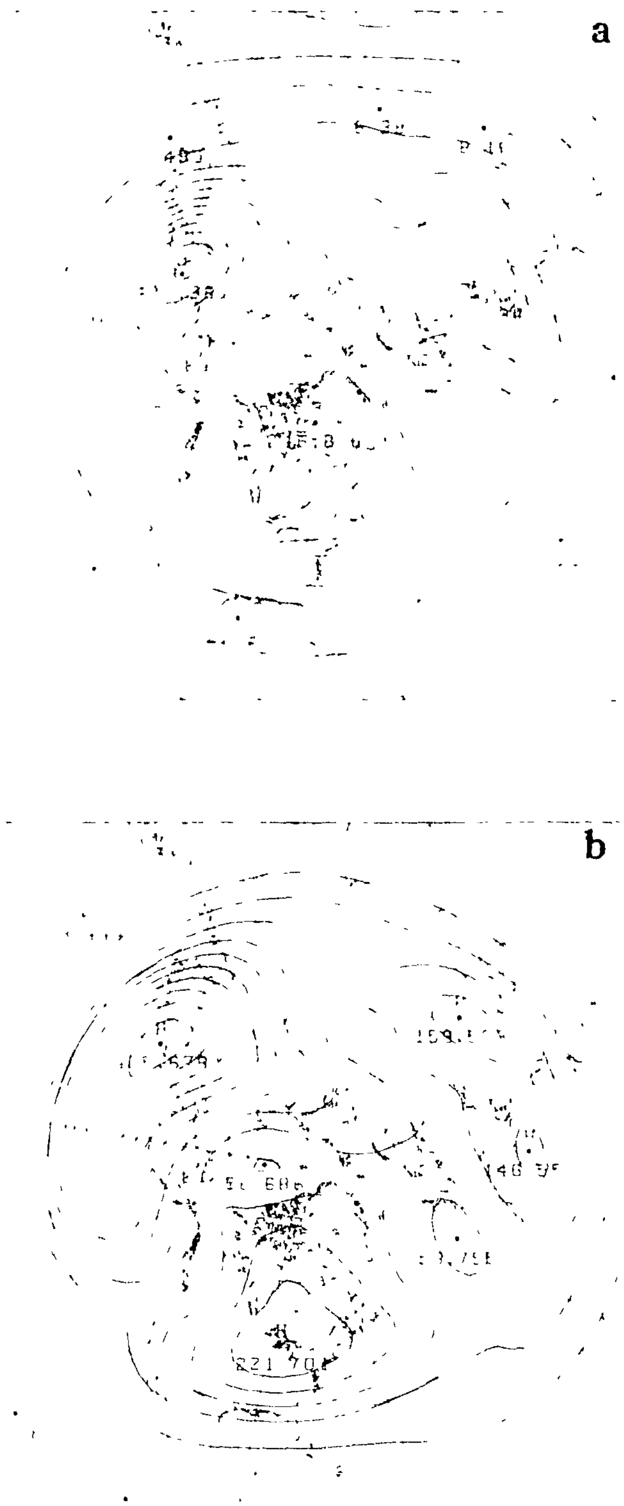

FIGURE 1

FIGURE 2

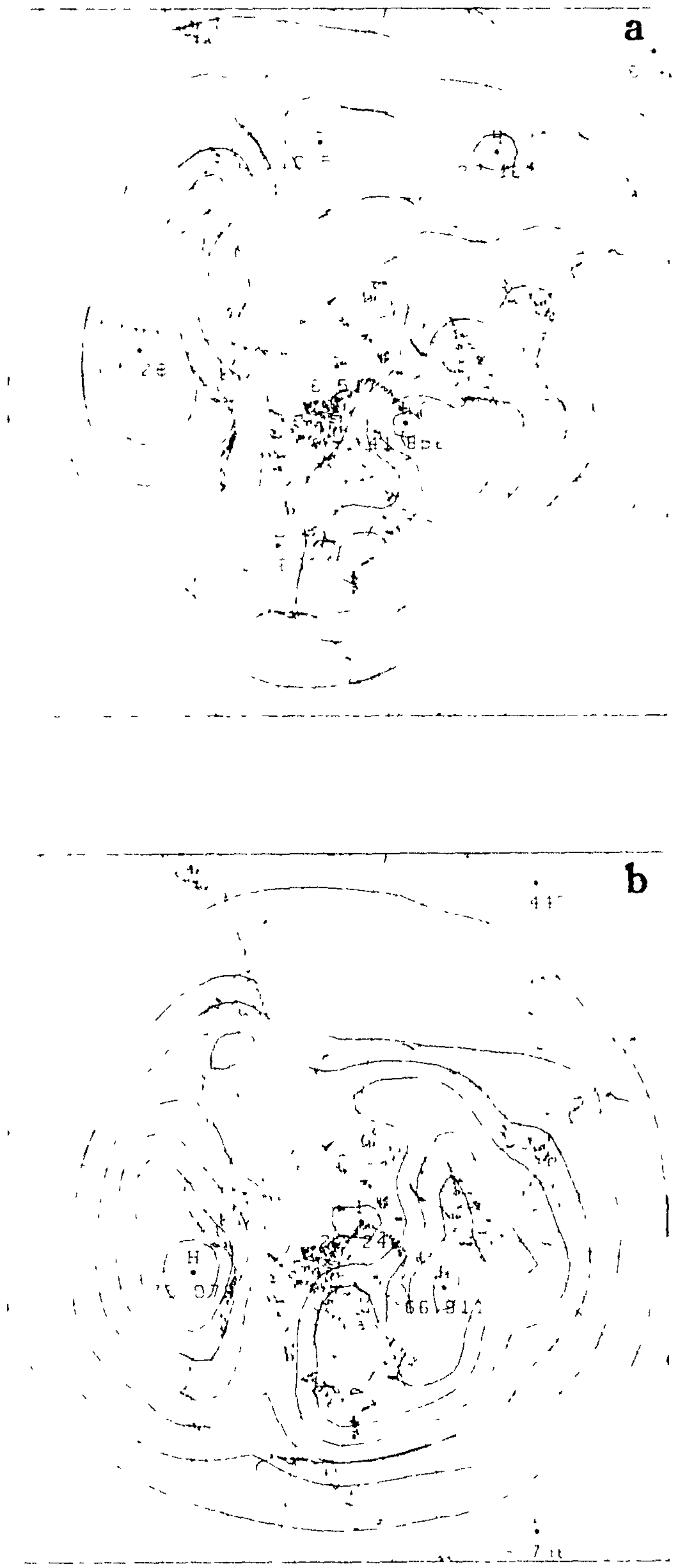

FIGURE 3

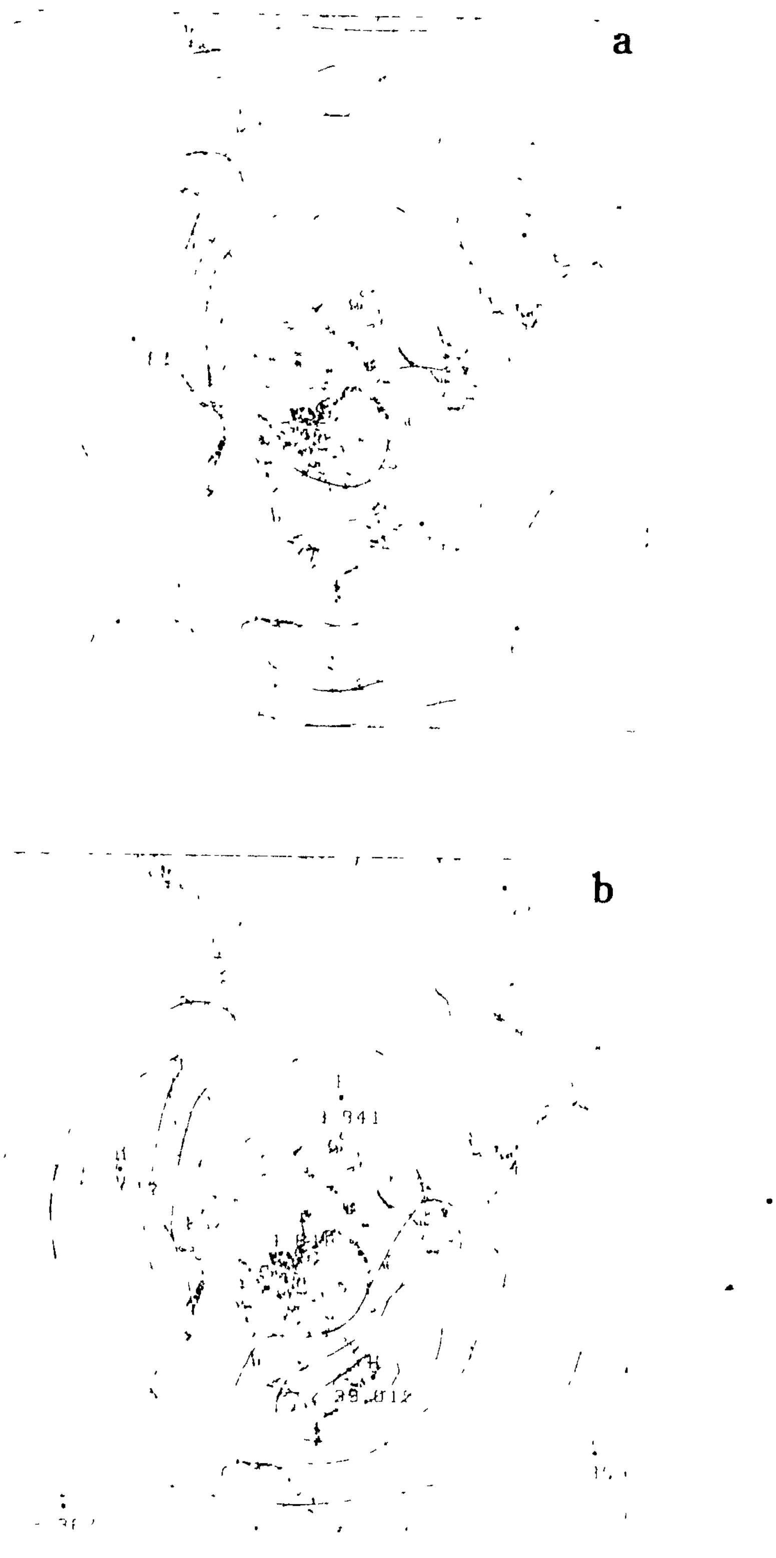

FIGURE 4

FIGURE 5

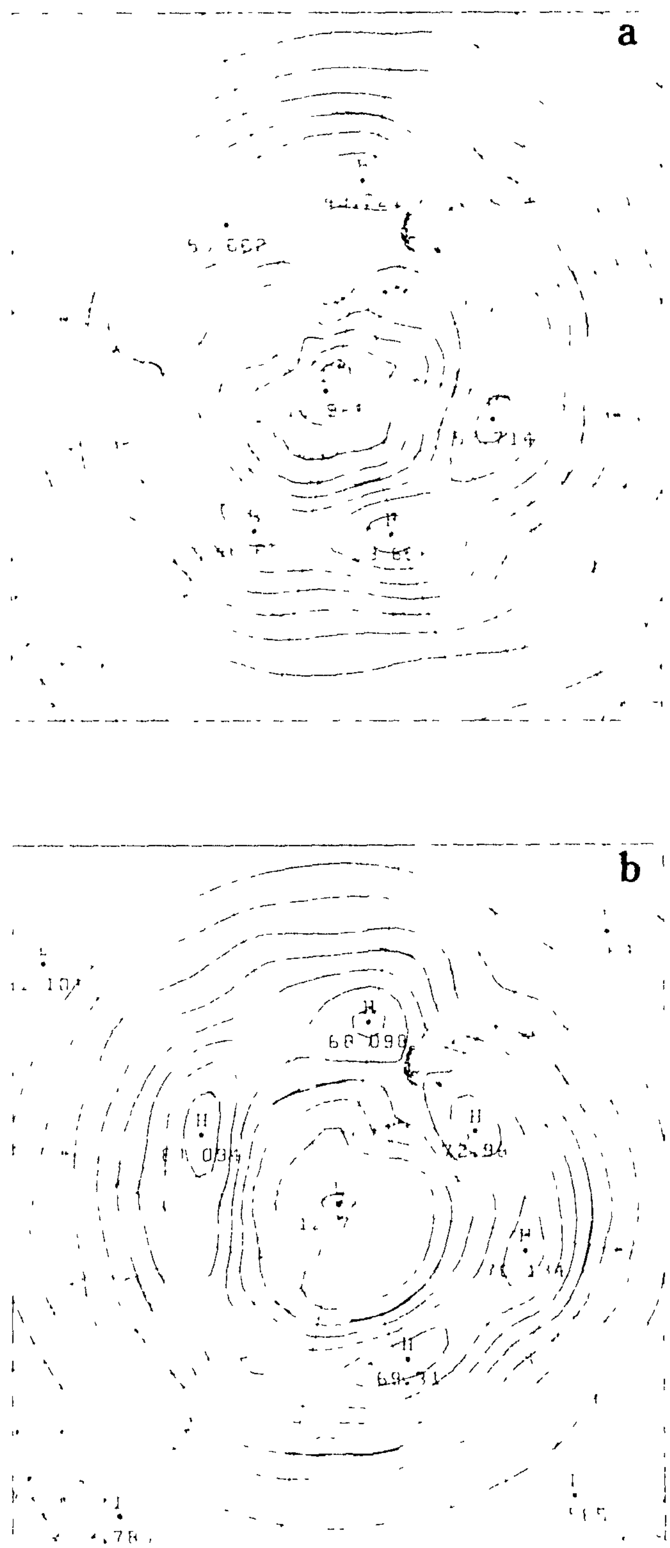

FIGURE 6

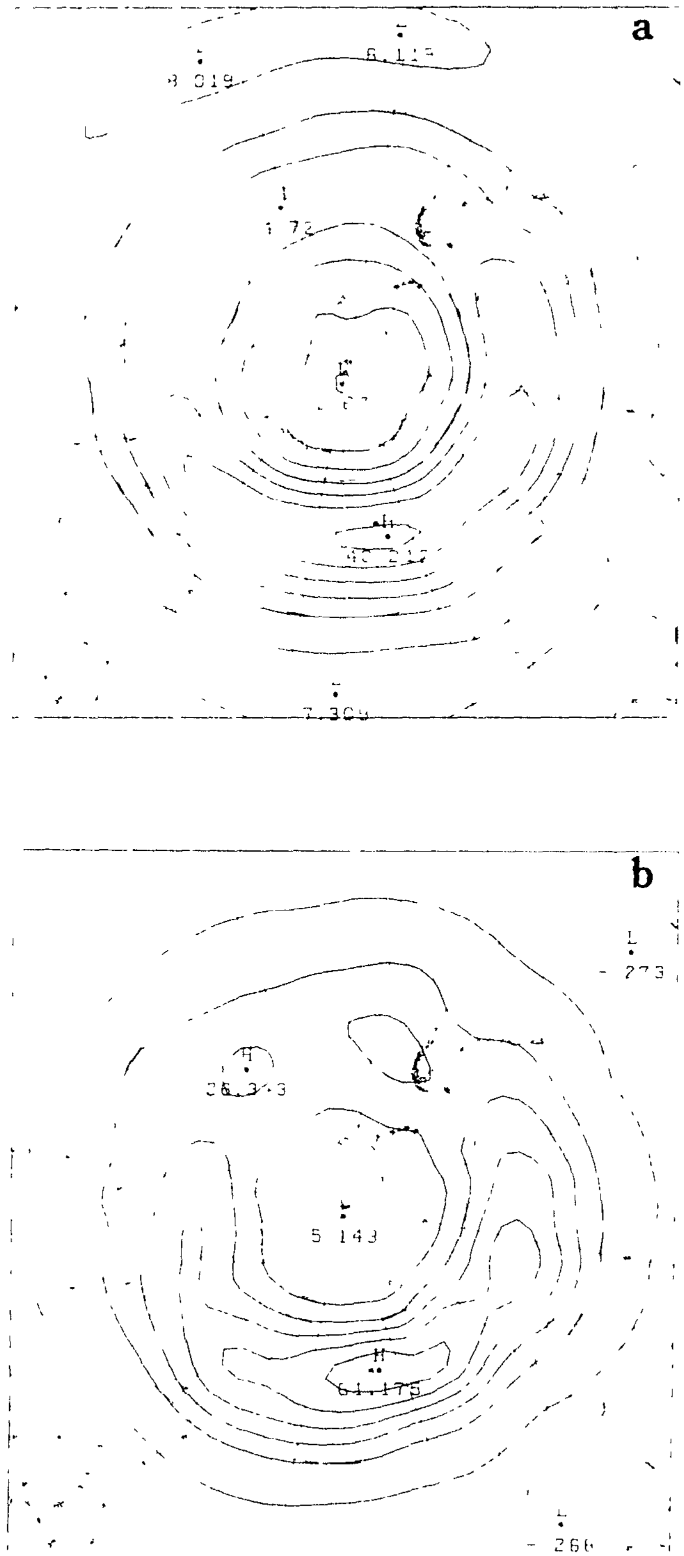

FIGURE 7

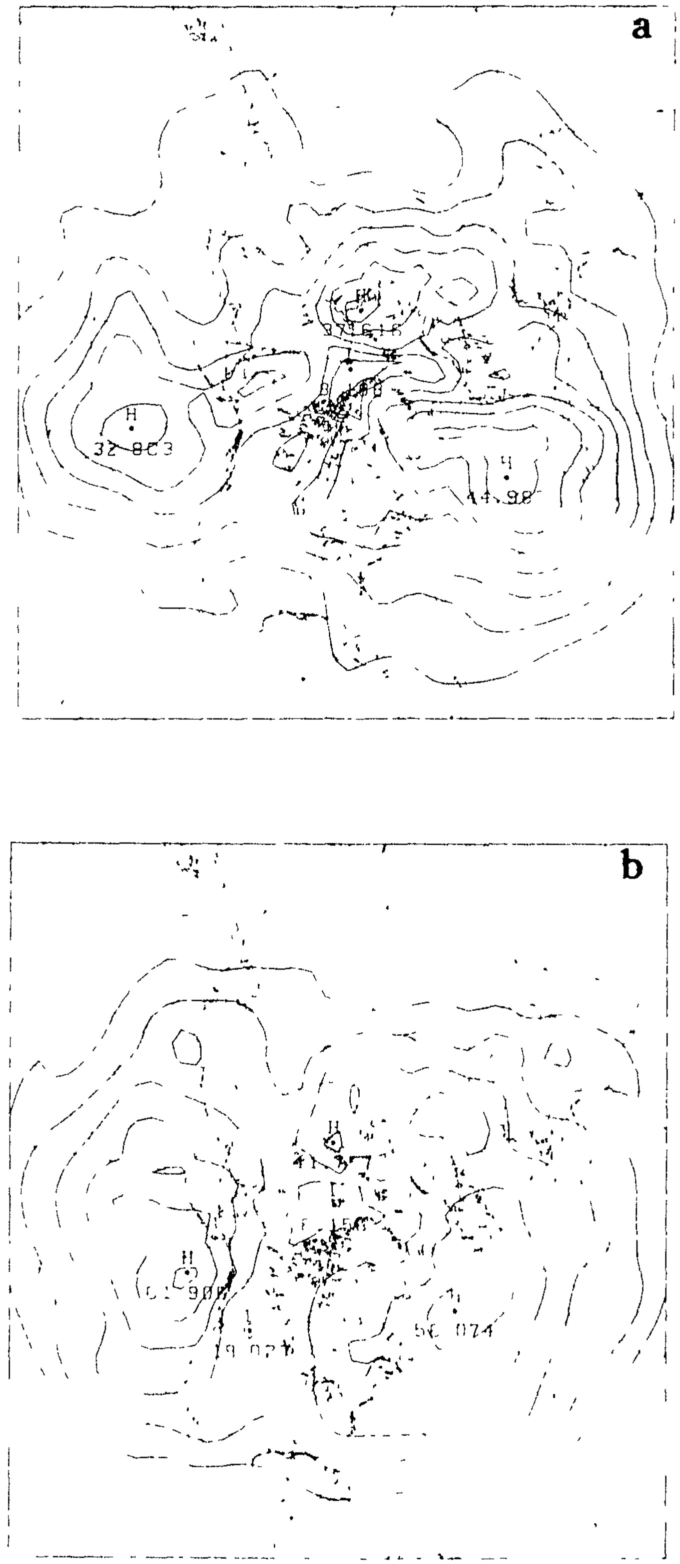

FIGURE 8

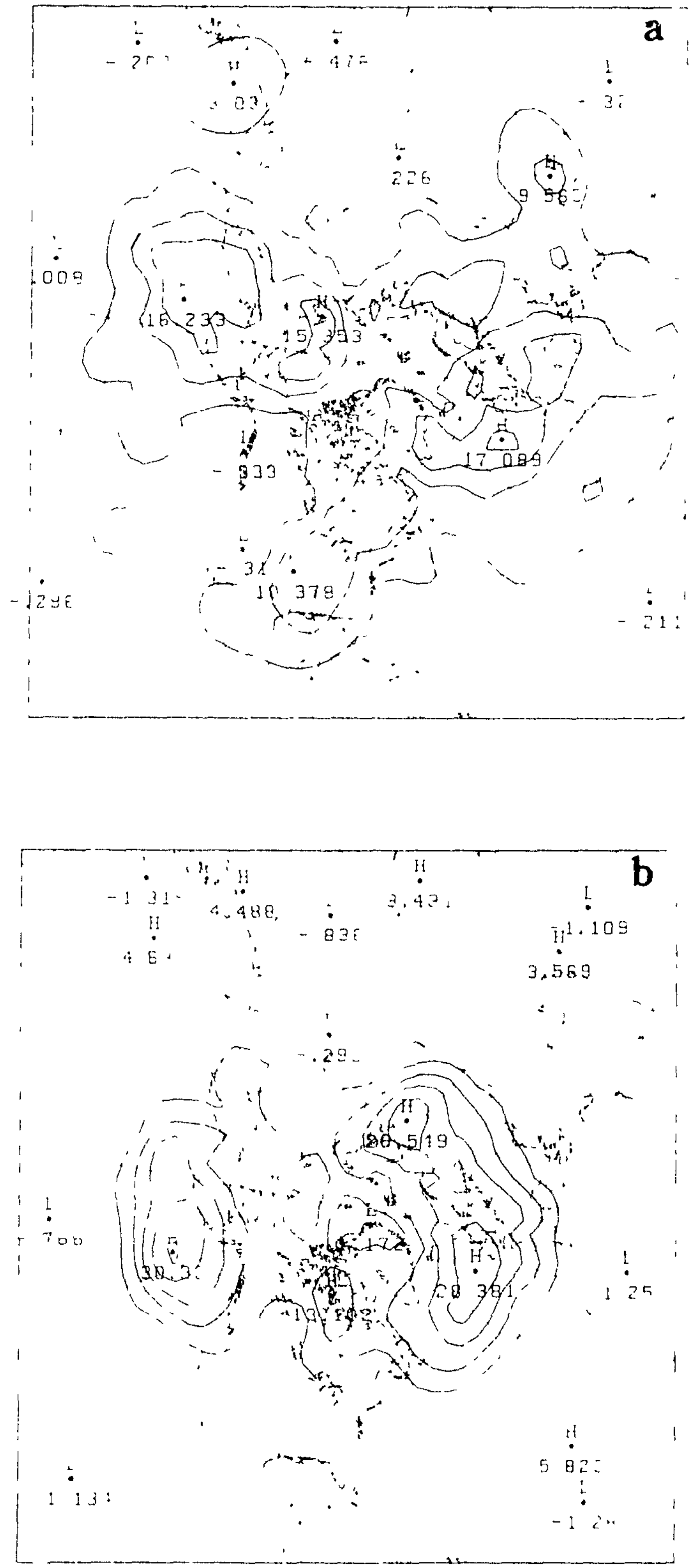

FIGURE 9

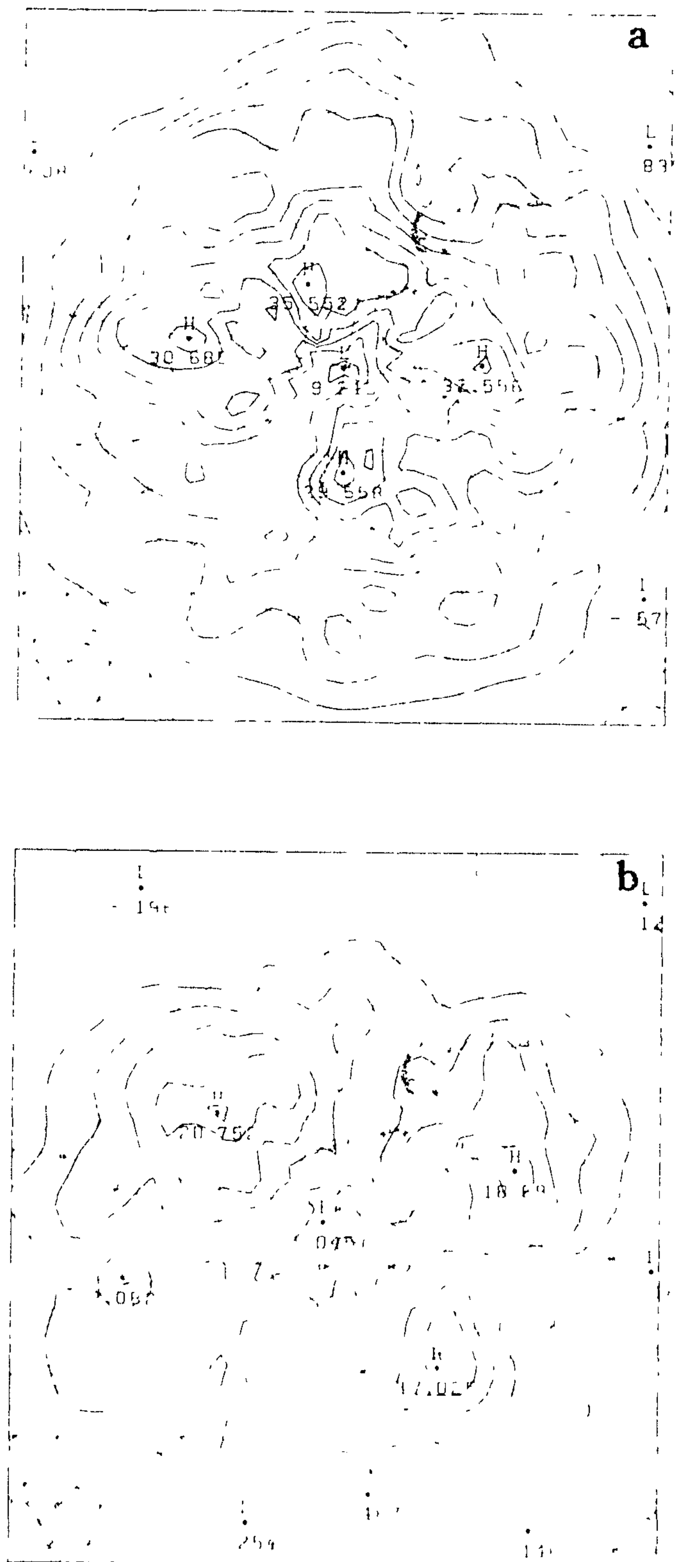

FIGURE 10

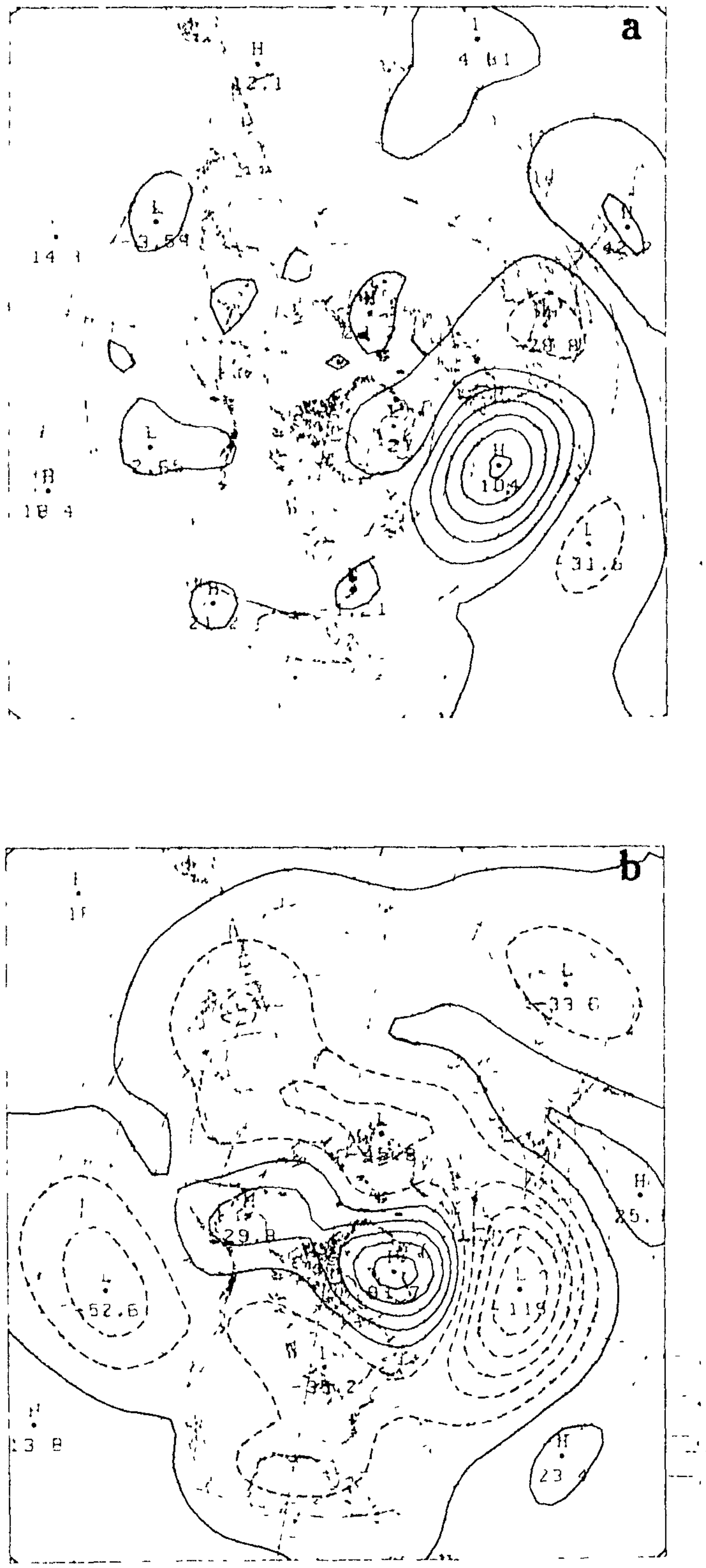

FIGURE 11

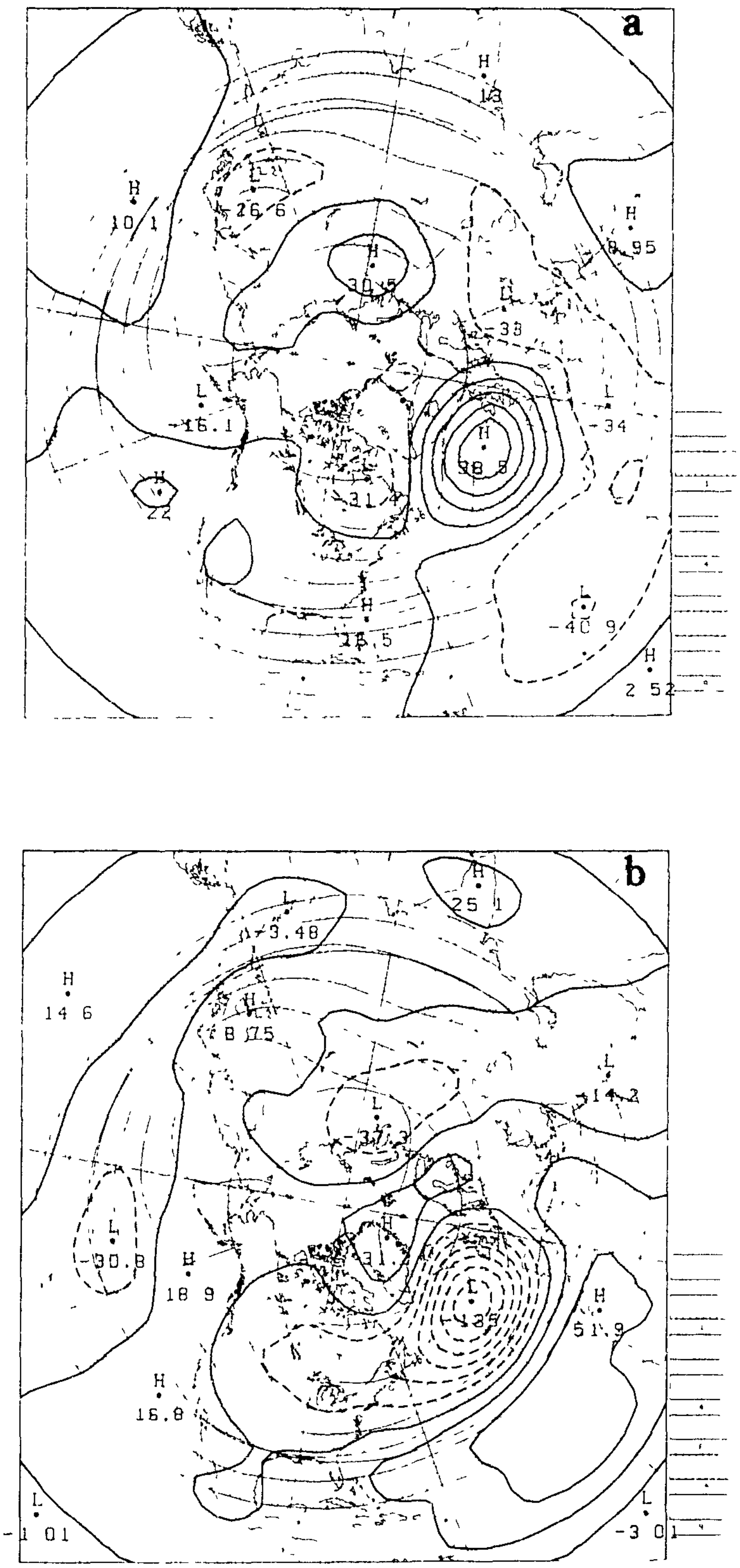

FIGURE 12

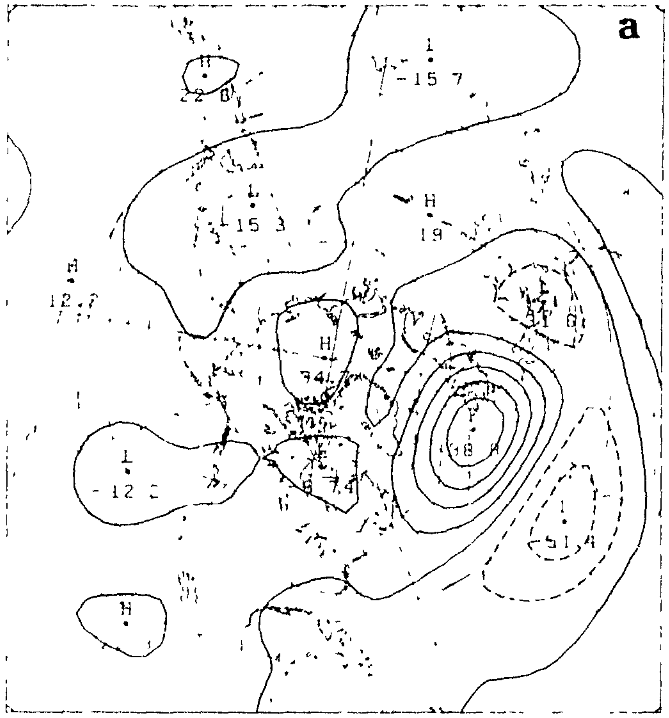

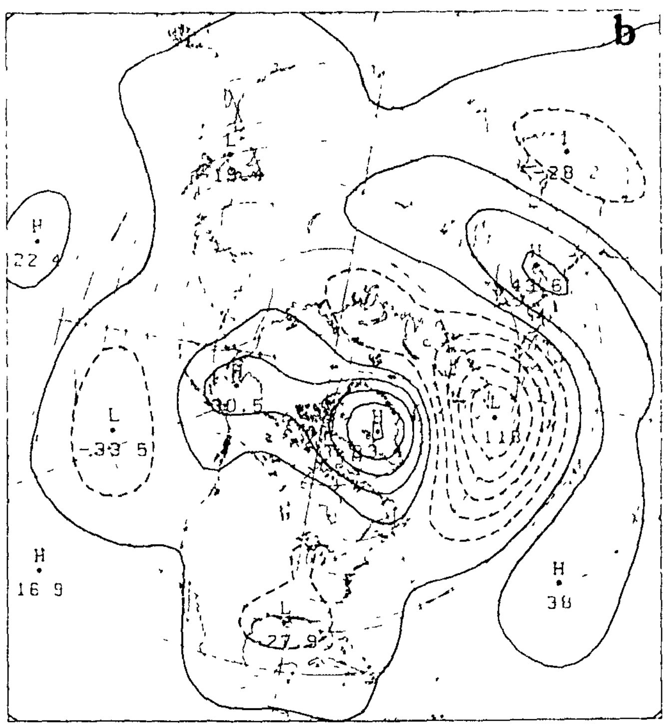

FIGURE 13

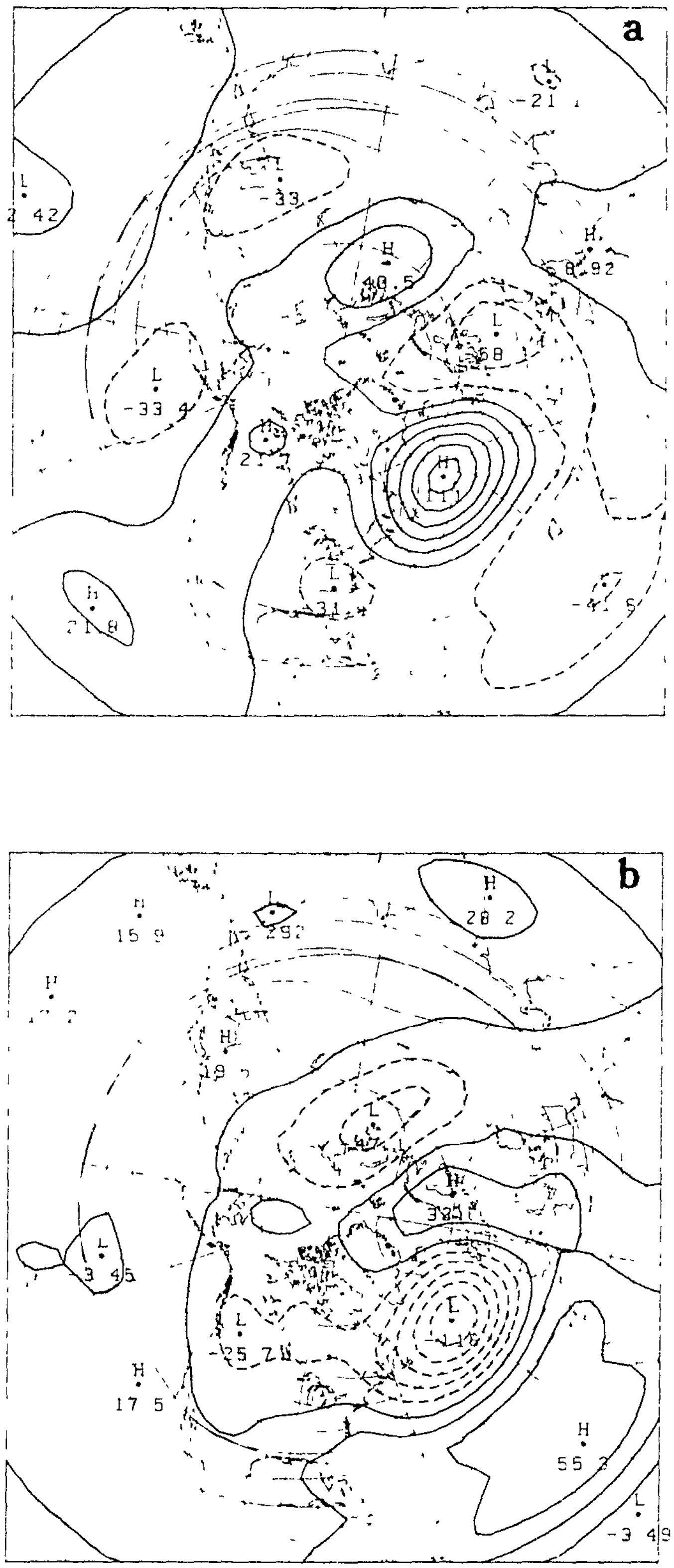

FIGURE 14

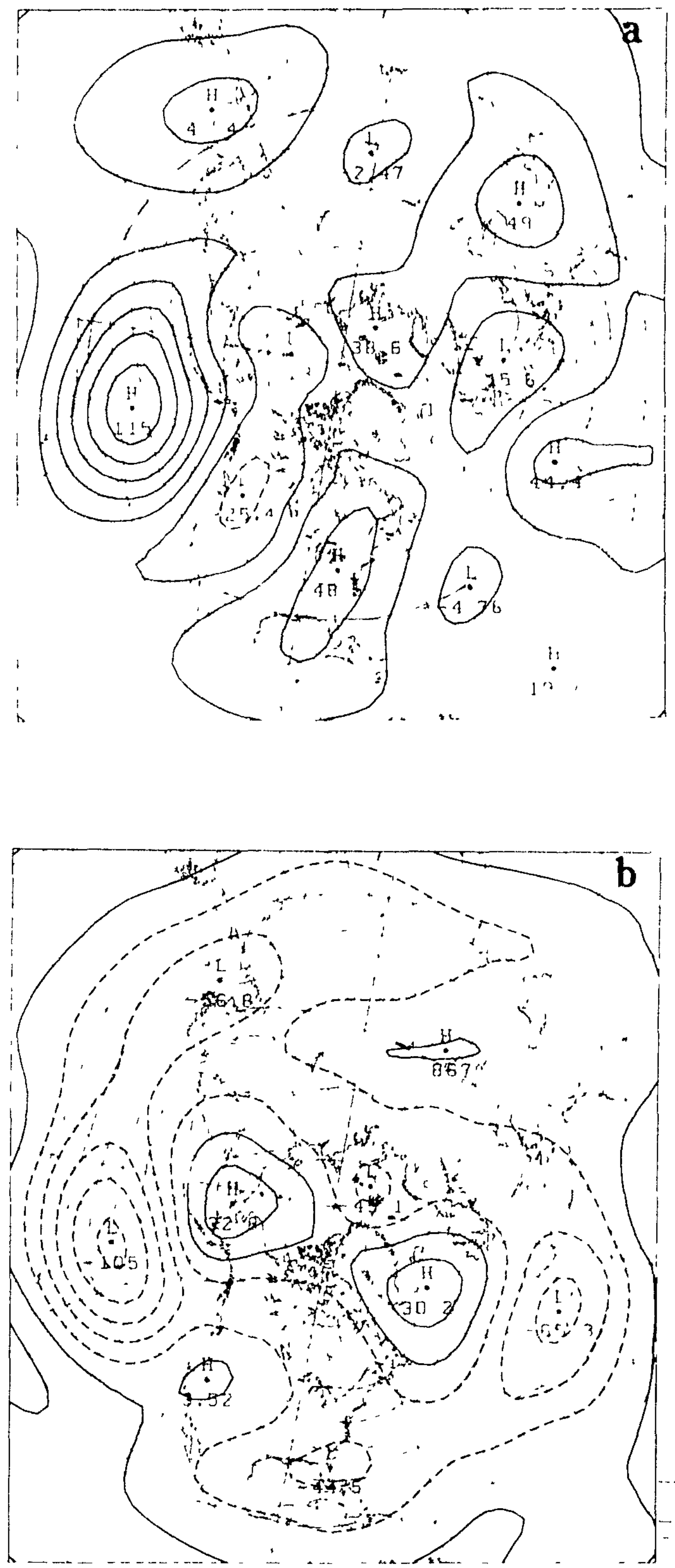

FIGURE 15

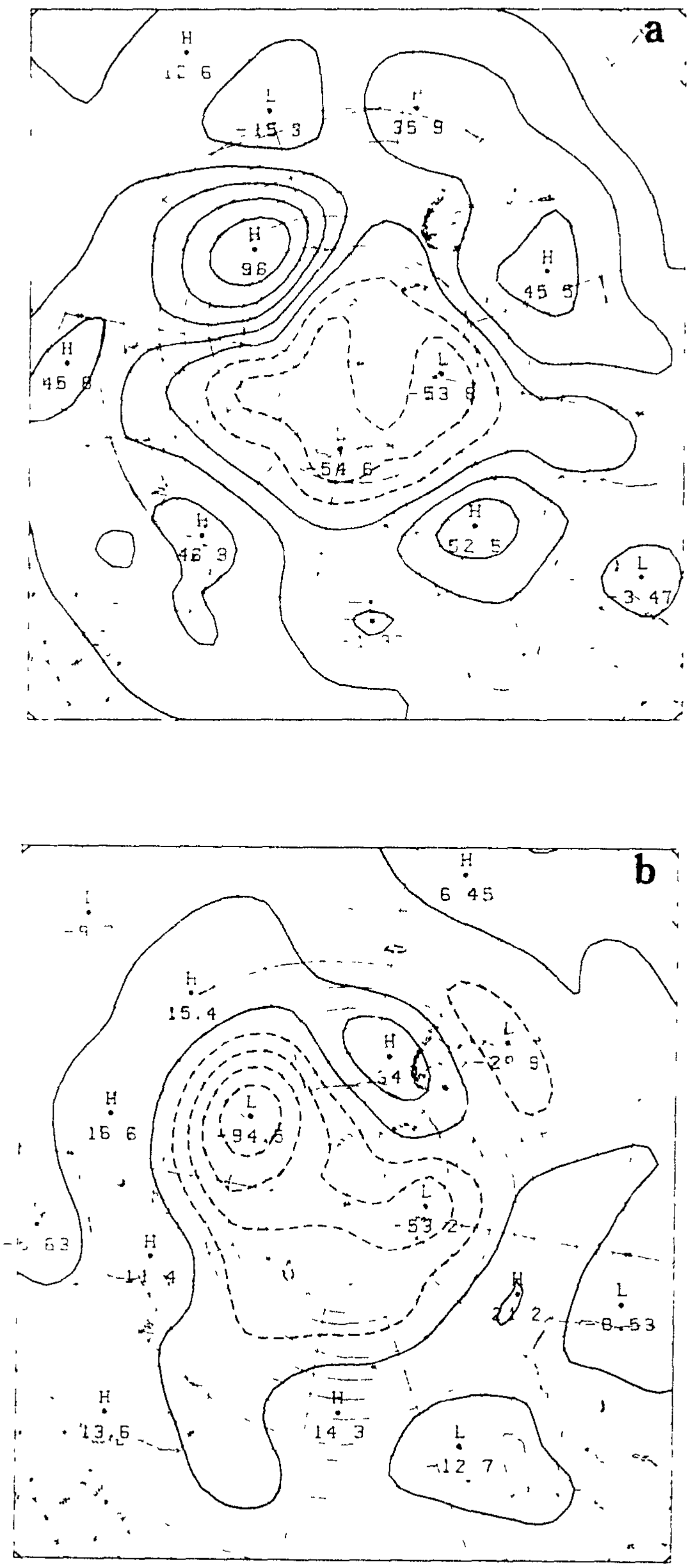
a
H
12 6
L
-15 3
35 9
H
96
H
45 5
H
45 8
L
-53 8
-54 6
H
46 3
H
52 5
L
-3 47
b
H
6 45
H
15.4
H
-34
L
-29 9
H
16 6
L
-94.5
L
-53 2
-5 63
H
11 4
L
-8 53
H
13 6
H
14 3
L
-12 7

FIGURE 16

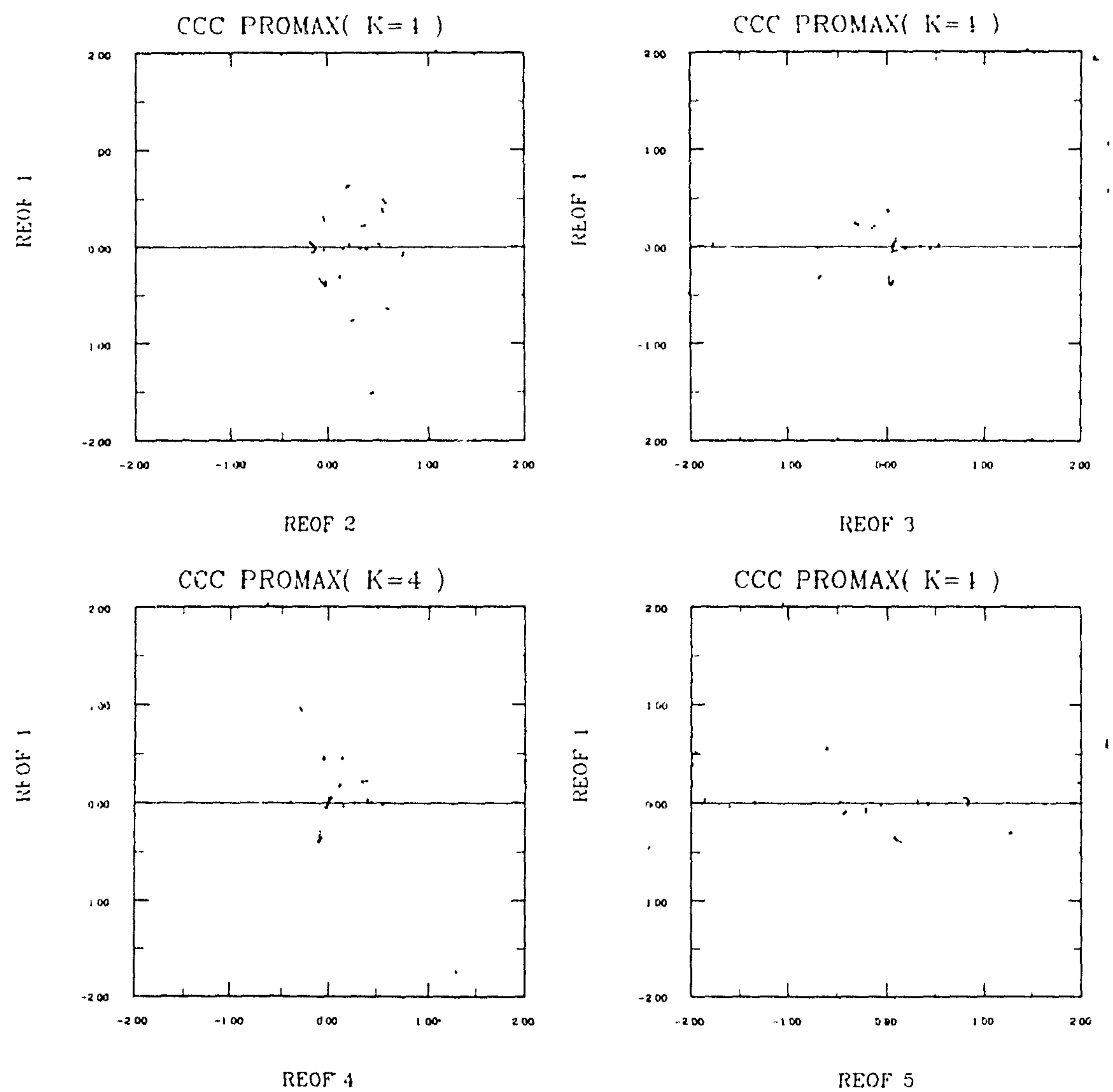
CCC PROMAX(K=4)
REOF 1
REOF 2
CCC PROMAX(K=4)
REOF 1
REOF 3
CCC PROMAX(K=4)
REOF 1
REOF 4
CCC PROMAX(K=4)
REOF 1
REOF 5

FIGURE 17

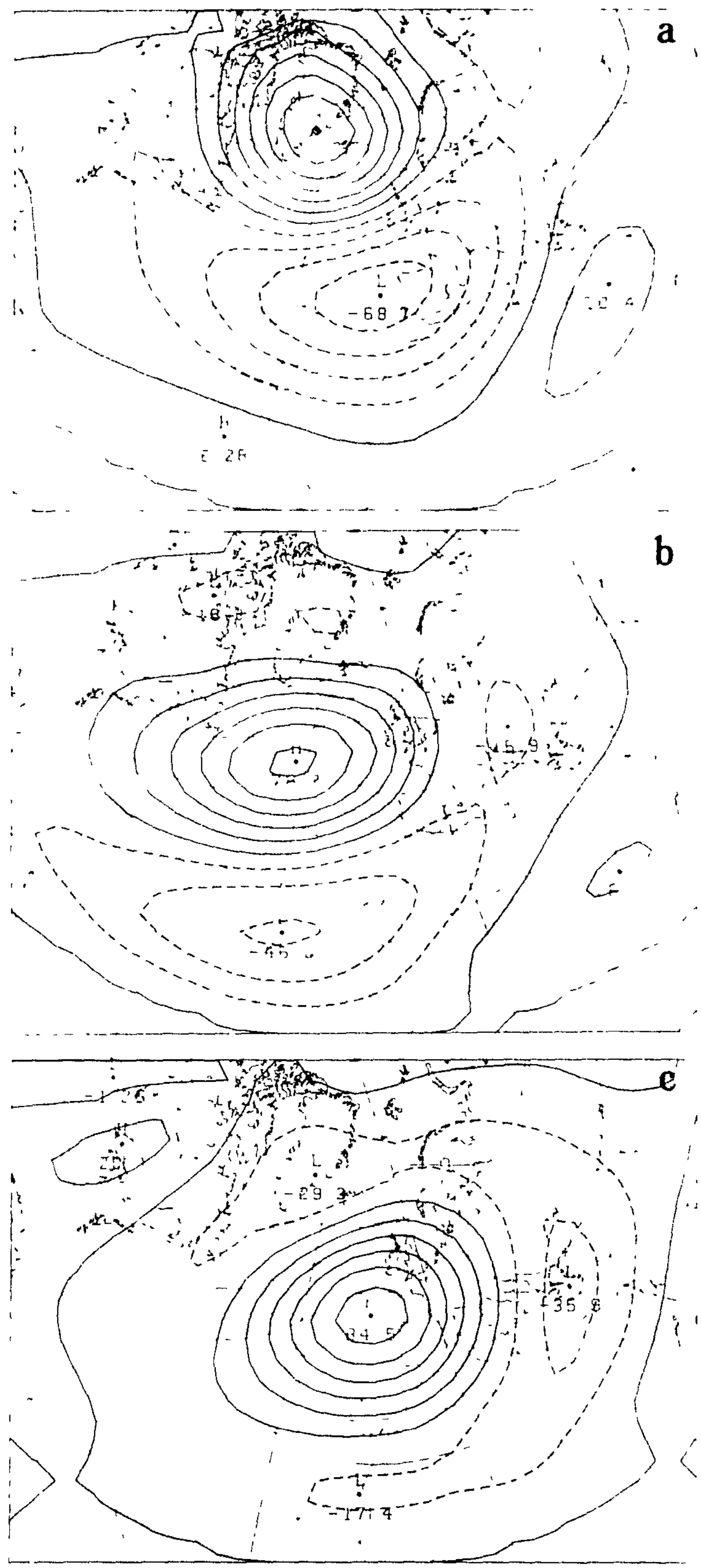

FIGURE 18

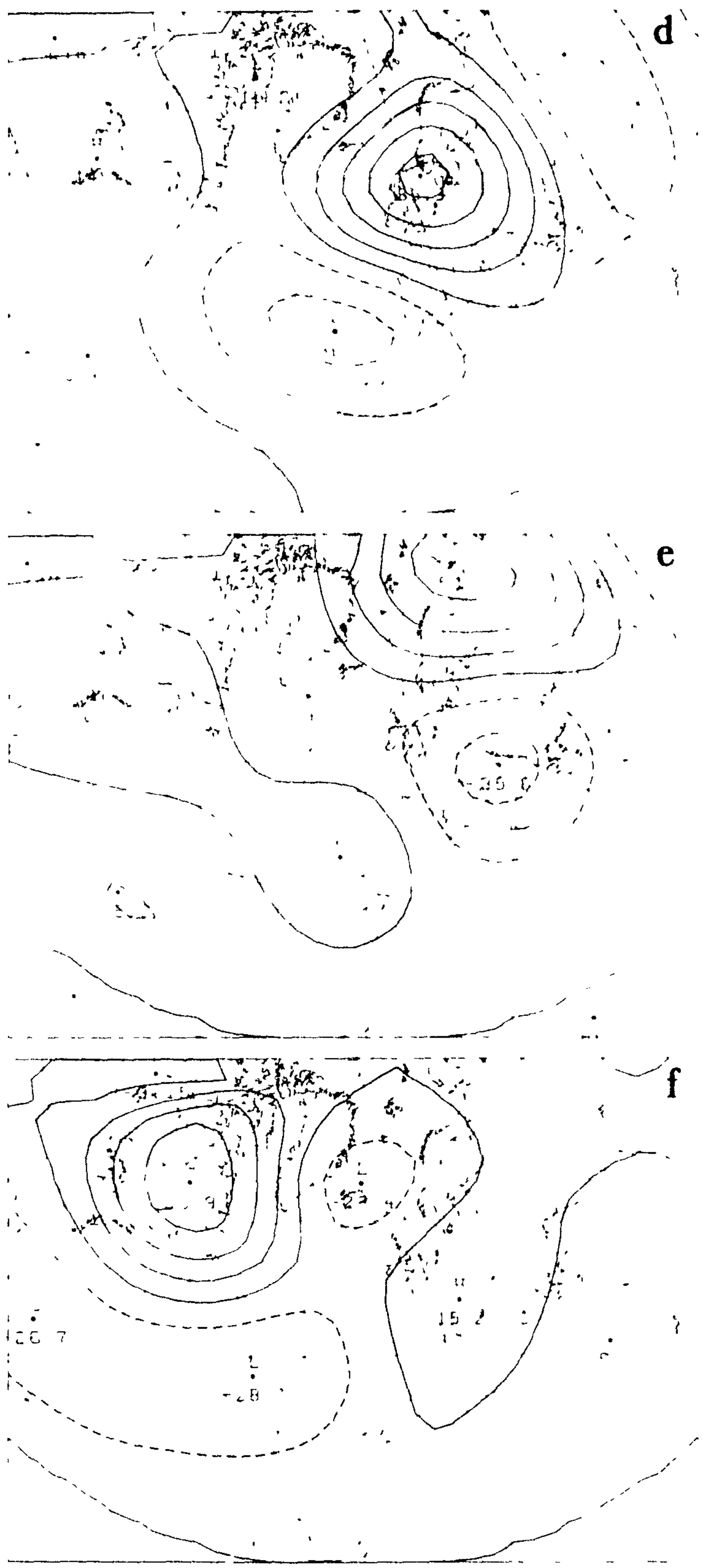

FIGURE 18

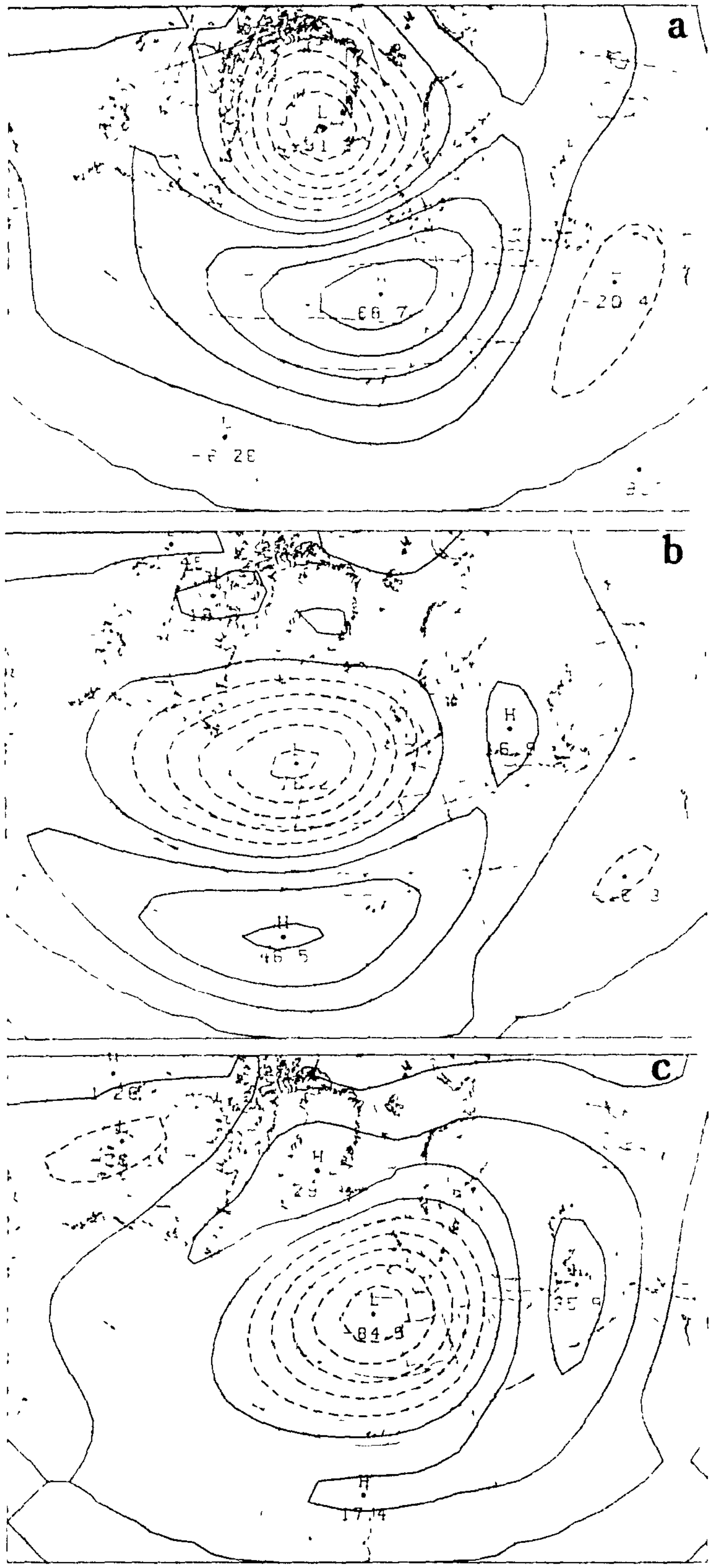

FIGURE 19

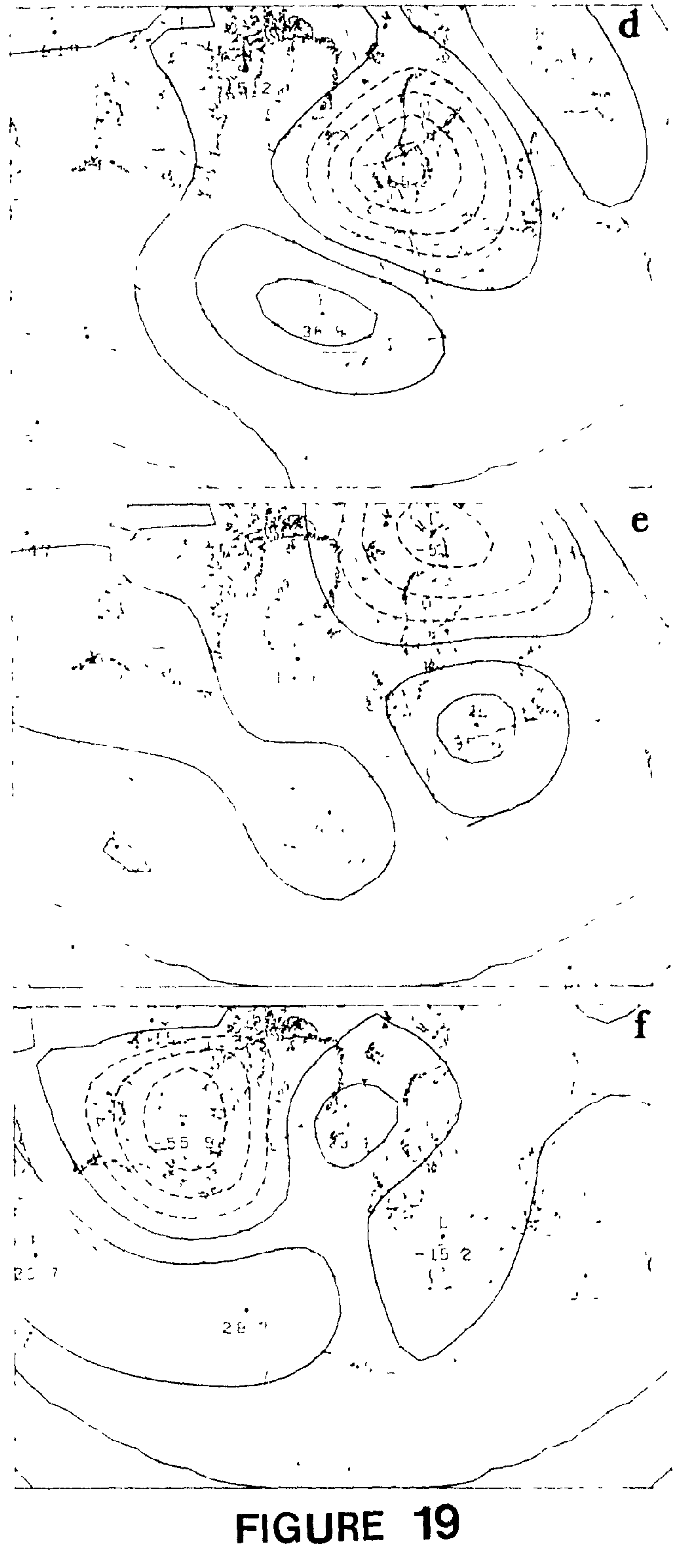

FIGURE 19

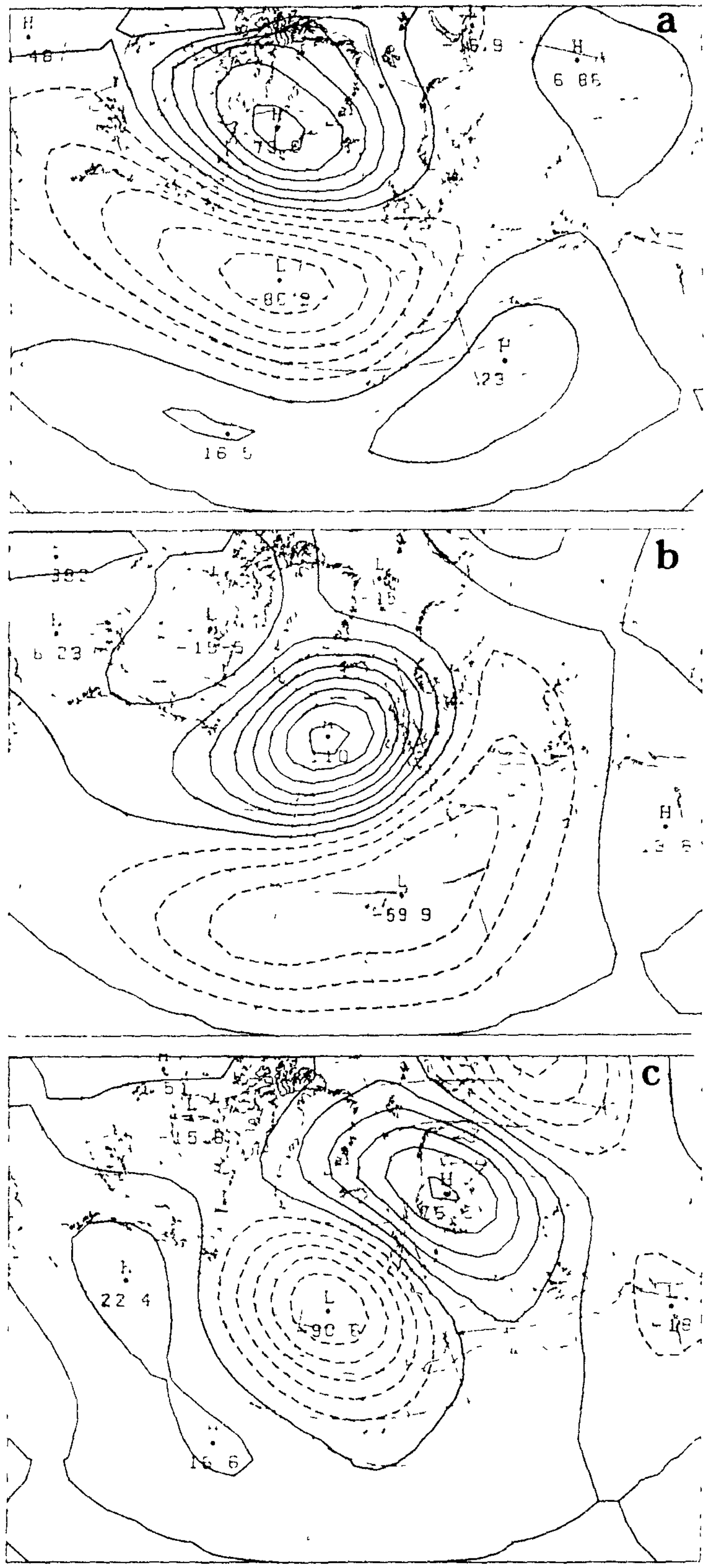

FIGURE 20

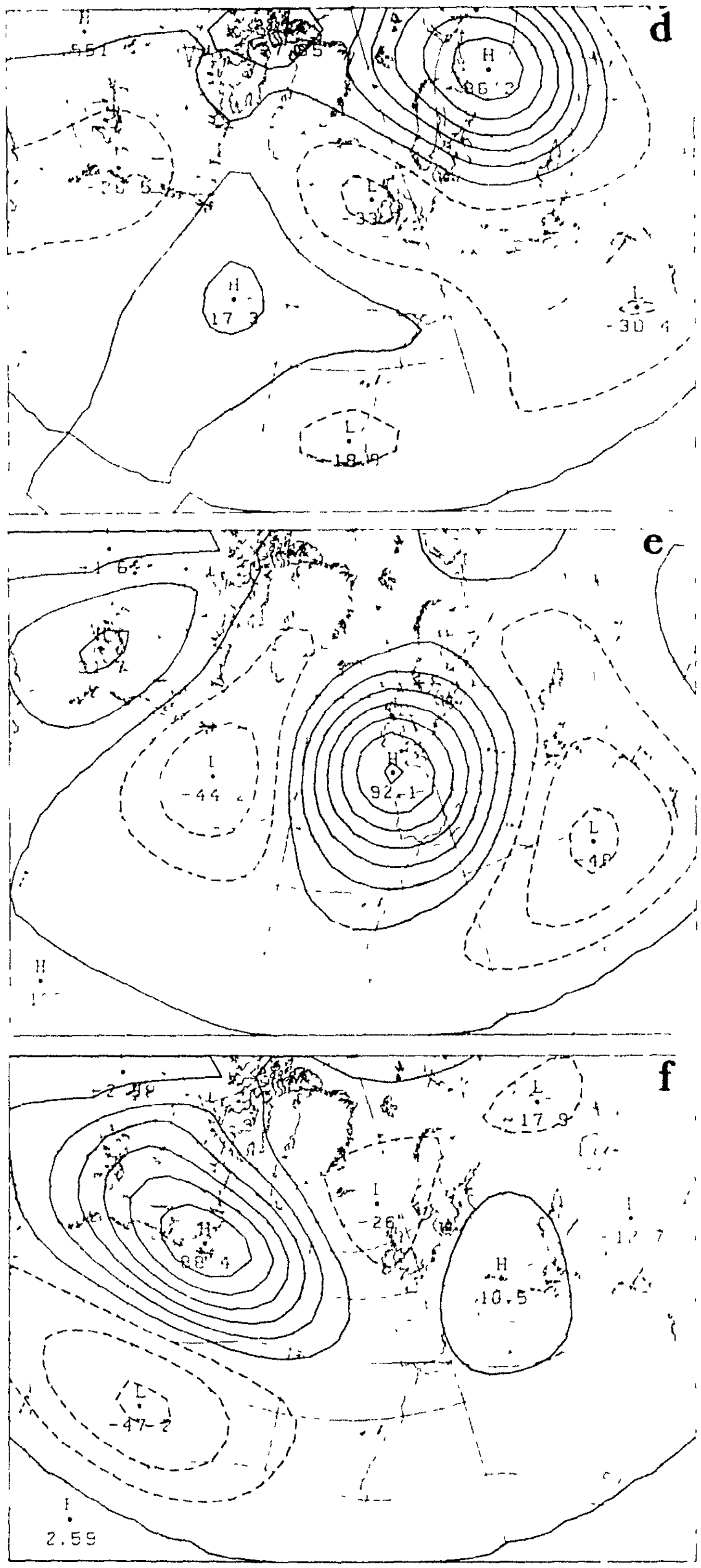

FIGURE 20

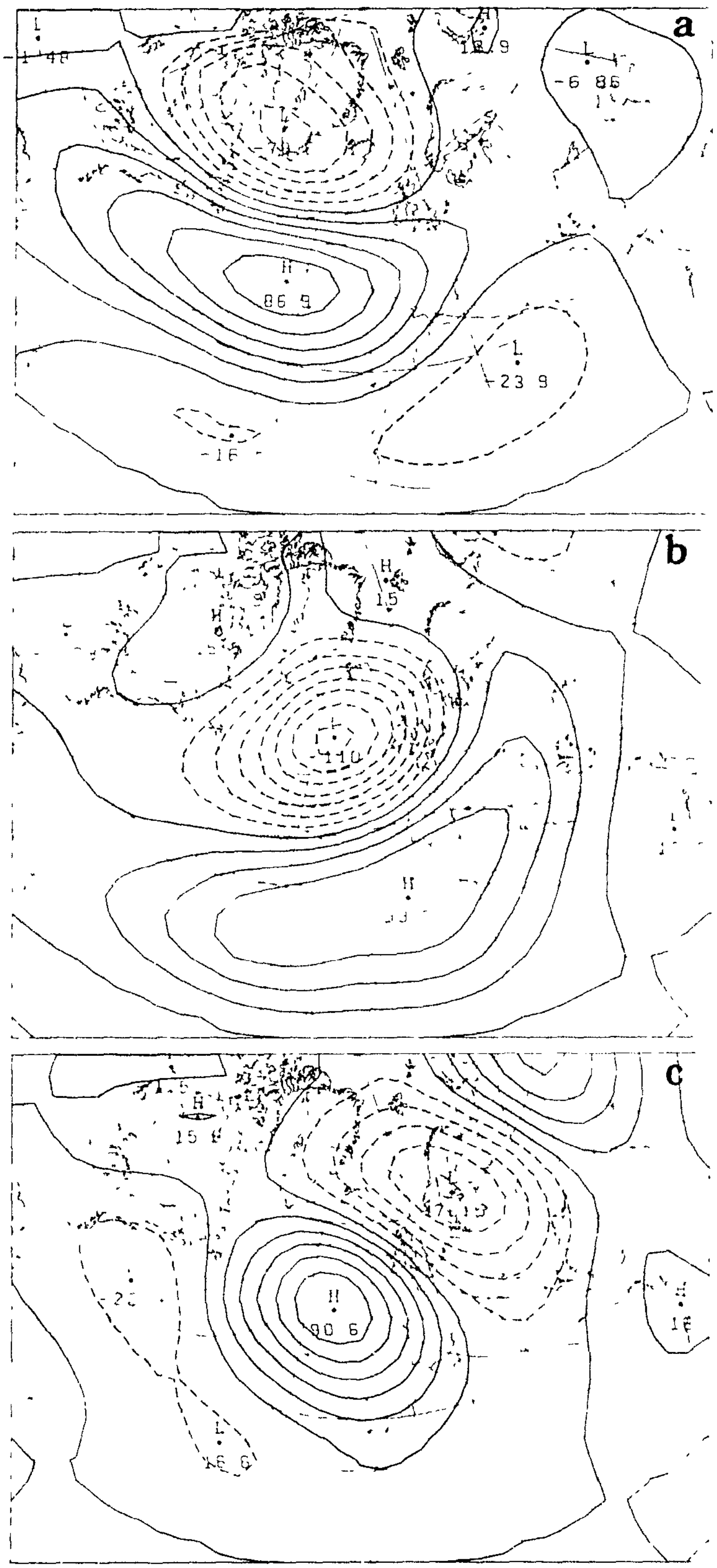

FIGURE 21

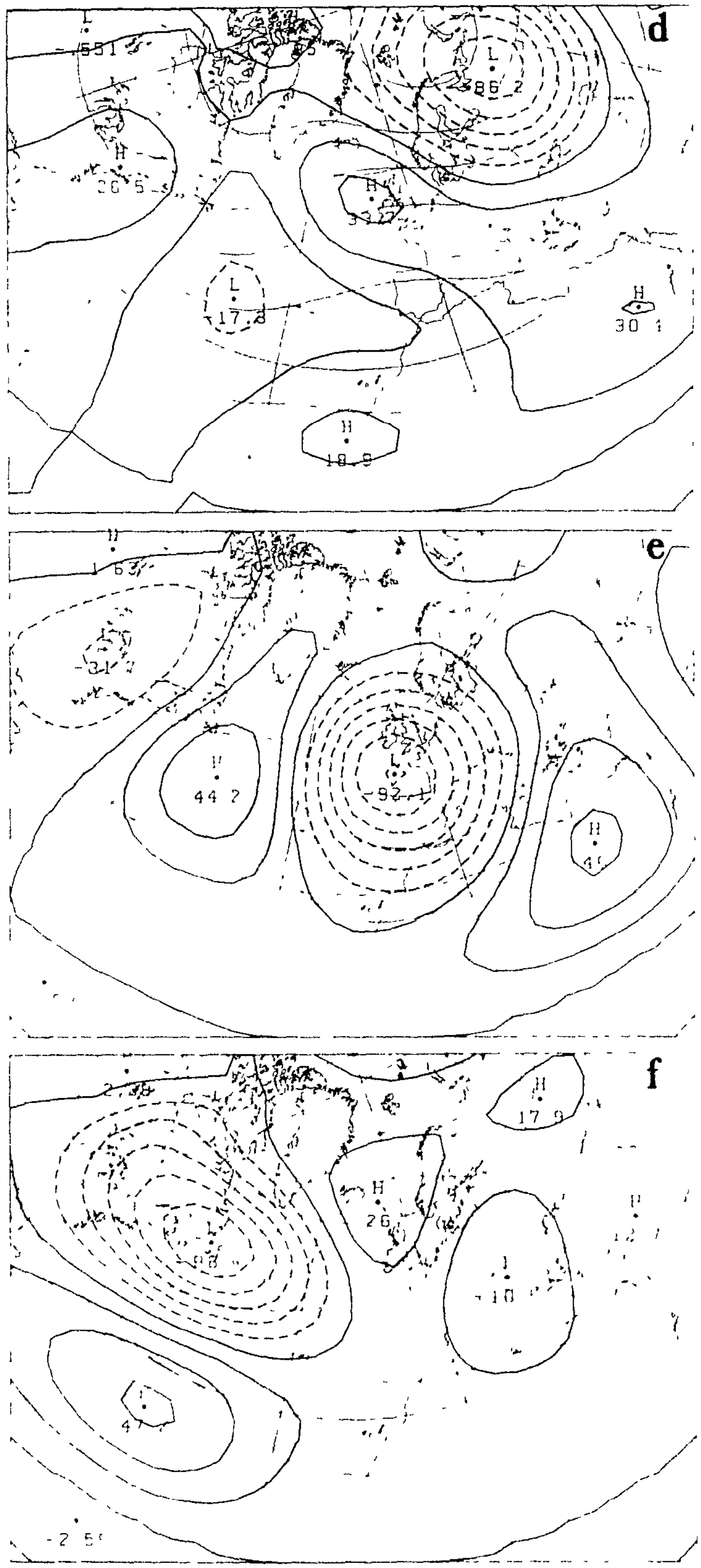

FIGURE 21

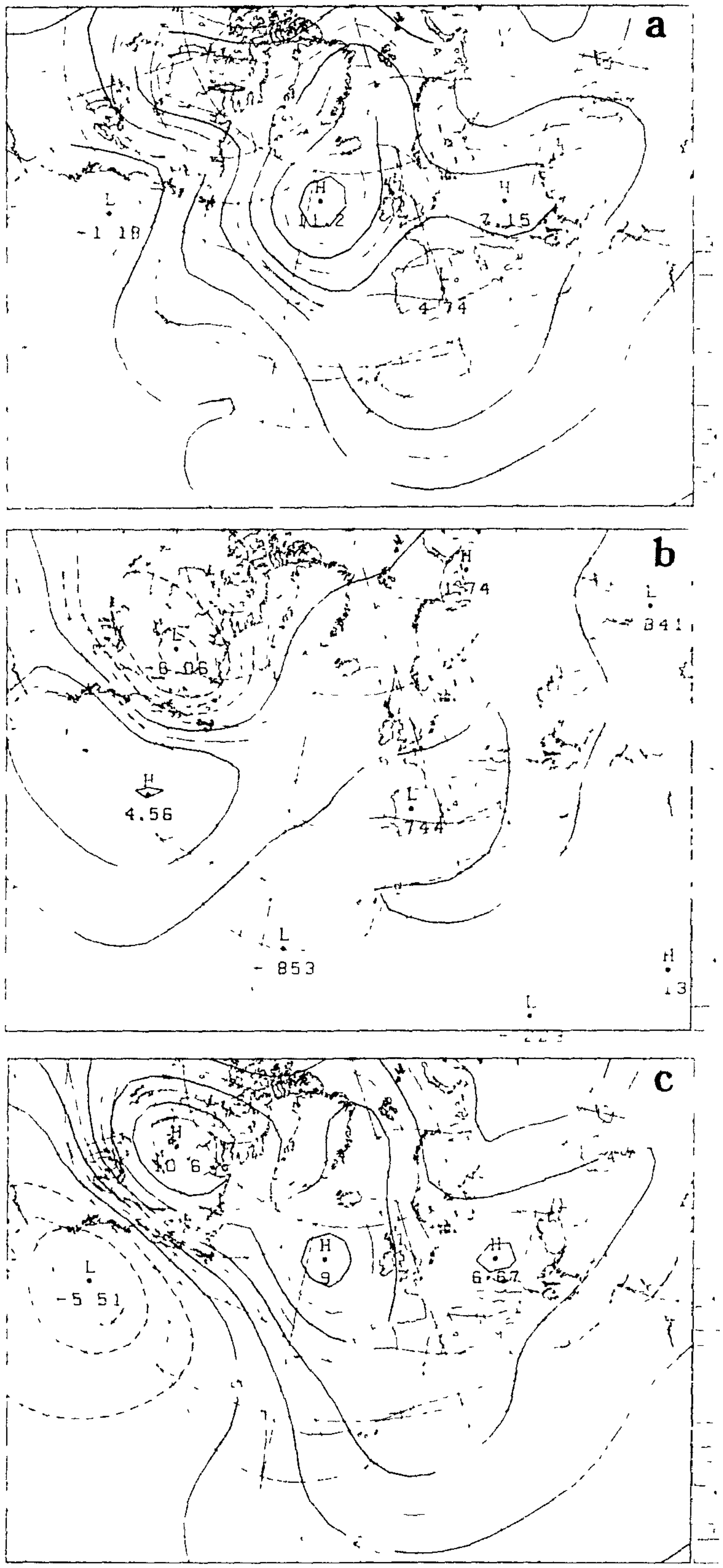

FIGURE 22

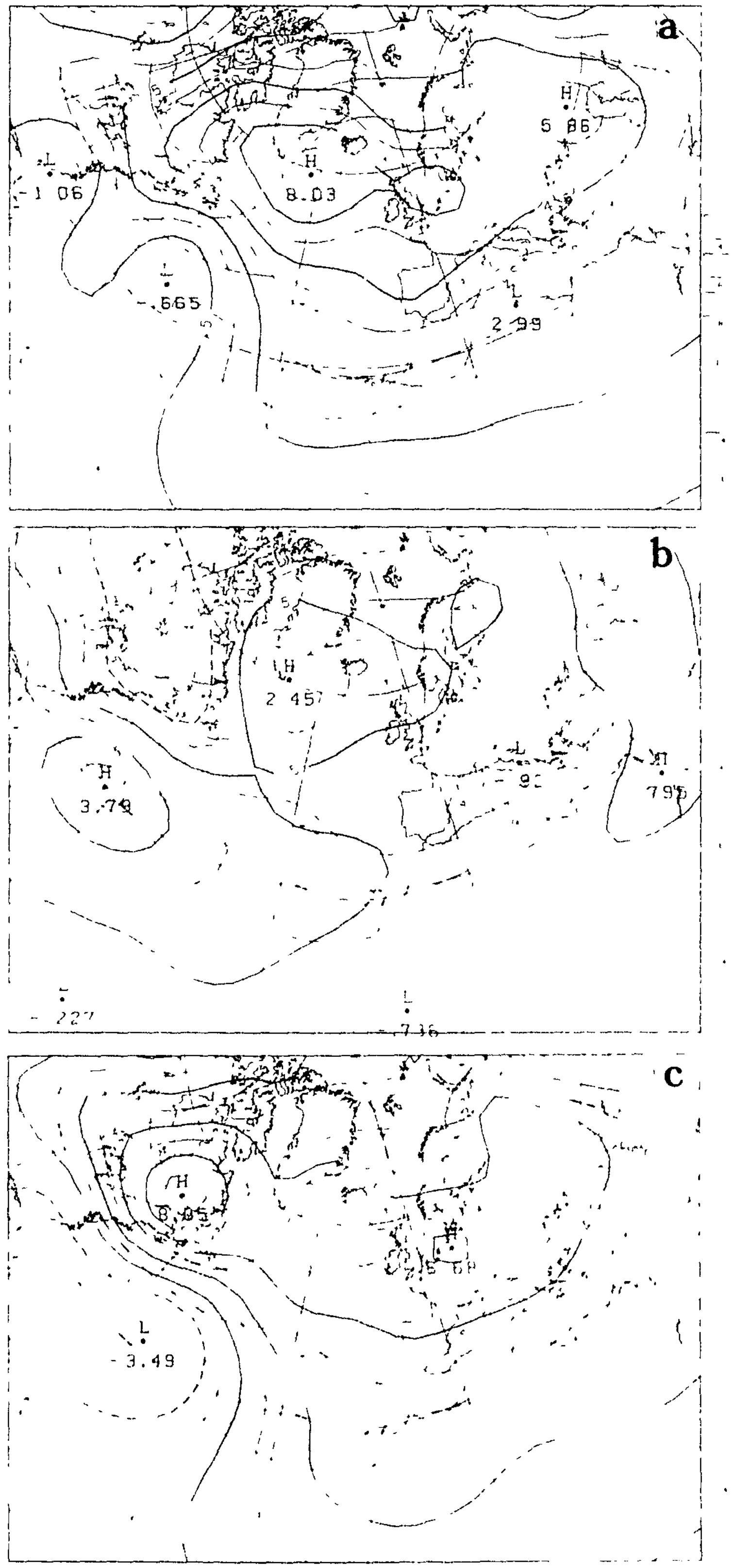

FIGURE 23

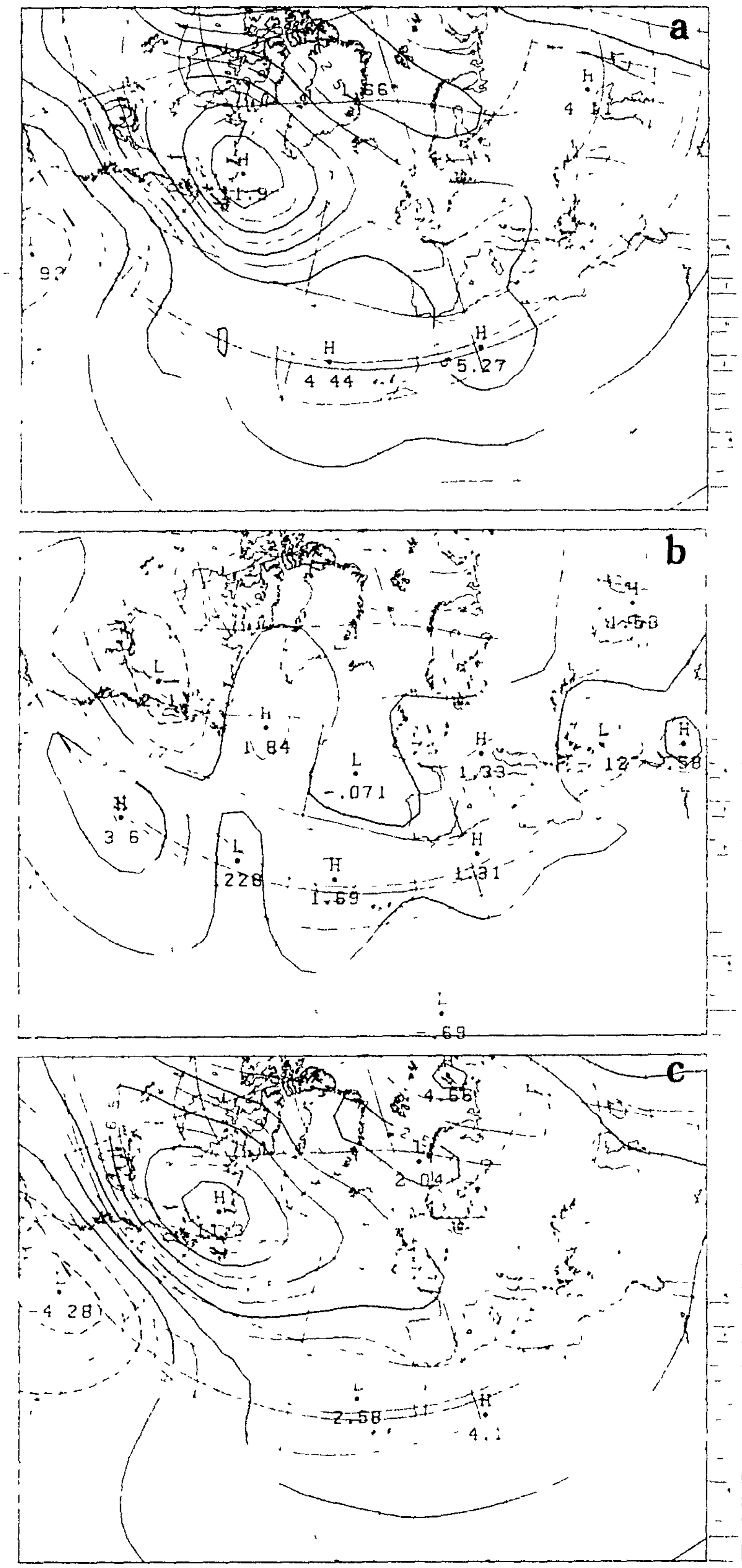

FIGURE 24

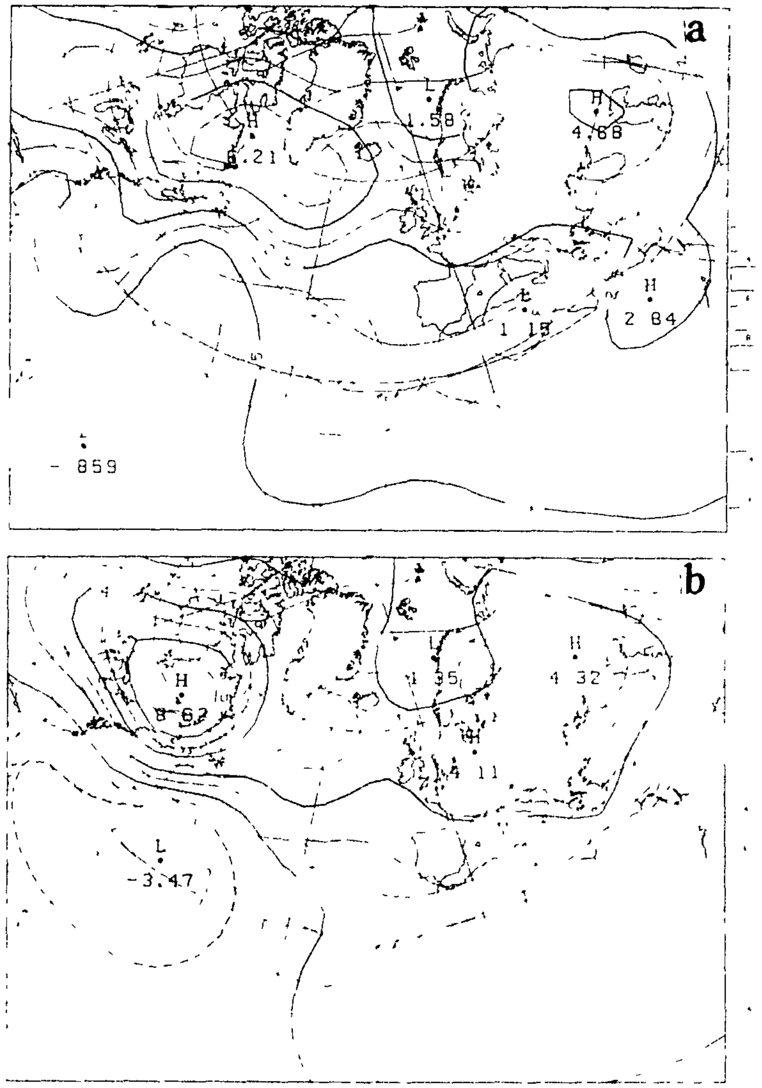

FIGURE 25

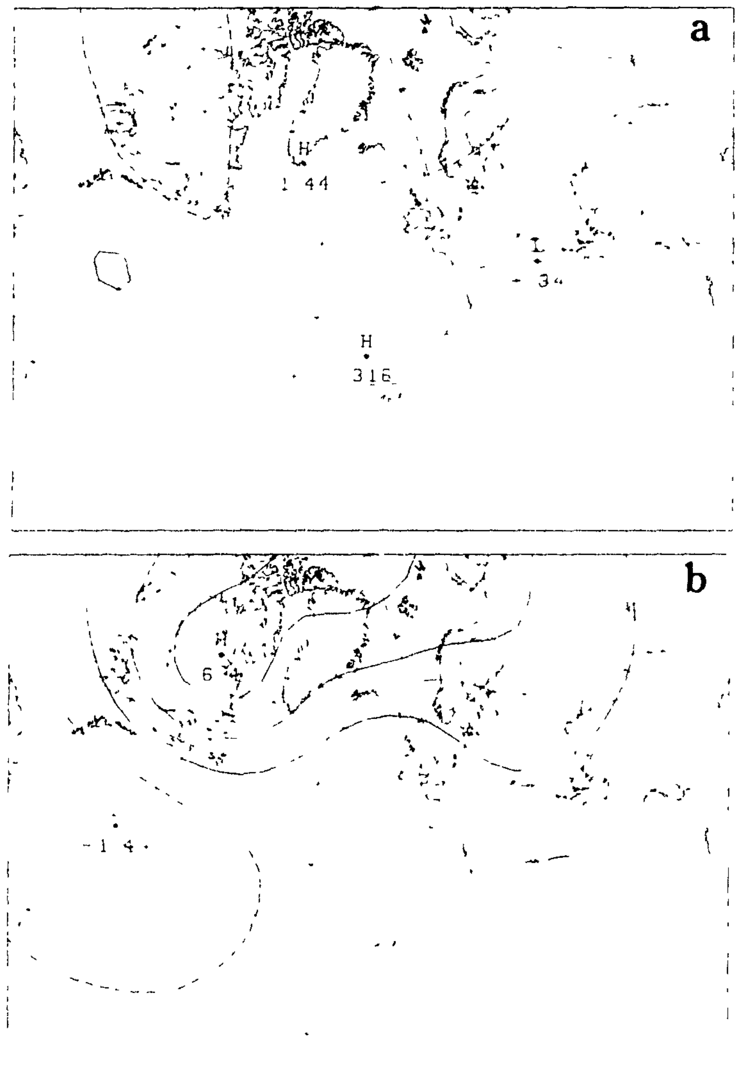

FIGURE 26

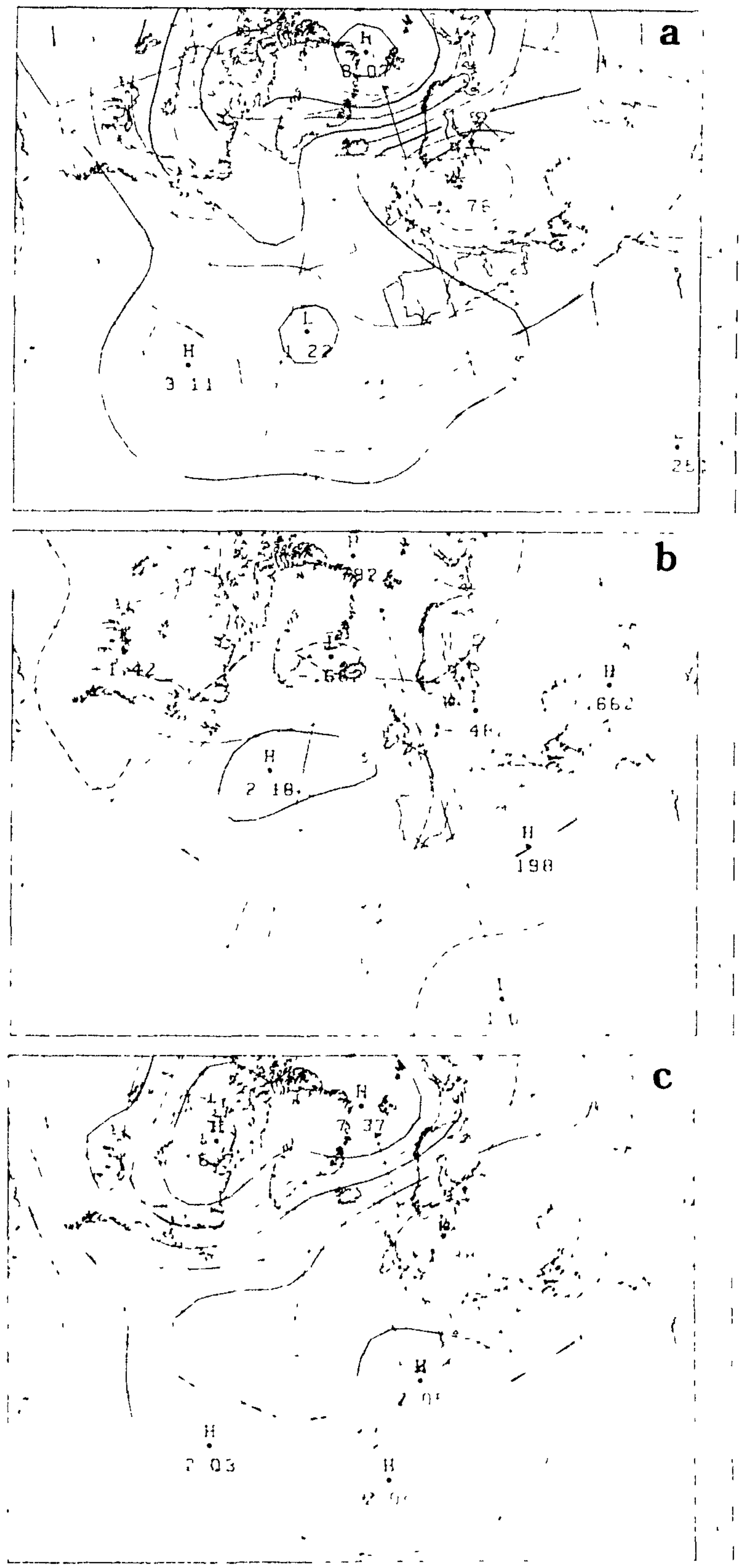

FIGURE 27

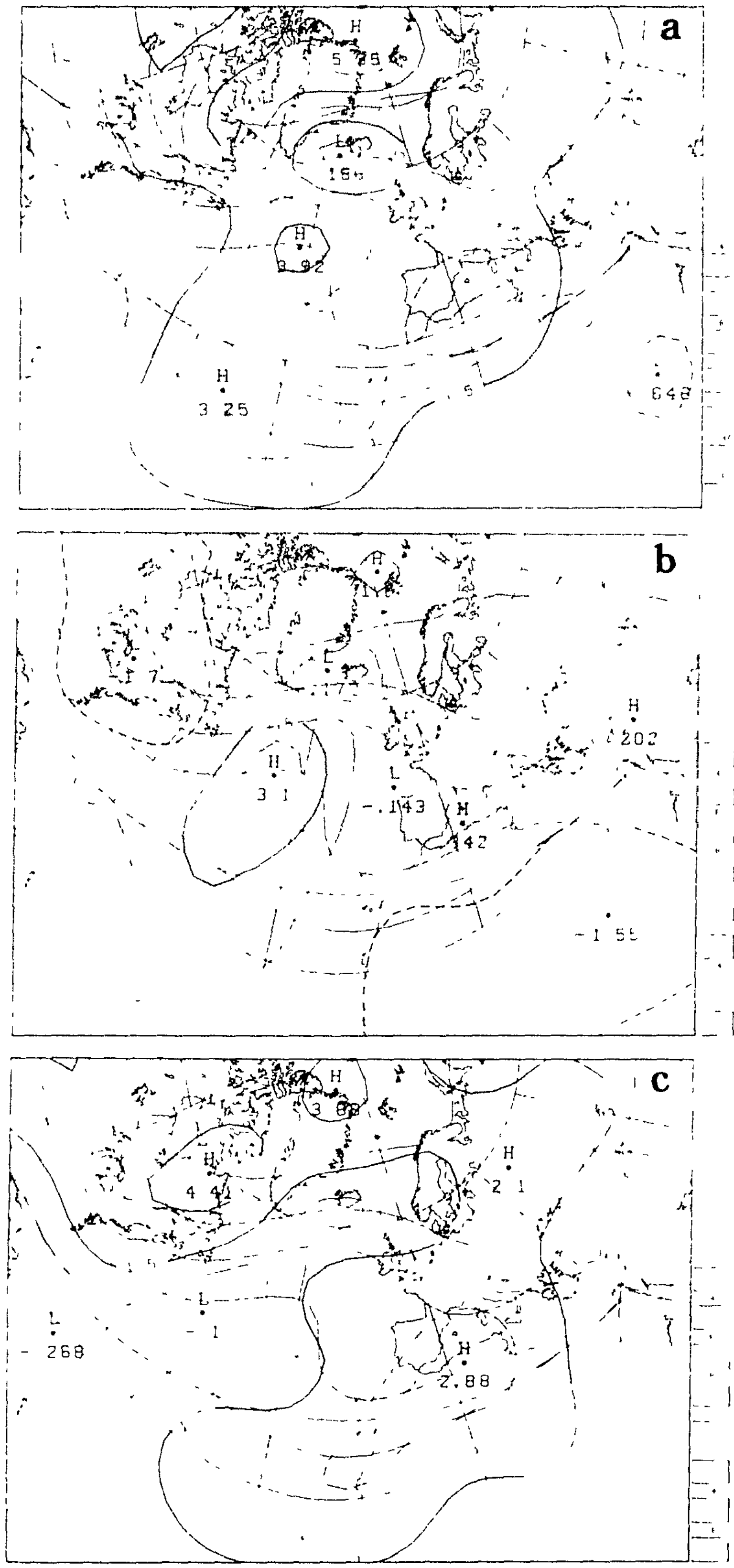

FIGURE 28

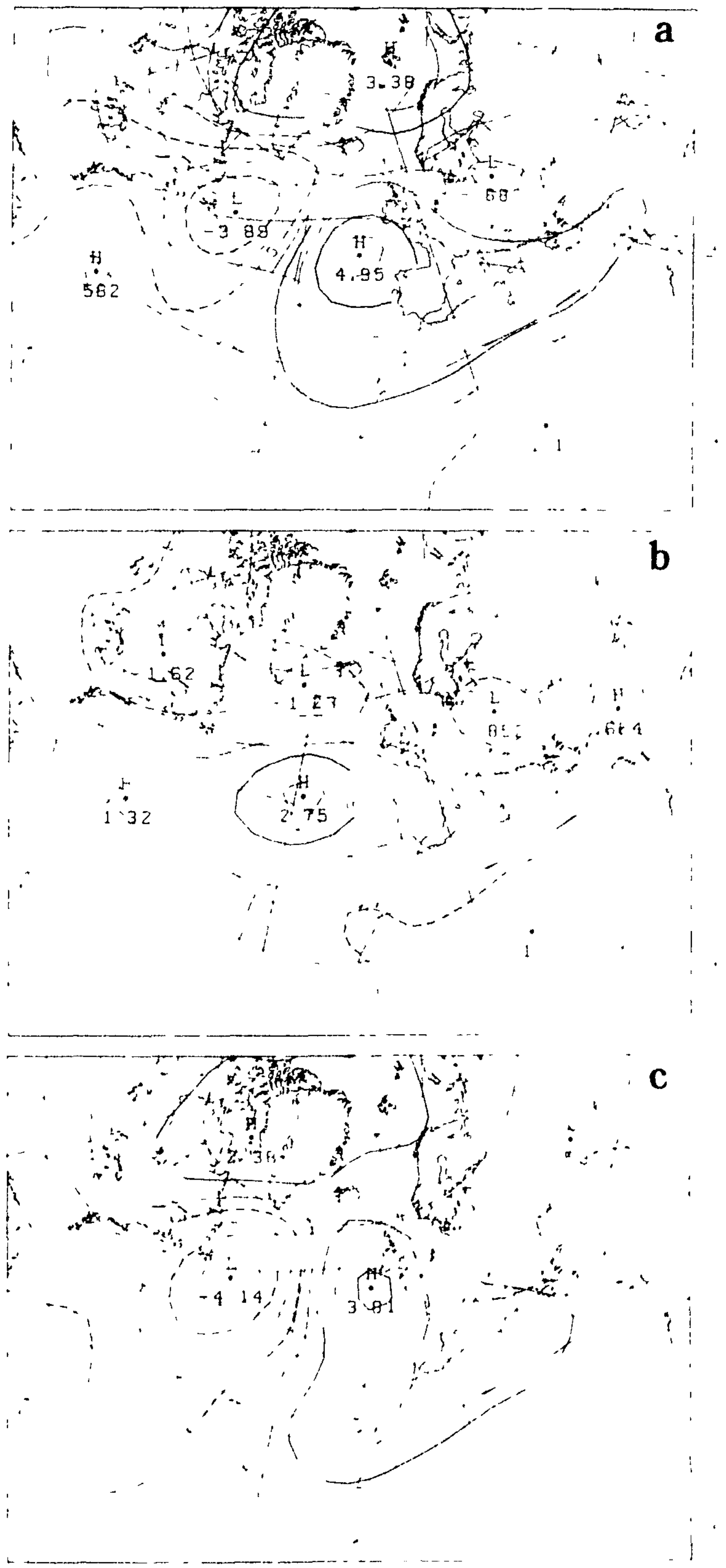

FIGURE 29

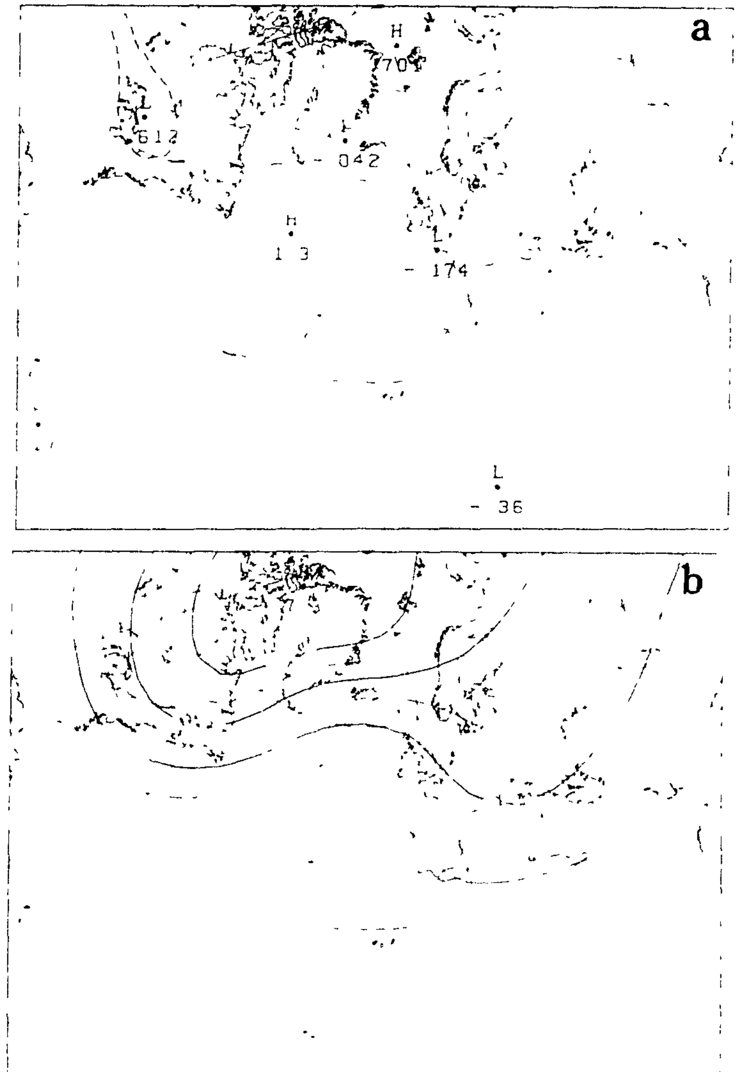

FIGURE 30

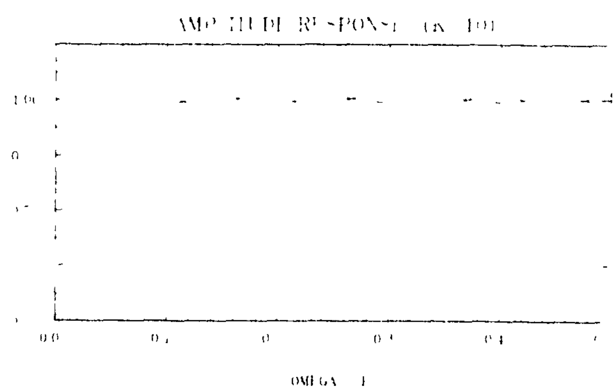

FIGURE A1